Three-Level, Viscous-Inviscid Interaction Technique for the Prediction of Separated Flow Past Rotating Wing

Sørensen, Jens Nørkær; Larsen, Poul Scheel; Pedersen, Bjarne Maribo; Jensen, Johannes Tejlgaard

Publication date:
1986

Document Version
Publisher's PDF, also known as Version of record

AFM 86-03 SEPTEMBER 1986

THREE-LEVEL, VISCOUS-INVISCID INTERACTION TECHNIQUE FOR THE PREDICTION OF SEPARATED FLOW PAST ROTATING WING

BY

JENS NØRKÆR SØRENSEN

DEPARTMENT OF FLUID MECHANICS

TECHNICAL UNIVERSITY OF DENMARK

Printed 1986
Department of Fluid Mechanics
Building 404,
Technical University of Denmark
DK-2800 Lyngby

PREFACE

This dissertation is submitted in partial fulfilment of the requirements for the Danish licentiate degree.
The dissertation is based on theoretical work carried out during the period August 1983 to September 1986 at the Department of Fluid Mechanics, The Technical University of Denmark. The work has been carried out under the guidance of Professors P.Scheel Larsen, B.Maribo Pedersen and J.Tejlgård Jensen.

I would like to express my appreciation to my instructors for their assistance and encouragement through the course of this work. Thanks are also due to my collegues at the Department whose kind co-operation I have appreciated. In particular I am grateful to Lic.Tech. Jess A.Michelsen for fruitful and inspiring discussions in the field of fluid dynamics.
I am indebted to Arnth Jensen, Bo Gervang, Knud Black and Tove Jørgensen for their kind assistance in preparing figures and correcting the manuscript. I am especially grateful to Mrs. Lizzie Krøyer for her patient and very skilful typing of the manuscript. Finally, I would like to give a special thank to B.Maribo Pedersen and the Wind Energy Group at the Department of Fluid Dynamics for their encouragement and invaluable financial support during the last part of the work.

September 1986
Jens Nørkær Sørensen

ABSTRACT

A computational model for predicting turbulent separated flows past rotating wings has been developed. The model makes use of a zonal approach in which the flow domain is divided into three levels, comprising the three-dimensional boundary layer, the external inviscid flow field and the inviscid flow field in the wake. Comparisons with two-dimensional calculations show that the effect of the rotation is to delay the onset of separation, to increase the lift coefficients by up to 30% in regions of highly separated flow, and to slightly decrease the drag coefficient. Comparisons of power and blade-root moment of a 15 m diameter wind turbine show that the computed results are in good agreement with measurements. Attempting to describe the actual physics of the flow, the model represents a considerable improvement to the classical blade-element theory.

ABSTRAKT

En numerisk beregningsmodel til bestemmelse af turbulent separeret strømning omkring en roterende vinge er blevet udviklet. Modellen er baseret på en zone antagelse, i hvilken strømningen er opdelt i tre niveauer bestående af det 3-dimensionale grænselag, den ydre inviskose strømning og den inviskose strømning i kølvandet. Sammenligninger med 2-dimensionale beregninger viser, at rotationen af vingen forsinker separation, øger opdriftskoefficienten med op til 30% ved stærkt separerede strømninger og formindsker modstandskoefficienten en anelse. Sammenligninger af effekt og blad-rods momenter for en 15 m diameter vindmølle viser at de beregnede resultater er i god overensstemmelse med målinger. Modellen repræsenterer en betragtelig forbedring af den klassiske blad-element teori, idet den søger at beskrive strømningens faktiske fysiske forløb.

NOMENCLATURE

a	Axial flow induction factor
a'	Tangential flow induction factor
a_1-a_4	Coefficients of the interaction flow
A	Van Driest damping constant
A_o	Area of streamtube far upstream of the rotor disk
A_D	Area of streamtube at the rotor disk
A_∞	Area of streamtube far downstream of the rotor disk
A_{ij}	Influence matrix of the potential flow
$\underline{\underline{A}}$	Influence matrix; alternative notation to A_{ij}
$\underline{\underline{A}}_j$	Matrix of the block elimination procedure
b	Viscosity parameter
b	Relaxation exponent
$(\underline{b}_1, \underline{b}_2, \underline{b}_3)$	Unit base vectors of surface fitted coordinate system
B	Number of rotor blades
B_{ij}	Influence matrix of the potential flow
$\underline{\underline{B}}$	Influence matrix; alternative notation to B_{ij}
$\underline{\underline{B}}_j$	Matrix of the block elimination procedure
c	Chord length
$c_{i,j}$	Element of influence matrix
C_L	Lift coefficient
C_D	Drag coefficient
C_T	Thrust coefficient
C_P	Power coefficient
C_ν	Turbulence parameter
$\underline{\underline{C}}$	Matrix of influence of the injection function
$\underline{\underline{C}}_j$	Matrix of the bloch elimination procedure

ds	Length of surface element
$d_{i,j}$	Coefficient of the interaction flow
D	Drag
$e_{i,j}$	Coefficient of the interaction flow
E	Transformed normal velocity component
F	Dimensionless velocity potential
F	Injection function
F_x	Normal force on blade element
F_y	Tangential force on blade element
g_{ij}	Metric tensor
G	Dimensionless velocity potential
h_1, h_3	Metric coefficients
h_j	Mesh size ; η-direction
$(\underline{i},\underline{j},\underline{k})$	Unit base vectors of Cartesian coordinate
k_n	Mesh size ; x-direction
K_n	Parameter of the interaction flow
K_1, K_3	Geodestic curvatures
K_{13}, K_{31}	Curvature parameters
L	Lift
L	Mixing length
$\underline{\underline{L}}$	Block-lower triangular matrix
m_z	Variable ; $m_z = W_e \delta_z^*$
m_1-m_{13}	Coefficients of the boundary layer equations
$\underline{n}$	Normal vector
N	Number of surface elements
p	Pressure
p_o	Atmospheric pressure
p_∞	Static pressure far downstream of the rotor disk

p_D^+	Static pressure just upstream of the rotor disk
p_D^-	Static pressure just downstream of the rotor disk
Δp	Pressure drop across the rotor disk
$(p_3)_j$- $(p_5)_j$	Coefficients of the velocity iterate
$\underline{p}_j$	Vector of the velocity iterate
P	Power
$(q_3)_j$- $(q_5)_j$	Coefficients of the displacement thickness iterate
$\underline{q}_j$	Vector of the displacement thickness iterate
$\bar{r}$	Distance from the axis of rotation to a point on the wing
r_i	Mesh size, z-direction
$(r_1)_j$- $(r_7)_j$	Residues of the Newton procedure
$\underline{r}_j$	Residue vector
R	Length of the wing
$(s_1)_j$- $(s_{26})_j$	Coefficients of iterates of the Newton procedure
Δs_k	Length of surface element no. k
$(t_3)_j$- $(t_4)_j$	Coefficient of the iterate of the spanwise skin-friction
$\underline{t}_j$	Vector of the iterate of the spanwise skin-friction
T	Thrust
$\underline{T}$	Non-dimensionalised spanwise shear parameter
T_w	Non-dimensionalised spanwise skin-friction
(u,v,w)	Boundary layer velocites
$\underline{u}$	Disturbance velocity vector
u_τ	Wall-friction velocity
u_x	Derivative of u

$-\overline{u'v'}$	Reynolds stress component
U	Non-dimensionalised chordwise velocity
(U_e, V_e, W_e)	Velocities evaluated at boundary layer edge
U_{te}	Total tangential velocity at boundary layer edge
U_{xe}	Derivative of U_e
$U_{x\infty}$	Component of $\underline{U}_\infty$, measured along the chord
$U_{y\infty}$	Component of $\underline{U}_\infty$, measured normal to the chord
$\underline{U}_\infty$	Resulting relative velocity
$\underline{U}_x$	Velocity component due to translating onset flow
$\underline{U}_y$	Velocity component due to translating onset flow
$\underline{U}_R$	Velocity due to rotating onset flow
$\underline{U}_i^{\infty r}$	Rotating onset flow
$\underline{U}_T$	Velocity due to translating onset flow
$\underline{U}_{wake}$	Velocity due to the wake
$\underline{\underline{U}}$	Block-upper triangular matrix
v_x	Tangential component of $\underline{v}_{ij}$
v_y	Normal component of $\underline{v}_{ij}$
$\underline{v}_{ij}$	Induced velocity
$(v_3)_j - (v_5)_j$	Coefficient of the iterate of the chordwise skin-friction
$\underline{v}_j$	Vector of iterate of the chordwise skin-friction
$-\overline{v'w'}$	Reynolds stress component
V	Non-dimensionalised chordwise shear-parameter
V_w	Chordwise wall-shear
V_o	Velocity of the undisturbed wind field

V_D	Wind velocity at the rotor disk
V_∞	Wind velocity far downstream of the rotor disk
V_t	Tangential velocity of the wake
$\underline{w}_i$	Resulting induced velocity
W	Non-dimensionalised spanwise velocity
W_{ref}	Spanwise reference velocity
(x,y,z)	Coordinates of surface fitted coordinate system
$(\bar{x},\bar{y},\bar{z})$	Coordinates of Cartesian coordinate system
$(\hat{x},\hat{y})$	Local chord orientated coordinate system
$\underline{Y}$	Right-hand side vector
$\underline{Z}$	Solution vector

α	Angle of attack
$\alpha_{i,j}$	Coefficient of three-point Lagrange interpolation
$\beta_{i,j}$	Coefficient of three-point Lagrange interpolation
γ	Pitch angle
γ_j	Vortex density at element no. j
Γ	Total vortex strength
$\underline{\underline{\Gamma}}_j$	Matrix of the block elimination procedure
δ	Boundary layer thickness
δ^*	Displacement thickness
$\underline{\delta}_j$	Vector of boundary layer iterates
$\Delta(\ )$	Iterate of Newton procedure
$\underline{\Delta}$	Solution vector of Newton procedure
ε	Criterium of convergence

η	Transformed normal coordinate
θ	Momentum thickness
θ	Angle between $\underline{b}_1$ and $\underline{b}_2$
θ_{11}	Chordwise momentum thickness
θ_{22}	Spanwise momentum thickness
θ_1, θ_2	Weighting coefficients
$\underline{\underline{\Lambda}}_j$	Matrix of the block elimination procedure
μ	Viscosity
ν	Kinematic viscosity
ν_i^t	Eddy viscosity ; inner formulation
ν_o^t	Eddy viscosity ; outer formulation
ρ	Fluid density
$\hat{\sigma}_j$	Source density of element no. j
$\hat{\sigma}_j^F$	Source density due to the injection function
τ_w	Wall friction
τ_{tw}	Total wall friction
ϕ	Coordinate , $\phi \equiv x$
$\overline{\phi}$	Velocity potential
(ϕ, Ψ)	Two-component velocity potential
ψ	Angle between the rotor plane and the relative velocity vector
$\underline{\underline{\Psi}}$	Matrix of the block elimination proces
ω	Relaxation parameter
Ω	Angular velocity
$\underline{\underline{\Omega}}_j$	Matrix of the block elimination procedure

Suffix

$( )'$	Derivative with respect to η
$( )_e$	Value at boundary layer edge
$( )_I$	Inviscid quantity
$( )_w$	Value at surface
$( )^*$	Quantity evaluated at off-body location
$\hat{( )}$	Normalised quantity
$\tilde{( )}$	Quantity taken in the wake

TABLE OF CONTENTS

1. INTRODUCTION

1.1 Introductory remarks

In the field of fluid dynamics some of the most complex and least understood phenomena are associated with the description of the flow past rotating blades. Assuming the flow to be incompressible and the inflow conditions to be steady, it is still necessary to cope with an essentially three-dimensional flow field subject to rotational effects in the boundary layer, such as the Coriolis and centrifugal forces. In addition, due to the presence of the rotor itself, the trailing and shedded vortices in the wake induce velocities that alter the inflow conditions of the external inviscid flow as well as the boundary layer.
Basically, the flow around a rotating blade section is similar to that about a two-dimensional airfoil. From experience it is known that the forces produced by rotating blades resemple the characteristics of the classical airfoil. It is commonly presumed, however, that rotationally induced radial flow to a certain extent influences skin friction and the location of separation, and that this effect may have a strong influence on the pattern of the flow in regions of separated boundary layers.

The aerodynamic theories for predicting thrust and power requirements of rotors have usually been based upon the use of two-dimensional airfoil data. Employing a blade-element theory, in which it is assumed that the blade-elements produce lift and drag independently of each other, performance estimates have been made of propellers, helicopters and wind turbine rotors. These theories, however, are found to have limited validity, at best restricted to describe flows around rotors at prestalled conditions. There is experimental evidence that the secondary flow in the boundary layer may alter the stalling characteristics of the airfoil section, and it is likely to assume that the limitations are attributed mainly to the use of two-dimensional airfoil data.

Although considerable effort, both analytically and experimentally, has been spent investigating the boundary layers of rotors, to date no adequate model, which cope with separated boundary layer flows, has been presented.
The aim of the present work, however, is to develop such a model. Before considering the scope of this thesis, however, it is appropriate to give a historical review of the pertinent literature which has been published to date.

1.2 Historical review

As early as in 1945 Himmelskamp (1945) investigated the boundary layer on a fan blade. Performing detailed measurements of the surface pressures, he discovered that in comparison to two-dimensional data the lift coefficient significantly increased yielding values greater than 3 near the hub. This phenomenon he attributed to secondary radial flows induced by the centrifugal force and to the Coriolis forces which act like an additional chordwise pressure gradient.

In the beginning of the 1950's the first analytical studies of laminar boundary layer flows on rotating blades was initiated by Sears and his collegues.
Based on the independence principle of the potential flow described by Sears (1950), Fogarty (1951) analysed attached laminar boundary layers on rotary wings. Assuming the chord to be small compared to distance from the axis of rotation, Fogarty concluded that the rotation only has a small effect on the growth of the boundary layer.
A later study performed by Rott & Smith (1956) confirmed this conclusion.
As this appears to be in disagreement to the results of Himmelskamp and the common view that three-dimensional effects on rotating blades are large, Fogarty (1951) suggested that the rotational effects only are pronounced in regions of separated flows.
By using chemical evaporation, pressure probe measurements and hot wire techniques, Tanner and Yaggy (1966) studied the bound-

ary layer properties of a full-scale hovering rotor. The aim of their study was to determine the effect of the rotation on the transition from laminar to turbulent flow, and to determine limiting streamlines and measure velocity profiles in the boundary layer. Compared to two-dimensional non-rotating results they discovered that there were no disagreement in the position of transition. Furthermore they found that no evidence of secondary radial flow in the boundary layer were present. In their study, however, only attached flows were analysed, which again indicates that if rotational effects do alter the boundary layer properties, it is only significant in the case of separated flows.
In an investigation performed by Harris (1966) it was suggested that the enhanced production of lift could be due to phenomena associated with the flow becoming yawed. This would tend to delay the stall and to some extent it could explain why the highest lift coefficient is obtained near the hub, where yaw is most pronounced.

In the late 60ths and the early 70ths intensive numerical and experimental studies on rotary wing boundary layers were carried out by McCroskey and co-wokers. Although the primary aim of this work was devoted to helicopters in forward flight, important conclusions of blades in pure rotation were drawn. Using a perturbation expansion of the boundary layer equations and a direct numerical integration based on the Crank-Nicolson scheme, it was shown that the crossflow velocities in fact do influence the separation characteristics of rotor blades as compared to two-dimensional airfoils. In the simple case of a flat-plate blade at zero angle of attack (McCroskey & Yaggy, 1968) it was found that the velocity profile of the laminar boundary layer could be expressed by similarity profiles determined uniquely by the ratio X/Z . Here X denotes the chordwise coordinate and Z the spanwise coordinate. For large values of X/Z , i.e. near the hub, the flow is dominated by the Coriolis force which forces the spanwise flow inward. Furthermore, as the hub is approached, the crossflow velocity derivative becomes large and through the equation of continuity the primary flow is significantly altered. At the

same time, the chordwise component of the centrifugal force exerts a strong accelerating force on the primary flow which increases the skin-friction and tends to stabilize the boundary layer. For small values of X/Z , however, this effect becomes less significant and for $X/Z < 0.1$ the primary velocity profile is close to its two-dimensional value.
In the case of a steadily rotating NACA0012 airfoil at zero incidence similar conclusions to those of the rotating flat plate were drawn (McCroskey & Dwyer, 1969). As the flow in this case was calculated as being laminar, it exhibited trailing edge separation.
In a later study Dwyer & McCroskey (1970) investigated the influence of the angle of attack on the separation characteristics of a rotating airfoil. This study involved as well numerical predictions as experimental techniques.
By increasing the pitch angle of the blade the effect of cross-flow was determined for stall onset.
Compared to two-dimensional calculations it was found that the separation line in the rotating case moved downstream. This delaying effect, however, was small and only present for collective angles of attack less than 5^{o}. Furthermore it was confined to the vicinity of the hub.

Using heated-film skin-friction gages, acenapthane sublimation and oil streaks McCroskey (1971) investigated the location of transition and the potential existence of laminar separation bubbles at the leading edge.
The most important conclusions drawn from this study was the strong similarity between the rotating and non-rotating behaviour of the airfoil. Thus the transition accured at approximately the same chordwise positions in both cases. Whether laminar or turbulent, the flow direction in the boundary layer seemed not to differ from the line representing the undisturbed flow direction. Furthermore it was found that for large angles of attack the numerical as well as the experimental results for separation agreed well with two-dimensional calculations. Finally, it was concluded that the main difference in the rotating and two-dimensional flow occurs within the

separation bubble, where centrifugal forces move the fluid outward significantly.

Parallel to the study of McCroskey and his collegues similar theoretical and experimental investigations were performed elsewhere. At Ohio State University flow visualization technique (Velkoff *et.al.*, 1971) as well as hot wire anemometry (Blaser & Velkoff, 1973) was employed to study the nature of the boundary layer on a model helicopter rotor. In addition, a momentum-integral method was developed and calculated results were compared with measurements. Young & Williams (1970) employed a series expansion solution to investigate the effects of rotation and forward flight on the boundary layer. Takematsu (1972) used a conformal coordinate system in order to take into account the influence curvature on the boundary layer solution of a rotating round-nosed blade. The most sophisticated analytically study to date, however, was carried out by Hicks & Nash (1971), who employed a finite difference technique to investigate the boundary layer behaviour of a rotating NACA 0012 airfoil. In their approach they employed a semi-empirical formulation of the external inviscid flow and a primitive variable formulation of the boundary layer equations in combination with an empirically modified turbulent-energy equation. From these studies, however, no further conclusions concerning rotors in pure rotation were drawn.

In general, it was concluded from the investigations that the dynamic stalling of retreting blades of helicopters in forward flight was the most important problem to be solved. Consequently, the investigations of hovering helicopters stopped, and the dynamic stall problem has dominated the research of helicopter aerodynamics since this time.

In the mid-70's the modern development of wind turbines took its beginning, and renewed attention was paid to the aerodynamics of steadily rotating blades. In general, the models which was developed to predict rotor performance of wind turbines have been based on momentum considerations and the classical blade element approach (see e.g. Wilson & Lissaman, 1974).

More advanced models which simulates the convection of the trailing vortex wake have also found their use. These models, however, are relatively computing costly and do not improve the accuracy much. A review of various calculation methods has been given by De Vries (1979). All of the existing models, however, are based on the use of empirical airfoil data, and as such they do not give any physical insight into the behaviour of the boundary layer. Comparisons of measurements with calculations clearly show that none of the current models are able to accurately predict the maximum rotor power or the post-peak power (see e.g. Rasmussen, 1983). This indicates that the three-dimensionality of the flow in the stalled regime might have a significant influence on the mechanisms which affects the production of the aerodynamic forces. Recent experiments seem to confirm this. In a wind tunnel study carried out by Milborrow & Ross (1984) the loading on a model rotor was investigated. From this study it was found that beyond the stall the effective lift coefficient was higher than that obtained from two-dimensional data. Using balanced wind vanes Savino & Nyland (1985) made it possible to visualize the flow direction on the surface of a 38 m diameter MOD-0 rotor blade. On the suction side of the blade a separation line clearly indicated the occurence of trailing edge separation. Upstream of the separation line flow was directed along the chord line. In the separated region, however, the flow was strongly radial with the vanes appearing almost motionless, indicating a stable flow direction. As compared to two-dimensional wind tunnel tests, it appeared that the position of the separation line deviated from 10 to 20 percent of a chord length.

1.3 Purpose of the present study

Seen in light of the investigations performed to date, considerable uncertainties still exist about the actual three-dimensional flow pattern on rotary wings. To get an insight into the nature of the aerodynamics of rotating wings, it is necessary therefore to develop a calculation method which is capable of handling three-dimensional stall. Against this

background, in the present study it was decided to develop a computational model which would enable us to calculate large regions of separated flow and thus overcome the limitations of the classical theories. Ideally, such a model should be capable of making actual performance predictions of rotors working in the stalled regime. In principle this would demand a solution of the Navier-Stokes equations. The solution of these equations for three-dimensional flows, however, are both difficult and time consuming. As a consequence it was found more appropriate to reduce the equations by dividing the flow into a viscous region, governed by the boundary layer equations , an inviscid region, represented by the Euler equations, and then to couple the two sets of equations by a viscous-inviscid matching procedure.
In the case of a two-dimensional flow past a NACA 4412 airfoil, a preliminary study (Sørensen, 1986) clearly showed that this approach represents an elaborate alternative to the Navier-Stokes equations. Compared to measurements by Coles & Wadcock (1979), C_{Lmax} was predicted within one percent accuracy. In addition, it was found that it was possible to extend the approach to describe three-dimensional separated flows.
As a consequence, the aim of the present study is to develop a computational model which, based on a viscous-inviscid interaction procedure, is able to calculate separated flows on rotating wings.

A detailed description of the various theories underlying the viscous-inviscid interaction technique is given in chapter 2. This chapter can be read independently of the remaining chapters and the reader who is familiar with these techniques may omit it.

2. VISCOUS-INVISCID INTERACTION

Although progress is being made in the solution of the time-averaged Navier-Stokes equations, with a suitable turbulence model, for turbulent flows, it is often very expensive to employ this approach for flow problems of technical importance. In particular, the solution of three-dimensional flow problems requires further advances in computer technology, turbulence modeling, and numerical techniques before the approach can be used routinely.

An alternative approach is to divide the flow into a viscous domain, governed by the boundary layer equations, and an inviscid domain, represented by the inviscid Euler equations, and then to couple the two sets of equations by a viscous-inviscid matching procedure. The advantage of this technique is that the boundary layer equations are parabolic and, if we presume incompressible and irrotational flow conditions, the equations of the inviscid flow are elliptic and linear. With these advantages, it is possible to keep both computer storage and computing time at a reasonable level.

Despite these advantages there remains one difficulty. The parabolic nature of the boundary layer equations apriori implies that the flow is uninfluenced by events downstream, hence special treatment is necessary at flow reversal. Furthermore, the boundary layer equations become singular at the separation point if the pressure gradient is prescribed as a boundary condition, as done in the direct method of calculation. This singularity, however, can be removed by instead prescribing the displacement thickness as a boundary condition, as done in the inverse method of calculation.

The following paragraphs are devoted to the analysis of general solution procedures which cope with the coupling of the viscous and inviscid domains and with flow reversal.

2.1 Matching techniques

In the following the basic concepts of viscous-inviscid matching techniques will be derived and explained. The derivation is mainly based on the review articles by Lock (1980, 1985).

2.1.1 Two-dimensional considerations

Considering a two-dimensional incompressible flow, we split the flow domain into two regions:
(i) A viscous boundary layer in the neighbourhood of the surface,
(ii) An inviscid flow external to the viscous layer.

The coupling between these two regions is achieved by the compatibility conditions at the edge of the boundary layer, $y = \delta$,

$$U_e = U_{Ie} \tag{2.1a}$$

$$V_e = V_{Ie} \quad , \tag{2.1b}$$

where U and V denotes the tangential and the normal velocity, respectively, suffix 'e' denotes values at the edge of the boundary layer, and suffix 'I' denotes values for the inviscid flow.

The conditions expressed by eqs. (2.1a) and (2.1b) can be used directly to specify the matching conditions as proposed by Mahgoub & Bradshaw (1979). However, it is more convenient to extend the inviscid flow into the viscous region which, in the notation of Lock (1980), is called the equivalent inviscid flow, and then to perform the coupling through the definition of a displacement thickness δ^* . For the equivalent inviscid flow, we allow the velocities to vary across the boundary layer region as sketched in fig. 2.1.

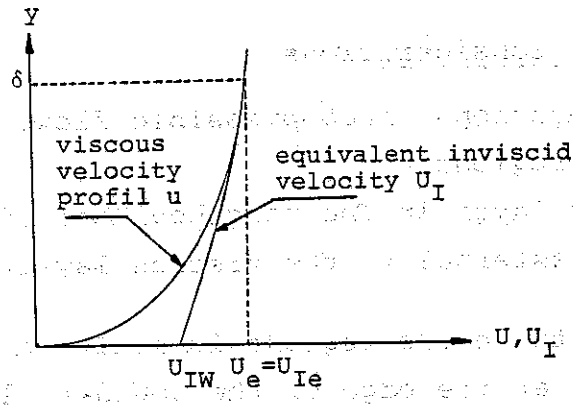

Fig. 2.1 Viscous and equivalent inviscid velocities in boundary layer.

Both the boundary layer flow and the equivalent inviscid flow obey the law of continuity,

$$\frac{\partial u}{\partial x} + \frac{\partial v}{\partial y} = 0 \quad , \tag{2.2}$$

$$\frac{\partial u_I}{\partial x} + \frac{\partial v_I}{\partial y} = 0 \quad , \tag{2.3}$$

where x defines the streamwise coordinate and y the direction normal to the surface.

Considering the difference between the equation of continuity for the viscous flow and the equivalent inviscid flow, we get the following equation

$$\frac{\partial}{\partial x}(u_I - u) + \frac{\partial}{\partial y}(v_I - v) = 0 \quad , \tag{2.4}$$

where surface curvature is neglected. Integrating eq. (2.4) across the viscous region, from $y = 0$ to $y = \delta$, and using the boundary conditions eqs. (2.1a) and (2.1b), we obtain the

following expression for the equivalent inviscid normal velocity at the wall

$$v_{Iw} = \frac{d}{dx}\left\{\int_o^\delta (u_I - u)\,dy\right\} \quad , \tag{2.5}$$

where suffix 'w' denotes values at the wall.

A generalized displacement thickness can then be defined as follows

$$\delta_A^* = \frac{1}{u_{Iw}} \int_o^\delta (u_I - u)\,dy \quad , \tag{2.6}$$

and the transpiration velocity, which gives the inner boundary condition for the inviscid flow, can be expressed in the general form

$$v_{Iw} = \frac{d}{dx}(u_{Iw}\delta_A^*) \quad . \tag{2.7}$$

Another way of finding an inner boundary condition for the inviscid flow is to look for a displacement surface which defines a streamline of the equivalent inviscid flow. This is accomplished by using the relation

$$\left.\frac{v_I}{u_I}\right|_{y=\delta_B^*} = \frac{d\delta_B^*}{dx} \quad , \tag{2.8}$$

where the displacement surface $\delta_B^*(x)$ determines the desired streamline.

Integrating eq. (2.2) from $y = 0$ to $y = \delta$, and taking advantage of the boundary condition $v = 0$ for $y = 0$, we get the following expression for the normal velocity at the edge of the boundary layer

$$V_e = -\int_o^\delta \frac{\partial u}{\partial x}\,dy \quad . \tag{2.9}$$

Integration of eq. (2.3) from y to δ gives

$$v_{Ie} - v_I = - \int_y^\delta \frac{\partial u_I}{\partial x} \, dy \quad . \tag{2.10}$$

Inserting eq. (2.1b) and eq. (2.9) into eq. (2.10) gives a general expression for the equivalent inviscid normal velocity at a distance y from the surface

$$v_I = \int_y^\delta \frac{\partial u_I}{\partial x} \, dy - \int_o^\delta \frac{\partial u}{\partial x} \, dy \quad . \tag{2.11}$$

Evaluation of eq. (2.11) at $y = \delta_B^*$ gives

$$v_I\Big|_{y=\delta_B^*} = \int_{\delta_B^*}^\delta \frac{\partial u_I}{\partial x} \, dy - \int_o^\delta \frac{\partial u}{\partial x} \, dy \quad . \tag{2.12}$$

Inserting eq. (2.12) into eq. (2.8), we get

$$u_I\Big|_{y=\delta_B^*} \frac{d\delta_B^*}{dx} = \int_{\delta_B^*}^\delta \frac{\partial u_I}{\partial x} \, dy - \int_o^\delta \frac{\partial u}{\partial x} \, dy \quad , \tag{2.13}$$

or, by use of the Leibnitz's rule for differentation of integrals,

$$u_I\Big|_{y=\delta_B^*} \frac{d\delta_B^*}{dx} = \frac{d}{dx} \left\{ \int_{\delta_B^*}^\delta u_I dy - \int_o^\delta u \, dy \right\} + u_I\Big|_{y=\delta_B^*} \frac{d\delta_B^*}{dx} \quad . \tag{2.14}$$

This equation is satisfied if

$$\int_{\delta_B^*}^\delta u_I dy = \int_o^\delta u \, dy \quad , \tag{2.15}$$

which simply expresses that the mass flow of the viscous flow in the region of the boundary layer must equal the mass flow of the equivalent inviscid flow between the displacement surface and the edge of the boundary layer.

Thus, we now have two alternative methods of performing the viscous-inviscid interaction procedure:

Model A The transpiration velocity method
In this method the inner boundary condition for the equivalent inviscid flow is given as a normal transpiration velocity, specified by eq. (2.7). The boundary condition is imposed at the surface of the body.

Model B The displacement surface method
In this method the surface of the body is replaced by the displacement surface $\delta_B^* = \delta_B^*(x)$, and the boundary condition for the equivalent inviscid flow is established by treating the surface δ_B^* as being impermeable.

When using a surface singularity method for the calculation of the inviscid flow, e.g. the method of Hess (1971), much computing time is taken up by the inversion of the influence matrix, which is only dependent of the geometry. In such a case it is of advantage to use model A, since the influence matrix only has to be inverted once. In contrast to this, model B demands a new inversion for each calculation of the displacement surface.

If we assume that no velocity gradient of the equivalent inviscid flow exists across the boundary layer, we have u_I = constant = U_e , and the displacement thicknesses given by eqs. (2.6) and (2.15) reduce to the standard definition

$$\delta^* = \int_o^\delta (1 - \frac{u}{U_e}) dy \quad . \tag{2.16}$$

Inserting eq. (2.16) into eq. (2.5) we get the expression for the transpiration velocity according to Lighthill (1958)

$$v_{Iw} = \frac{\partial}{\partial x}(U_e \delta^*) \quad . \tag{2.17}$$

Eq. (2.16) and eq. (2.17) give a first-order approximation to the boundary conditions, and they should not be used in cases where the boundary layer cannot be considered as being thin. Such cases exist for flows which either are separated or are approaching separation.

Furthermore, if the streamline curvature becomes important, pressure gradients will be generated across the boundary layer. According to Lock (1985), this can be accounted for by correcting the pressure P as follows (see fig. 2.2)

$$P_w = P_{Iw} - \kappa^* \rho U_e^2 (\delta^* + \theta) \quad , \tag{2.18}$$

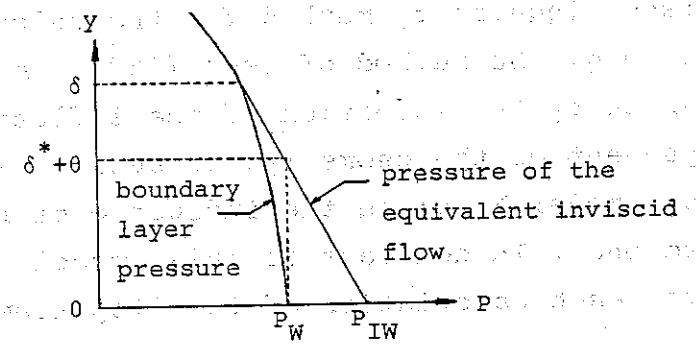

Fig. 2.2 Pressure variation through boundary layer.

where $\kappa^* \cong \frac{d^2\delta^*}{dx^2}$ the curvature of the displacement surface

ρ the density of the fluid

$\theta = \int_0^\delta \frac{u}{U_e}\left(1 - \frac{u}{U_e}\right)dy$ the momentum thickness ,

and P_w and P_{Iw} denotes the wall pressure of the real flow and the equivalent inviscid flow, respectively. Evaluating the pressure of the equivalent inviscid flow at $y = \delta^* + \theta$, Lock (1985) has shown that one gets the wall pressure of the actual fluid flow. This is especially usefull when establishing the Kutta condition.

2.1.2 Extension to three dimensions

The foregoing two-dimensional analysis forms the basic understanding for an extension to the general three-dimensional case. Again we distinguish between two alternative methods of performing the viscous-inviscid interaction.

Model A The transpiration velocity method

The three-dimensional equation of continuity is, for the viscous flow,

$$\frac{\partial u}{\partial x} + \frac{\partial v}{\partial y} + \frac{\partial w}{\partial z} = 0 \quad , \tag{2.19}$$

and, for the inviscid flow,

$$\frac{\partial u_I}{\partial x} + \frac{\partial v_I}{\partial y} + \frac{\partial w_I}{\partial z} = 0 \quad , \tag{2.20}$$

and the difference between these equations is

$$\frac{\partial}{\partial x}(u_I - u) + \frac{\partial}{\partial y}(v_I - v) + \frac{\partial}{\partial z}(w_I - w) = 0 \quad , \tag{2.21}$$

where w denotes the velocity in the z-direction.

As in the two-dimensional case we integrate eq. (2.21) across the boundary layer from $y = 0$ to $y = \delta$ and obtain the following expression for the normal transpiration velocity

$$v_{Iw} = \frac{\partial}{\partial x}\int_0^\delta (u_I - u)dy + \frac{\partial}{\partial z}\int_0^\delta (w_I - w)dy \quad . \tag{2.22}$$

The displacement thicknesses in the x- and z-directions are then defined as follows

$$\delta^*_{xA} = \frac{1}{u_{Iw}}\int_0^\delta (u_I - u)dy \quad , \tag{2.23}$$

$$\delta^*_{zA} = \frac{1}{w_{Iw}}\int_0^\delta (w_I - w)dy \quad . \tag{2.24}$$

Hence, the transpiration velocity is given as

$$v_{Iw} = \frac{\partial}{\partial x}(u_{Iw}\delta^*_{xA}) + \frac{\partial}{\partial z}(w_{Iw}\delta^*_{zA}) \quad . \tag{2.25}$$

If there is no gradient of the equivalent inviscid velocity across the boundary layer, the standard expressions replace eqs. (2.23), (2.24) and (2.25),

$$\delta_x^* = \int_o^\delta \left(1 - \frac{u}{U_e}\right) dy \quad , \tag{2.26}$$

$$\delta_z^* = \int_o^\delta \left(1 - \frac{w}{W_e}\right) dy \quad , \tag{2.27}$$

$$v_{Iw} = \frac{\partial}{\partial x}\,(U_e \delta_x^*) + \frac{\partial}{\partial z}\,(W_e \delta_z^*) \quad . \tag{2.28}$$

Model B The displacement surface method
In this case $\delta_B^*(x,z)$ is assumed to be an impermeable stream surface, hence the vector (u_I, v_I, w_I) is tangent to the surface $y = \delta_B^*$ (see fig. 2.3).

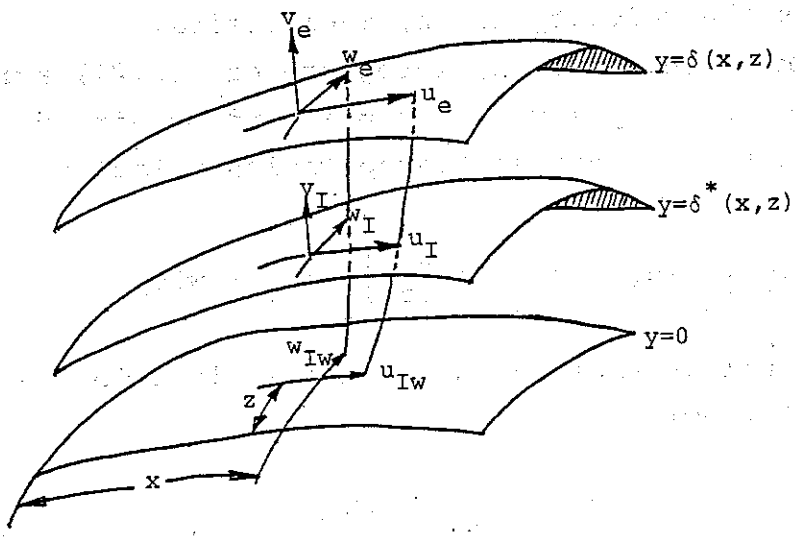

Fig. 2.3 Inviscid velocity field and displacement surfaces.

Thus, at $y = \delta_B^*$ we have

$$v_I(y = \delta_B^*) = u_I \frac{\partial \delta_B^*}{\partial x} + w_I \frac{\partial \delta_B^*}{\partial z} \quad . \tag{2.29}$$

Integrating eq. (2.19), from $y = 0$ to $y = \delta$, yields

$$V_e = - \int_o^\delta \frac{\partial u}{\partial x} dy - \int_o^\delta \frac{\partial w}{\partial z} dy \quad , \tag{2.30}$$

and integration of eq. (2.21) from y to δ gives

$$V_e - v_I = - \int_o^\delta \frac{\partial u_I}{\partial x} dy - \int_y^\delta \frac{\partial w_I}{\partial z} dy \quad . \tag{2.31}$$

Evaluating eq. (2.31) at $y = \delta_B^*$ and taking advantage of eqs. (2.29) and (2.30), we obtain the following expression, at $y = \delta_B^*$

$$u_I \frac{\partial \delta_B^*}{\partial x} + w_I \frac{\partial \delta_B^*}{\partial z} = \int_{\delta_B^*}^\delta \frac{\partial u_I}{\partial x} dy + \int_{\delta_B^*}^\delta \frac{\partial w_I}{\partial z} dy - \int_o^\delta \frac{\partial u}{\partial x} dy - \int_o^\delta \frac{\partial w}{\partial z} dy \quad . \tag{2.32}$$

Using the Leibnitz rule for the differentiation of integrals, eq. (2.32) gives the relation defining the displacement surface $\delta_B^*(x,z)$,

$$\frac{\partial}{\partial x} \left\{ \int_{\delta_B^*}^\delta u_I dy - \int_o^\delta u \, dy \right\} + \frac{\partial}{\partial z} \left\{ \int_{\delta_B^*}^\delta w_I \, dy - \int_o^\delta w \, dy \right\} = 0 \quad . \tag{2.33}$$

If we neglect the gradient of the equivalent inviscid velocity across the boundary layer, that is if we put $u_I = \text{constant} = U_e$ and $w_I = \text{constant} = W_e$, we obtain

$$\frac{\partial}{\partial x} \left\{ (\delta - \delta_B^*) U_e - \int_o^\delta u \, dy \right\} + \frac{\partial}{\partial z} \left\{ (\delta - \delta_B^*) W_e - \int_o^\delta w \, dy \right\} = 0 \quad . \tag{2.34}$$

Inserting the standard expressions for the displacement thicknesses eqs. (2.26) and (2.27), we get the defining equation of the displacement surface according to Moore (1953)

$$\frac{\partial}{\partial x} \left[U_e (\delta_B^* - \delta_x^*) \right] + \frac{\partial}{\partial z} \left[W_e (\delta_B^* - \delta_z^*) \right] = 0 \quad . \tag{2.35}$$

In three dimensions, a simplified approximation for correcting the presence of pressure gradients normal to the surface can be imposed in a way similar to that of the two-dimensional case (recall eq. 2.18),

$$P_w = P_{Iw} - \kappa_s^* \rho U_e^2 (\delta^* + \theta_{11} + \theta_{22}) \quad , \tag{2.36}$$

where κ_s^* is the curvature of the displacement surface. This curvature is measured in a plane which is normal to the body surface and contains the external streamline.

The momentum thicknesses θ_{ii} are defined by

$$\theta_{11} = \int_o^\delta \left(\frac{u}{U_e}\right)\left(1 - \frac{u}{U_e}\right) dy \quad , \tag{2.37}$$

$$\theta_{22} = -\int_o^\delta \left(\frac{w}{U_e}\right)^2 dy \quad . \tag{2.38}$$

Typically, θ_{22} is small compared to θ_{11}, and if streamline coordinates of the external flow are used, eq. (2.36) reduces to the two-dimensional counterpart eq. (2.18).

2.2 Numerical procedures of viscous-inviscid interaction

In order to give the basic concepts of the numerical treatment of viscous-inviscid interaction, we will confine ourselves to two-dimensional flows in the following passage.

2.2.1 Numerical treatment of the boundary layer equations

We assume that the flow is steady and incompressible, and that the equations of the boundary layer form an adequate mathematical model for the viscous region.

The boundary layer equations, in terms of continuity and momentum, are given by

$$\frac{\partial u}{\partial x} + \frac{\partial v}{\partial y} = 0 \quad , \tag{2.39}$$

$$u \frac{\partial u}{\partial x} + v \frac{\partial u}{\partial y} = U_e \frac{dU_e}{dx} + \frac{\partial}{\partial y}(\nu^* \frac{\partial u}{\partial y}) \quad , \tag{2.40}$$

where the pressure gradient has been replaced by the velocity gradient according to the free stream condition

$$-\frac{1}{\rho}\frac{dP}{dx} = U_e \frac{dU_e}{dx} \quad . \tag{2.41}$$

In eq. (2.40) $\nu^* = \nu + \nu^t$, ν being the kinematic viscosity and ν^t the eddy viscosity.

The boundary conditions are given by

$$y = 0 \quad : \quad u = v = 0 \quad , \tag{2.42a}$$

$$y = \delta \quad : \quad u = U_e \quad . \tag{2.42b}$$

Furthermore, the displacement thickness is given by its standard definition

$$\delta^*(x) = \int_o^\delta \left(1 - \frac{u}{U_e}\right) dy \quad . \tag{2.43}$$

If the boundary layer equations are solved in the direct manner, with the pressure gradient of eq. (2.41) prescribed as boundary condition, one finds - when separation is approached - that the calculation stalls, and it becomes impossible to reach a solution. This behaviour is called the Goldstein singularity after S. Goldstein (1948), who investigated the boundary layer equations in the vicinity of the point of separation and found the solution to be singular at separation.

This singularity, however, is not a physical property of the boundary layer but a characteristic property related to the numerical technique chosen. For an actual flow, the physical properties are given by the mutual influence between the boundary layer and the external flow, in which the presence of the boundary layer alters the pressure distribution by an amount that is proportional to the displacement thickness. This fact led Catherall & Mangler (1966) to formulate the inverse method of calculation in which the boundary condition of the pressure gradient is replaced by that of the displacement thickness (eq. 2.43). Later, Klineberg & Steger (1974) showed that the singularity could also be removed by specifying the skin friction as a boundary condition.

An interesting phenomenological investigation of the influence of the relation between the distributions of displacement thickness $\delta^*(x)$, external velocity $U_e(x)$, and wall shear $\tau_w(x)$ on the numerical solution has been given by Drela & Thompkins (1983). They express the distribution of the displacement thickness δ^* and that of the external velocity U_e through the definition of the gradient parameters,

$$\beta_u = \frac{x}{U_e} \frac{dU_e}{dx} \quad , \tag{2.44}$$

$$\beta_{\delta^*} = \frac{x}{\delta^*} \frac{d\delta^*}{dx} \quad . \tag{2.45}$$

By a systematic change of δ^* they made it possible to express β_u and τ_w as function of β_{δ^*} at a specific boundary layer station. Such relations are shown in Fig. 2.4, for the case where the flow just upstream of the station considered corresponds to the Blasius flow of zero pressure gradient.

The figures show that for a positive pressure gradient, that is for $\beta_u < 0$, there exist two values of β_{δ^*} that are solutions to the problem. These two solutions collapse into a saddle point at separation.

Furthermore, β_u exhibits a minimum at separation. This implies that, if a direct problem were being solved and if the specified U_e were less than the one given by the minimum, no solution would exist. Despite the doubleness for $\beta_u < 0$ it is still possible to reach solutions by using the direct procedure. This is due to the fact that a typical solution procedure proceeds in a way that the initial guesses for δ^* and the velocity profiles are estimated from the values at the previous station. Thus, the procedure usually converges toward the physically correct solution because it is the one closest to the initial guess. As expected, however, this is not the case for a flow situation where the known upstream velocity profile is close to separation as sketched in fig. 2.5.

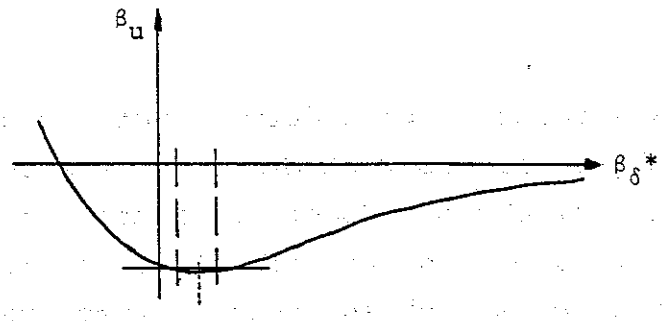

Fig. 2.4a β_u-β_δ* relation far from separation.

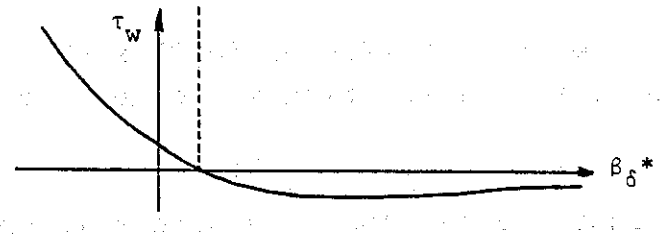

Fig. 2.4b τ_w-β_δ* relation far from separation.

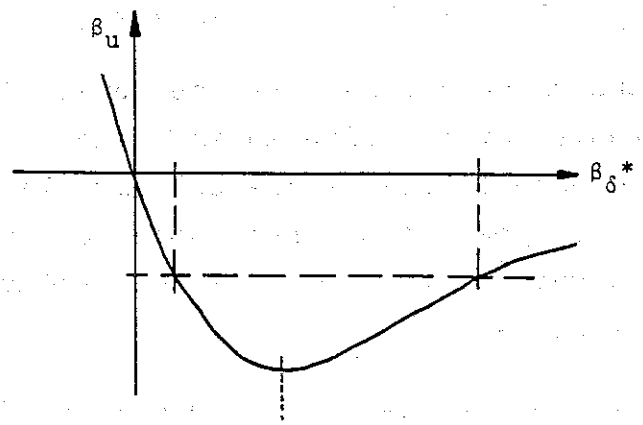

Fig. 2.5a β_u-β_δ* relation near separation.

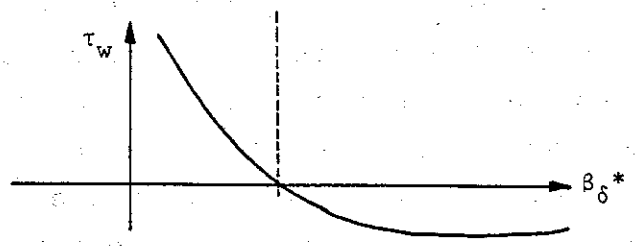

Fig. 2.5b τ_w-β_δ* relation near separation.

Here, the iterative solution procedure cannot decide which solution is the physically correct one since the two possible values of δ^* are quite close together. Hence, it is impossible to reach a solution, and the iterative scheme of the direct solution will move back and forth between the two possible solutions without achieving convergency.

If the inverse problem were solved by specifying δ^* or τ_w, it is readily seen that the solution would be unique in all cases.

In general, the figures show, that the direct method is best suited for the calculation of a boundary layer far from separation, whereas the inverse method is best suited for the calculation of a separated boundary layer. This is explained by the fact, that β_{δ^*} is quite insensitive to changes of β_u for the values of β_u greater than zero, and that β_u is nearly independent of β_{δ^*} for flows where $\tau_w \leq 0$.

When continuing the calculations past the separation point one encounters the problem of marching against the streamwise velocity. This problem occurs because the boundary layer equations are of the parabolic type, hence their solution in regions of reversed flow requires information from downstream if stability problems are to be prevented.

This problem was solved by Reyhner & Flügge-Lotz (1968) by introducing an approximation which allows the use of forward-marching schemes in regions with negative wall shear. This approximation, usually termed FLARE, is made by neglecting or altering the streamwise convective term in the boundary layer equations. In practise, this is accomplished by replacing the convective term in eq. (2.40), $u\,\partial u/\partial x$, by the term $C|u|\partial u/\partial x$, where $C = 1$ for $u > 0$ and C = a small positive constant, or zero, for $u \leq 0$.

A discussion of the accuracy in using the FLARE approximation is given by Pletcher (1978), who concluded, that for the test-case of Simpson (1974) the solutions were within plotting

accuracy when using the values $C = 0.0$, 0.2 or 0.4 . Furthermore, Carter & Wornom (1975) have pointed out that the use of FLARE gives quite a good accuracy for reversed flow velocities less than $0.10\ U_e$.

It is possible to obtain a higher accuracy by using an upstream-downstream iteration in the reversed flow region. Such an iteration, called the DUIT procedure, has been developed by Williams (1975). An investigation carried out by Cebeci, Keller & Williams (1979) showed that convergence could be obtained in three to four upstream-downstream sweeps by using the DUIT procedure.

2.2.2 Numerical treatment of the interaction

The simplest way to perform a viscous-inviscid interaction is to use the effect of the displacement thickness iteratively, as a correction to the inviscid flow solution. Specifically, the iterative cyclus may consist of the following steps.

The solution of the inviscid part gives a velocity distribution U_{Ie} , which is used directly as an outer boundary condition for the viscous boundary layer calculation. The calculation of the viscous region is thus carried out in the direct manner, yielding an updated distribution of displacement thickness $\delta^{*(n)}$. This distribution is then used to recalculate the inviscid velocity distribution $U_{Ie}^{(n+1)}$, taking $\delta^{*(n)}$ as the displacement surface, or using eq. (2.7) to predict the equivalent transpiration velocity. The iteration is continued until a certain convergency criterium is satisfied. This iterative procedure, which usually is referred to as the direct method of viscous-inviscid interaction, will only converge if δ^* is small, and if the flow considered is unseparated.

A natural way to extend the foregoing method to handle separated flows is to solve both the inviscid flow and the boundary layer inversely, as shown by Carter & Wornom (1975). This is referred to as the inverse method of viscous-inviscid interaction.

Introducing a formal (quasi) operator notation (See Veldman, 1980), a compact formulation of the direct and the inverse iteration is given in figs. 2.6 and 2.7, respectively.

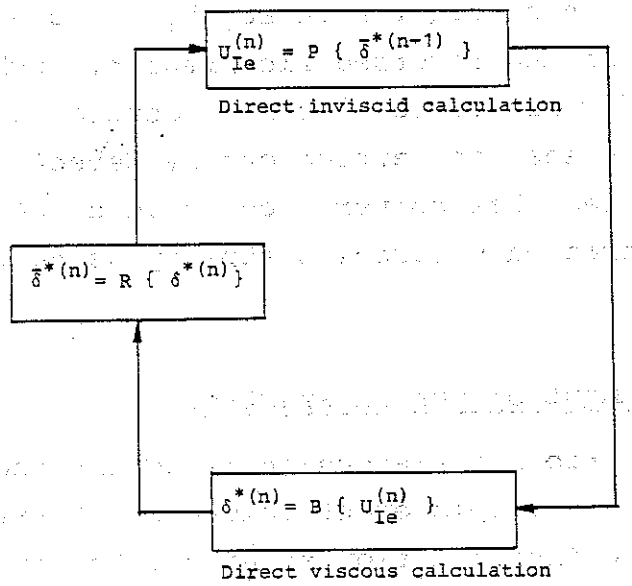

Fig. 2.6 Direct interaction.

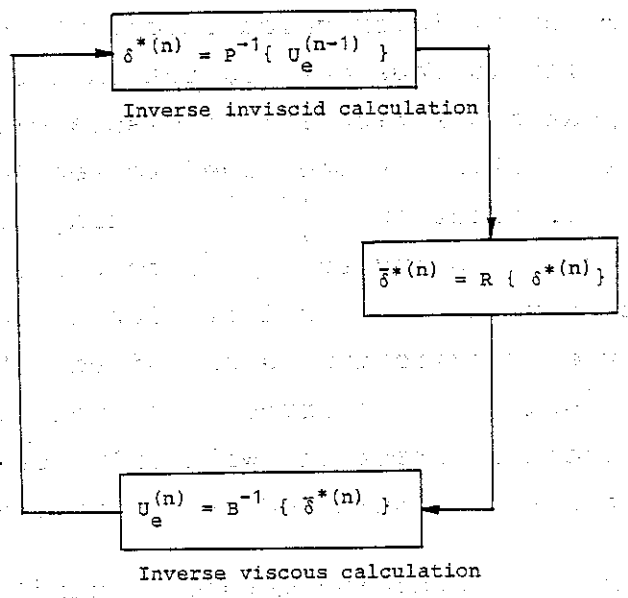

Fig. 2.7 Inverse interaction.

Here, the operator P denotes a direct potential flow calculation, B denotes a direct boundary layer calculation, and R is a relaxation operator. Superscript 'n' denotes the iteration count, and P^{-1} and B^{-1} formally denote the inverse of P and B, respectively.

For both the direct and the inverse interaction, it is necessary to use under-relaxation which has the drawback of requiring a large number of iterations to achieve convergence. To overcome this shortcoming Carter (1979) developed the socalled semi-inverse interaction. This interaction is based on the use of a relaxation scheme in which δ^* is determined on the basis of knowledge of the variation of U_e. Carter noted that a local increase in U_e caused a decrease in δ^*, and that a local decrease in U_e caused an increase in δ^*, hence small perturbations in the global variables U_e and δ^* tend to preserve the volume flow-rate in the boundary layer, i.e. $U_e\delta^* \cong$ constant (See Kwon & Pletcher 1979).

The semi-inverse interaction is performed such that the external flow is calculated in the direct manner and the boundary layer is calculated in the inverse manner. The resulting free stream velocities, U_{Ie} and U_e, are then used to update the displacement thickness according to the following relaxation scheme

$$\delta^{*(n)} = \delta^{*(n-1)} \left\{1 + \omega\left[\frac{U_e^{(n)}}{U_{Ie}^{(n)}} - 1\right]\right\} \quad , \qquad (2.46)$$

where ω is a relaxation parameter, $\omega \in [0,2]$. The updated δ^* is then used as boundary condition for the calculation of both the external flow and the boundary layer. The procedure for the semi-inverse interaction is shown in fig. 2.8.

In order to prevent numerical instabilities the value of ω must be chosen carefully, and in general it depends heavily upon the properties of the flow. For the solution of a flow in which a laminar separation bubble is induced by a trough on

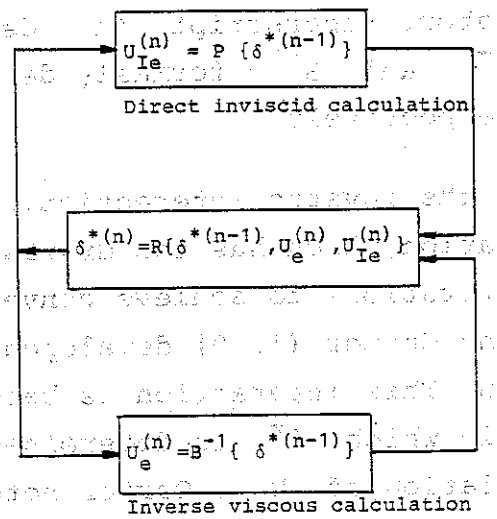

Fig. 2.8 Semi-inverse interaction.

a flat surface, Kwon & Pletcher (1979) employed over-relaxation with ω varying over the range from 1.2 to 1.8 . For flows about an airfoil with trailing edge separation, it becomes necessary to use under-relaxation, see Sørensen (1986).

A modification of eq. (2.46) has been given by Lee & Pletcher (1985), who employed an updating formula of the following form

$$\delta^{*(n)} = \delta^{*(n-1)} \left\{1 + \omega\left[\left(\frac{U_e^{(n)}}{U_{Ie}^{(n)}}\right)^b - 1\right]\right\} \quad , \qquad (2.47)$$

where use of the exponent b $(b > 1)$ gives greater weight to the local discrepancy between U_e and U_{Ie} , with the result that convergence is accelerated, whilst stability is still maintained.

To overcome the problem of selecting a proper value of ω , Le Balleur (1978) developed a self correcting relaxation scheme based on a linearized analysis of the viscous-inviscid

interaction process. In this analysis, the governing equations are linearized and decomposed into their Fourier components, and the growth or decay of wavelengths of the order of a streamwise step length determines the optimum value of the relaxation parameter.

It is characteristic of all of the methods mentioned above (i.e. the direct, the inverse, and the semi-inverse methods) that edge velocities and displacement thicknesses are successively updated after the completion of a boundary layer sweep. Hence, the methods allow only a weak, delayed interaction.

From triple-deck theory (Stewartson 1979), it is well-known that there is no definite hierarchy between the viscous region and the inviscid region, hence the coupling between the two regions has a more simultaneous character. This is particularly true for separated flows where it is the local, mutual coupling between U_e and δ^* which determines the flow properties.

As a consequence of this, Veldman (1979) formulated the socalled quasi-simultaneous interaction method. In this method, a linear combination of the edge velocity and the displacement thickness is prescribed as a boundary condition for the boundary layer flow calculation. This relation is established by way of the equations for the equivalent inviscid flow subject to a transpiration velocity as boundary condition. Veldman employs the following relation

$$U_e(x) = U_{Ie}^{(o)}(x) + \frac{1}{\pi}\int_{X_A}^{X_B} \frac{\frac{d(U_e\delta^*)}{dx}}{x-\zeta}\, d\zeta \quad , \qquad (2.48)$$

where the Hilbert integral is an approximate expression (from thin-airfoil theory) which gives the influence of the displacement thickness on the potential flow solution. $U_{Ie}^{(o)}(x)$ is the edge velocity from a first order potential flow solution, and the interval $[X_A, X_B]$ denotes the region in which the interaction is assumed to be important. The expression $d(U_e\delta^*)/dx$ is readily recognized as the normal transpiration velocity v_w (recall eq. 2.17).

Discretization of eq. (2.48) yields an equation of the following form

$$U_{e_i} = U_{Ie_i}^{(o)} + \sum_{j=1}^{N} \alpha_{ij} U_{e_j} \delta_j^* \quad , \qquad (2.49)$$

where α_{ij} is an influence coefficient depending only of the discretization of eq. (2.48). Subscript 'i' denotes the boundary layer station considered, and $j = 1, 2, \ldots, N$ refers to stations which are presumed to have an influence on the properties of station 'i'.

Because of the elliptic nature of eq. (2.49) several sweeps have to be performed before convergence is achieved. As a consequence of this, eq. (2.49) is solved in a Gauss-Seidel manner, such that variables upstream of station 'i' are updated, while the old (not-updated) values are retained downstream from this station. Thus, in the n-th sweep eq. (2.49) can be rearranged as

$$U_{e_i}(1 - \alpha_{ii} \delta_i^*) = r_i \quad , \qquad (2.50)$$

where

$$r_i = U_{Ie_i}^{(o)} + \sum_{j=1}^{i-1} \alpha_{ij} U_{e_j}^{(n)} \delta_j^{*(n)} + \sum_{j=i+1}^{N} \alpha_{ij} U_{e_j}^{(n-1)} \delta_j^{*(n-1)} \quad . \qquad (2.51)$$

To perform a quasi-simultaneous boundary layer calculation eq. (2.50) is employed as a boundary condition in addition to those given by eqs. (2.42) and (2.43). Denoting the interaction law of eq. (2.50) by the symbol I the method of quasi-simultaneous interaction proceeds as shown in fig. 2.9. Here the index 'k' denotes the iteration count for the boundary layer solution.

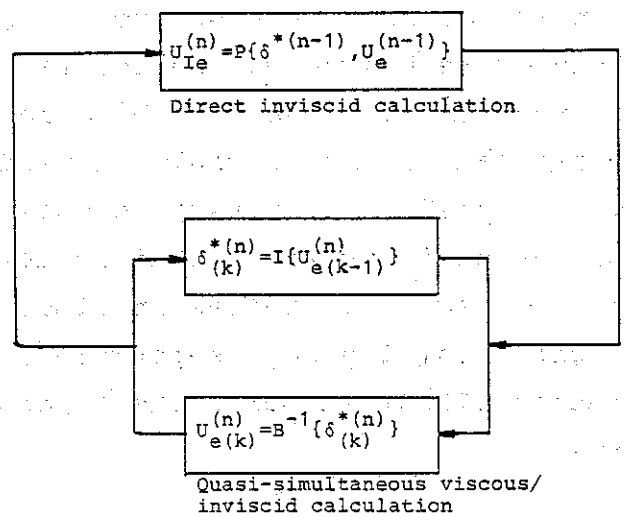

Fig. 2.9 Quasi-simultaneous interaction.

In order to increase the rate of convergence of the viscous/inviscid cycles, Cebeci, Clark, Chang, Halsey & Lee (1985) combined the quasi-simultaneous procedure with an over-relaxation scheme similar to the one proposed by Carter (eq. 2.46). But instead of updating by way of the displacement thickness, they updated via the transpiration velocity, according to the formula

$$v_{Iw}^{(n)} = v_{Iw}^{(n-1)}\left\{1 + \omega\left[\frac{U_e^{(n)}}{U_{Ie}^{(n-1)}} - 1\right]\right\} \quad , \qquad (2.52)$$

where $v_{Iw}^{(n-1)}$ is the transpiration velocity computed from the current displacement thickness, and $v_{Iw}^{(n)}$ is the updated distribution which is used to compute the new inviscid velocity.

A comparison of the efficiencies of the semi-inverse method and the quasi-simultaneous method for a separated diffuser flow have been made by Edwards & Carter (1985). Two main conclusions

resulted from this comparison. First, as the separated region increased in size the quasi-simultaneous procedure converged at a faster rate than the semi-inverse procedure. Secondly, the quasi-simultaneous technique was easier to use (when first implemented) than the semi-inverse one, because it was found that the same relaxation parameter could be used independently of the flow being analysed. In contrast to this, the relaxation parameter of the semi-inverse technique must be decreased as the separated flow region increases in size. For the flow about an airfoil with trailing edge separation, an investigation made by Sørensen (1986) supports the foregoing conclusions of Edwards & Carter.

3. THREE-LEVEL, VISCOUS-INVISCID INTERACTION MODELLING OF THE FLOW FIELD ABOUT A ROTATING BLADE

In order to describe the complex three-dimensional flow field about a rotor, a model based on a viscous-inviscid zonal approach has been developed. This model, which will be presented in the following, describes the flow field in three levels of complexity, comprising the viscous near-field (the boundary layer), the inviscid near-field (the potential flow), and the inviscid far-field (the shedded vortices).

The viscous near-field is determined by solving the three-dimensional boundary layer equations. These are formulated quite general in a rotating non-orthogonal coordinate system, hence making the solution appropriate to arbitrary-shaped blades. In order to improve the solution procedure of the equations, a transformation, in which the normal coordinate is non-dimensionalised by the displacement thickness, is employed. This is an alternative to the traditional Falkner-Skan formulation, which is found not to work satisfactorily for turbulent boundary layer flows developing under strong pressure gradients (see Sørensen, 1986). The transformed equations are discretized by using the Keller-box scheme when the flow is attached, and the zig-zag scheme when the flow is separated. Initial conditions are established by employing the infinite-swept-wing assumption and the stagnation line equations. The discretized, non-linear equations are linearized by using the Newton method, and the resulting linearized equations are solved by a block elimination method (see Bradshaw, Cebeci & Whitelaw, 1981).

The inviscid near-field denotes the potential flow field external to the boundary layer. This is calculated using a strip-theory in which the inviscid spanwise velocity component at a given cross-section is treated as being independent of the flow at the remaining cross-sections. Thus, the inviscid near-field is described by a set of two-dimensional potential flow equations. The solution of these equations is carried out by use of the panel-method of Hess (1971). By employing this

method, the blade surface is replaced by a number of singularities (sources and vortices) which are used to satisfy the Neumann conditions at the blade surface. The solution is accomplished by superposition of the disturbed, singularity induced flow, and the undisturbed onset flow.

The solution of the inviscid flow provides the boundary conditions for the solution of the boundary layer equations. The retarded viscous flow in turn affects the boundary conditions for the inviscid equations, thus the two sets of equations must be matched iteratively. This matching is performed by use of a three-dimensional viscous-inviscid interaction procedure, where the two sets of boundary conditions are coupled together by a normal transpiration velocity.

The inviscid far-field, which denotes the shedded vortices in the wake, is predicted by incorporating a multiple-streamtube model into the equations, according to the propeller theory of Glauert (1963). Using this model, the influence of the wake on the inviscid flow field is determined as a induced velocity, locally altering the onset flow.

The influence of the wake depends on the forces acting on the rotor, which in turn is a function of the onset flow altered by the induced velocities. As a consequence, the overall solution is carried out iteratively between the aforementioned three levels.

3.1 The coordinate systems and their transforms

The geometry of the blade is defined in a Cartesian coordinate system $(\bar{x},\bar{y},\bar{z})$ which rotates with angular velocity Ω about its $\bar{y}$-axis, as shown in fig. 3.1. The $\bar{z}$-axis is measured outward in the spanwise direction from the center of rotation. In order to retain standard two-dimensional airfoil terminology, the $\bar{x}$-axis defines a left-handed coordinate system.

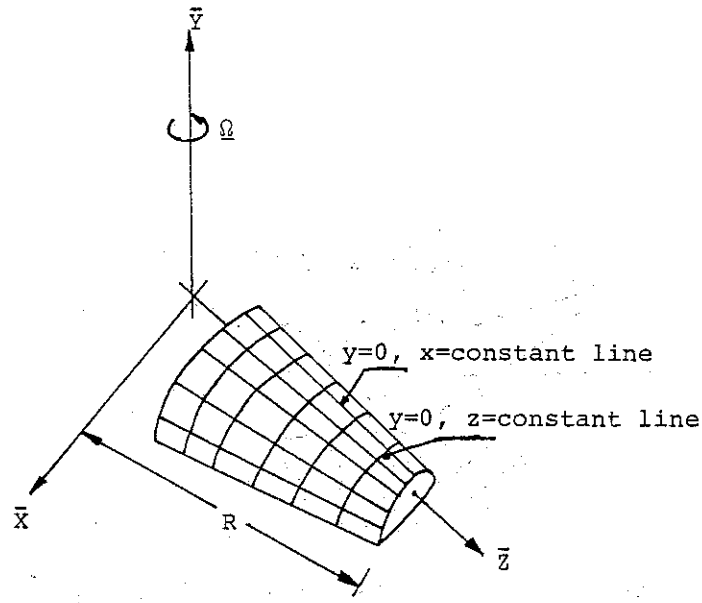

Fig 3.1 The rotating coordinate system

On the surface of the blade is embedded a body-fitted coordinate system (x,y,z) which defines the net on which the boundary layer equations are to be solved. As shown in fig. 3.1 and fig. 3.2, the spanwise cross-sections are given by curves of z = constant, and y is measured in the direction of the surface normal. As independent z-variable we employ the Cartesian $\bar{z}$-coordinate, non-dimensionalised by the length of the blade R ; $z = \bar{z}/R$.

The transformation between the Cartesian system and the body-fitted system has to be bijective in order to prevent ambiguity. For example, if we use chordwise locations to define the x-coordinates, we see that a given chordwise location defines two points; one on the upper surface and one on the lower surface. Therefore, this definition causes the transformation to be ambiguous. It is also impossible to define the x-coordinates by way of the surface arc lengths , since cross-sections are not necessarily similar.

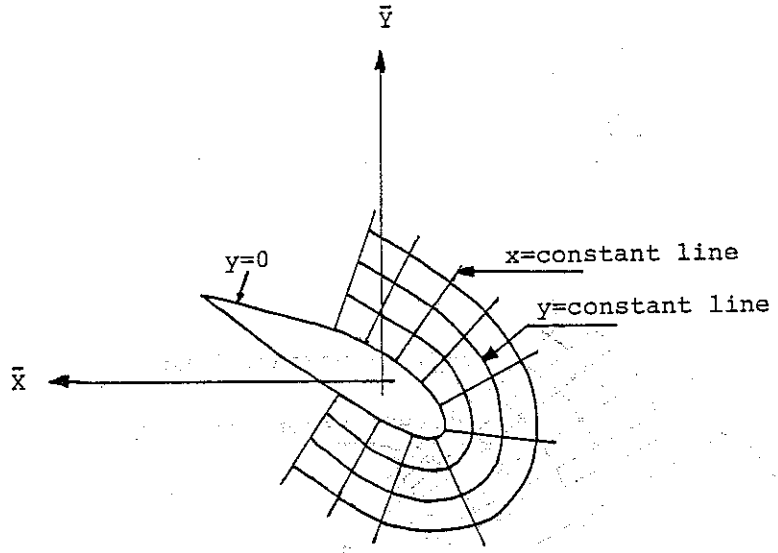

Fig 3.2 Cross-sectional view of the blade and and coordinates

To circumvent these problems, we inscribe the cross-sections in half circles and let the x-coordinate be defined by the angle ϕ, as shown in fig. 3.3 (see Cebeci, Kaups & Ramsey, 1977). The point P defining a surface coordinate is then defined by projecting a point S on the half circle into the surface contour in the direction parallel to $\hat{y}$. Coordinate axes $(\hat{x},\hat{y})$ defines a local coordinate system with $\hat{x}$ lying along the chord and $\hat{y}$ measured penpendicular on this, having the origin at the airfoil leading edge.

Denoting the local chord length by c, the transformation is

$$\frac{\hat{x}}{c} = 1 - \cos\phi \quad . \tag{3.1}$$

Here, negative values of ϕ define coordinates on the lower surface, whereas positive values of ϕ refer to those on the upper surface. Specifically, $\phi = 0$ corresponds to the leading edge, and $\phi = -\pi/2$ and $\phi = \pi/2$ correspond to the trailing edge at lower and upper surface, respectively.

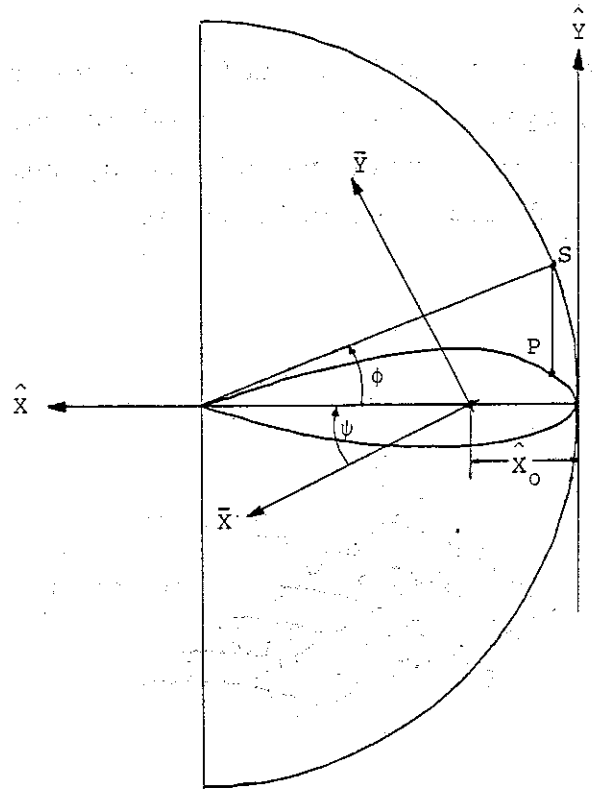

Fig. 3.3 Definition of surface coordinates

In general, the blade is twisted and has a pitch angle different from zero. Therefore, the Cartesian reference system $(\bar{x},\bar{y})$ and the local coordinate system $(\hat{x},\hat{y})$ differ in orientation by an angle denoted ψ. At a specific cross-section, denoting the chordwise distance from the leading adge to the $\bar{z}$-axis of the Cartesian system by $\hat{x}_o$, we obtain the following transformation between the Cartesian coordinate system and the local cross-sectional coordinate system,

$$\left(\frac{\bar{x}}{c}\right) = \left(\frac{\hat{x}-\hat{x}_o}{c}\right)\cos\psi - \left(\frac{\hat{y}}{c}\right)\sin\psi \qquad (3.2)$$

$$\left(\frac{\hat{y}}{c}\right) = \left(\frac{\hat{x}-\hat{x}_o}{c}\right)\sin\psi + \left(\frac{\hat{y}}{c}\right)\cos\psi \qquad (3.3)$$

The independent variables z and ϕ define a nonorthogonal curvilinear coordinate system which is fitted to the blade surface. The relation between this coordinate system and the Cartesian one is given through the definition $z = \bar{z}/R$ and eqs.(3.1)-(3.3).

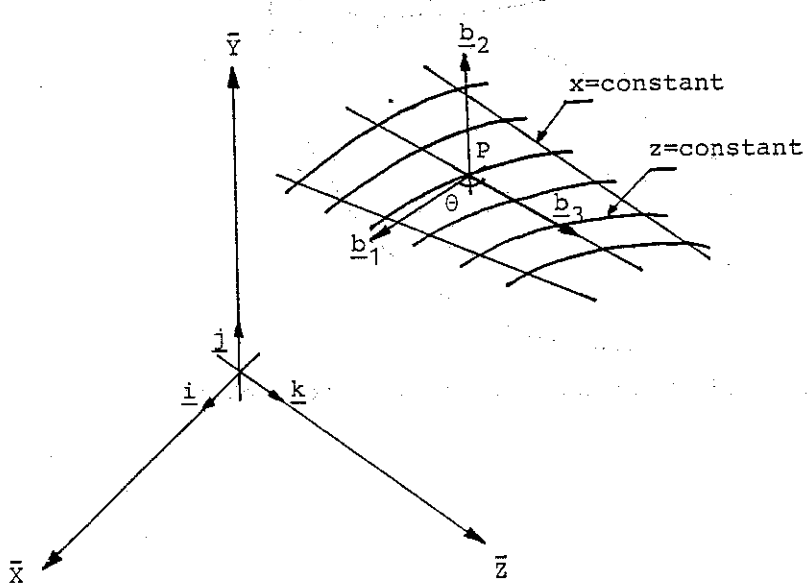

Fig 3.4 Basis vectors of coordinate systems

At a point P on the blade surface, the coordinate curves of the surface-fitted system define a non-orthogonal base with unit base vectors $(\underline{b}_1, \underline{b}_2, \underline{b}_3)$, as shown in fig. 3.4. The unit tangent vector $\underline{b}_1$ along z = constant is given by

$$\underline{b}_1 = \frac{1}{h_1} \frac{\partial \bar{x}}{\partial \phi} \underline{i} + \frac{1}{h_1} \frac{\partial \bar{y}}{\partial \phi} \underline{j} \quad , \tag{3.4}$$

where h_1 is a metric coefficient defined by

$$h_1 = \left(\frac{\partial \bar{x}}{\partial \phi}\right)^2 + \left(\frac{\partial \bar{y}}{\partial \phi}\right)^2 \tag{3.5}$$

The unit tangent vector $\underline{b}_3$ along ϕ = constant is given by

$$\underline{b}_3 = \frac{1}{h_3}\frac{\partial \bar{x}}{\partial z}\,\underline{i} + \frac{1}{h_3}\frac{\partial \bar{y}}{\partial z}\,\underline{j} + \frac{1}{h_3}\,R\,\underline{k} \quad , \tag{3.6}$$

with the corresponding metric coefficient

$$h_3 = \left(\frac{\partial \bar{x}}{\partial z}\right)^2 + \left(\frac{\partial \bar{y}}{\partial z}\right)^2 + R^2 \quad . \tag{3.7}$$

As the y-coordinate is measured in the direction of the normal to the surface, the unit tangent vector $\underline{b}_2$ is established by the vector product

$$-\sin\theta\,\underline{b}_2 = \underline{b}_1 \times \underline{b}_3 \quad , \tag{3.8}$$

where θ denotes the local angle between $\underline{b}_1$ and $\underline{b}_3$. Note that the minus-sign appears because the coordinate system is defined as left-handed. Thus eq.(3.8) yields

$$\underline{b}_2 = \frac{1}{h_1 h_3 \sin\theta}\left[-R\frac{\partial \bar{y}}{\partial \phi}\,\underline{i} + R\frac{\partial \bar{x}}{\partial \phi}\,\underline{j} - \left(\frac{\partial \bar{x}}{\partial \phi}\frac{\partial \bar{y}}{\partial z} - \frac{\partial \bar{x}}{\partial z}\frac{\partial \bar{y}}{\partial \phi}\right)\underline{k}\right]. \tag{3.9}$$

The angle θ is given by the dot product

$$\cos\theta = \underline{b}_1 \cdot \underline{b}_3 \quad , \tag{3.10}$$

thus yielding

$$\cos\theta = \left(\frac{\partial \bar{x}}{\partial \phi}\frac{\partial \bar{x}}{\partial z} + \frac{\partial \bar{y}}{\partial \phi}\frac{\partial \bar{y}}{\partial z}\right)/h_1 h_3 \quad . \tag{3.11}$$

Altogether, eqs.(3.4)-(3.11) define the transformation between the Cartesian coordinate system $(\underline{i},\underline{j},\underline{k})$ and the curvilinear coordinate system $(\underline{b}_1,\underline{b}_2,\underline{b}_3)$.

For convenience, the boundary layer coordinate ϕ is replaced by x, $x \equiv \phi$, in the following.

3.2 The inviscid far-field: The shedded vortices

For a rotor exposed to a stream of air, the bound vorticity on the blades and the trailing vortices behind the rotor induce velocities that alters the velocity field about the rotor. Hence, the inflow conditions, defining the local onset flow on the blades, are also altered and have to be determined when calculating the near-field properties of the flow.

A general discussion of performance prediction methods of various kinds of rotors has been given by Glauert (1963), who investigated the aerodynamics of both airplane propellers, helicopter rotors and horizontal axis wind turbines. Although the aerodynamics of these rotating devices may seem similar, the induced velocities of airplane propellers and helicopter rotors are small compared to the speed of flight, whereas the induced velocities of wind turbines in most cases are appreciable in comparison to the undisturbed velocity field. A review of fluid dynamic aspects of various kinds of wind energy conversion systems has been carried out by de Vries (1979) and a description, with particular emphasis on practical performance calculations of wind turbines, has been given by Wilson & Lissaman (1974).

In the following, one of the most popular methods of performance predictions, the so-called blade-element - or multiple streamtube method, will be presented. Using this model, the induced velocities are predicted by assuming that the flow through the rotor occurs in non-interacting streamtubes.

3.2.1 The idealized rotor: Axial momentum theory

Replacing the rotor by an actuator disc, the flow is assumed to be entirely axial with no rotational motion (an actuator disc can be thought of as an idealized rotor constructed by by two counter rotating rotors, each consisting of infinite many frictionless blades). Far upstream of the disc, we denote the velocity of the wind field as V_o and the atmospheric pressure as p_o. The presence of the disc causes the incoming

air gradually to slow down, with an increase in the static pressure as a result. When passing through the disc, energy of the air is absorbed causing a drop in the static pressure from, say, p_D^+ in front of the disc to $p_D^\div$ behind the disc (see fig. 3.5). The axial velocity of the air decreases continously from V_o far upstream of the disc to V_D at the plane of the disc. Downstream of the disc, the velocity decreases further until it stabilizes at a value of V_∞, whereas the pressure climbs back to the atmospheric value p_o.

The streamtube containing the disc has a cross-sectional area, A_D, which is larger than the area far upstream of the disc, A_o, and smaller than A_∞, the area far downstream of the disc. According to the law of conservation of mass, we get

$$A_o V_o = A_D V_D = A_\infty V_\infty \quad . \tag{3.12}$$

Applying the Bernoulli equation separately to the upstream and downstream sections of the streamtube yields

$$p_o + \frac{1}{2}\rho V_o^2 = p_D^+ + \frac{1}{2}\rho V_D^2 \quad . \tag{3.13}$$

$$p_D^\div + \frac{1}{2}\rho V_D^2 = p_o + \frac{1}{2}\rho V_\infty^2 \quad , \tag{3.14}$$

where ρ denotes the density of the air.

Combining these equations, the pressure drop $\Delta p = p_D^+ - p_D^\div$ can be expressed as

$$\Delta p = \frac{1}{2}\rho (V_o^2 - V_\infty^2) \quad . \tag{3.15}$$

In terms of change of momentum the pressure drop is obtained as

$$\Delta p = \rho V_D (V_o - V_\infty) \quad , \tag{3.16}$$

hence, the velocity at the disc is given by

$$V_D = \frac{1}{2}(V_o + V_\infty) \quad , \tag{3.17}$$

which is the average of the initial and final velocities.

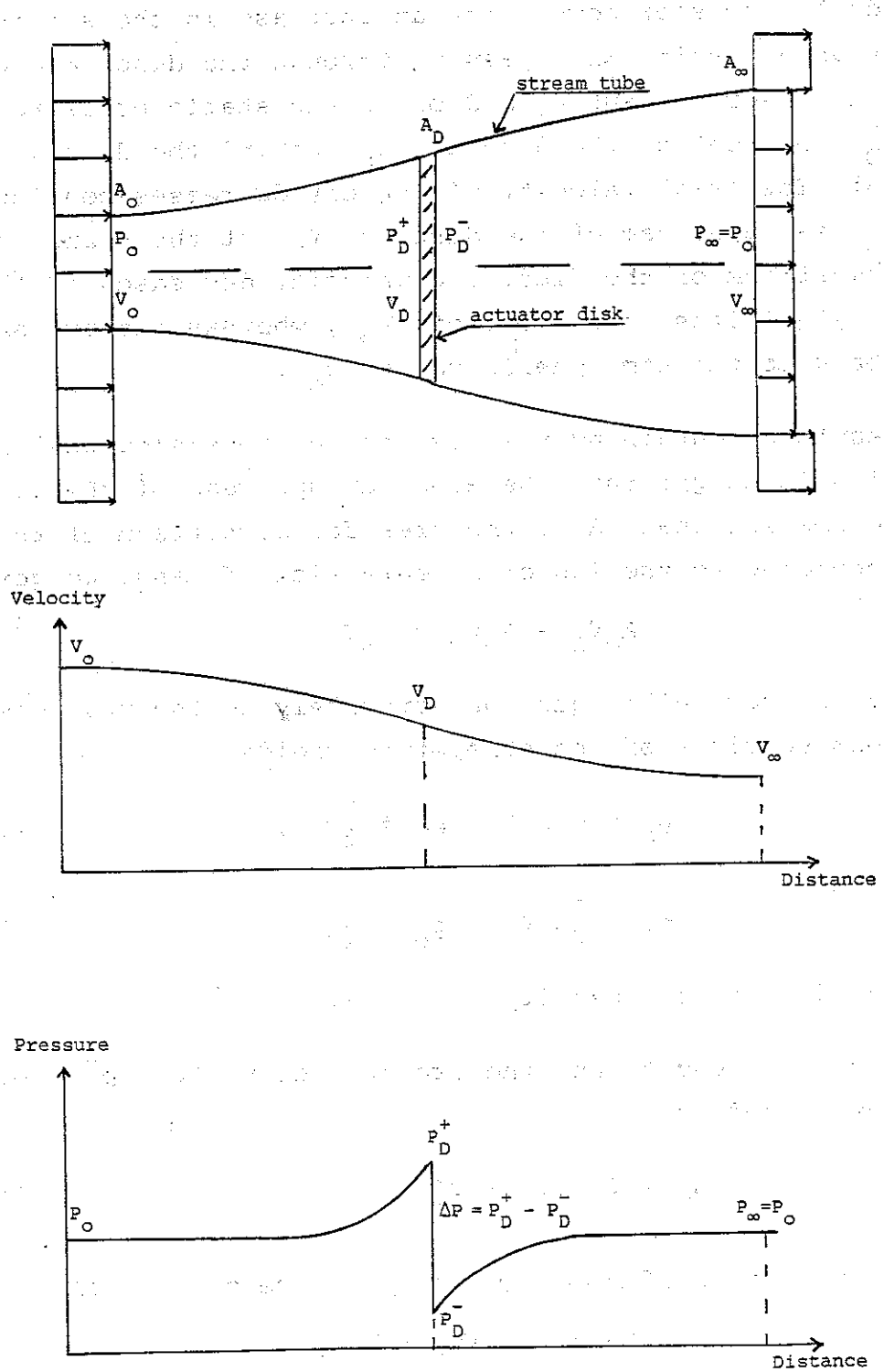

Fig. 3.5 One-dimensionel flow past wind turbine.

It is convenient to introduce the axial flow induction factor, a, by

$$V_D = (1 - a)V_o \quad , \tag{3.18}$$

where $a V_o$ is the induced velocity at the disc.

Combining eq.(3.17) and eq.(3.18), we obtain

$$V_\infty = (1 - 2a)V_o \quad . \tag{3.19}$$

The axial pressure force, i.e. the thrust acting on the disc, is obtained as

$$T = \Delta p A_D \quad , \tag{3.20}$$

and, from the first law of thermodynamics, the power extraction from the air is given by

$$P = \frac{1}{2} \rho V_D (V_o^2 - V_\infty^2) A_D \quad . \tag{3.21}$$

Combining eq.(3.20) with eq.(3.16) and eq.(3.19), and eq.(3.21) with eq.(3.19), we obtain

$$T = 2 \rho a (1 - a) V_o^2 A_D \quad , \tag{3.22}$$

$$P = 2 \rho a (1 - a)^2 V_o^3 A_D \quad . \tag{3.23}$$

Defining the thrust coefficient C_T and the power coefficient C_P as

$$C_T = \frac{T}{\frac{1}{2} \rho V_o^2 A_D} \quad , \tag{3.24}$$

and

$$C_P = \frac{P}{\frac{1}{2} \rho V_o^3 A_D} \quad , \tag{3.25}$$

in terms of the axial induction factor, a, we obtain

$$C_T = 4 a (1 - a) \quad , \tag{3.26}$$

and

$$C_P = 4 a (1 - a)^2 \quad . \tag{3.27}$$

Note, that in the absence of the actuator disc, the denominator of eq.(3.25) represents the available power in the air.

Evaluating eq.(3.27), it is recognized that C_P exhibits a maximum, $C_P = 16/27$, at $a = 1/3$. Hence, the maximum power that can be extracted from the wind by an idealized rotor is given by

$$C_{P_{max}} = 16/27 \quad . \tag{3.28}$$

This is usually referred to as the Betz limit.

For $a < 0$, eq.(3.27) shows that energy is added to the wake flow, hence the rotor acts like a propeller. For $a > 0$, energy is extracted from the flow, and the rotor works in its wind turbine state. For $a > \frac{1}{2}$, the velocity of the wake flow V_∞ becomes negative. In this state, the one-dimensional momentum theory is no longer valid, and empirical modifications have to be made.

3.2.2 The tangential flow induction factor

The idealized rotor does not cause any rotation of the wind field. A real rotor, however, imposes a rotating slipstream on the wake. Hence the streamlines of the wake follow a helical path resulting from the superposition of translational and rotational velocities.

As the flow is assumed to be frictionless, the tangential velocity in front of the rotor is zero, and the transfer of rotational motion takes place entirely across the thickness of the rotor. In the plane of rotation, the induced tangential velocity is assumed to have a value of $\Omega \bar{z} a'$, where a' denotes the tangential flow induction factor. Assuming $\Omega \bar{z} a'$ to be the average of the tangential velocity in front of the rotor and the tangential velocity immediately behind the rotor, the tangential velocity of the wake immediately behind the rotor is given as

$$V_t = 2 \Omega \bar{z} a' \quad . \tag{3.29}$$

If there is no expansion of the slipstream, V_t remains constant throughout the wake.

3.2.3 Blade-element theory

To model the aerodynamics of a real rotor having a finite number of blades, it is assumed that the flow through the rotor occurs in annular streamtubes, which do not influence each other.

Combining this assumption with the knowledge about the local two-dimensional airfoil characteristics, the induced velocities can be determined by pure momentum considerations. Usually, this is accomplished by letting the axial force on the blades be set equal to the rate of change of axial momentum and the torque on the blades to be put equal to the rate of change of angular momentum of the flow. The axial force and the torque on the blades depend on both the lift force and the drag force. The induced velocities, however, are only produced by the lift forces, whereas the loss of momentum produced by the drag is due to shear stresses in the boundary layer, see for example de Vries (1979). Therefore, these assumptions bring up inconsistencies in the formulation. An alternative formulation, which circumvents these inconsistencies, is to put the total rate of change of momentum (axial and tangential) equal to the corresponding blade force (which is in fact the lift force). This formulation was originally given by Øye (1983).

In fig. 3.6 is shown a cross-sectional element of a blade at blade radius $\bar{z}$. Denoting the angle between the resulting relative velocity, U_∞, and the rotor plane as ψ, and the local pitch angle as γ, the angle of attack is given by

$$\alpha = \psi - \gamma \quad . \tag{3.30}$$

Denoting the resulting induced velocity as $\underline{w}_i$, from the figure it is seen that

$$U_\infty = (V_o^2 + \Omega^2 \bar{z}^2 - w_i^2)^{\frac{1}{2}} \quad . \tag{3.31}$$

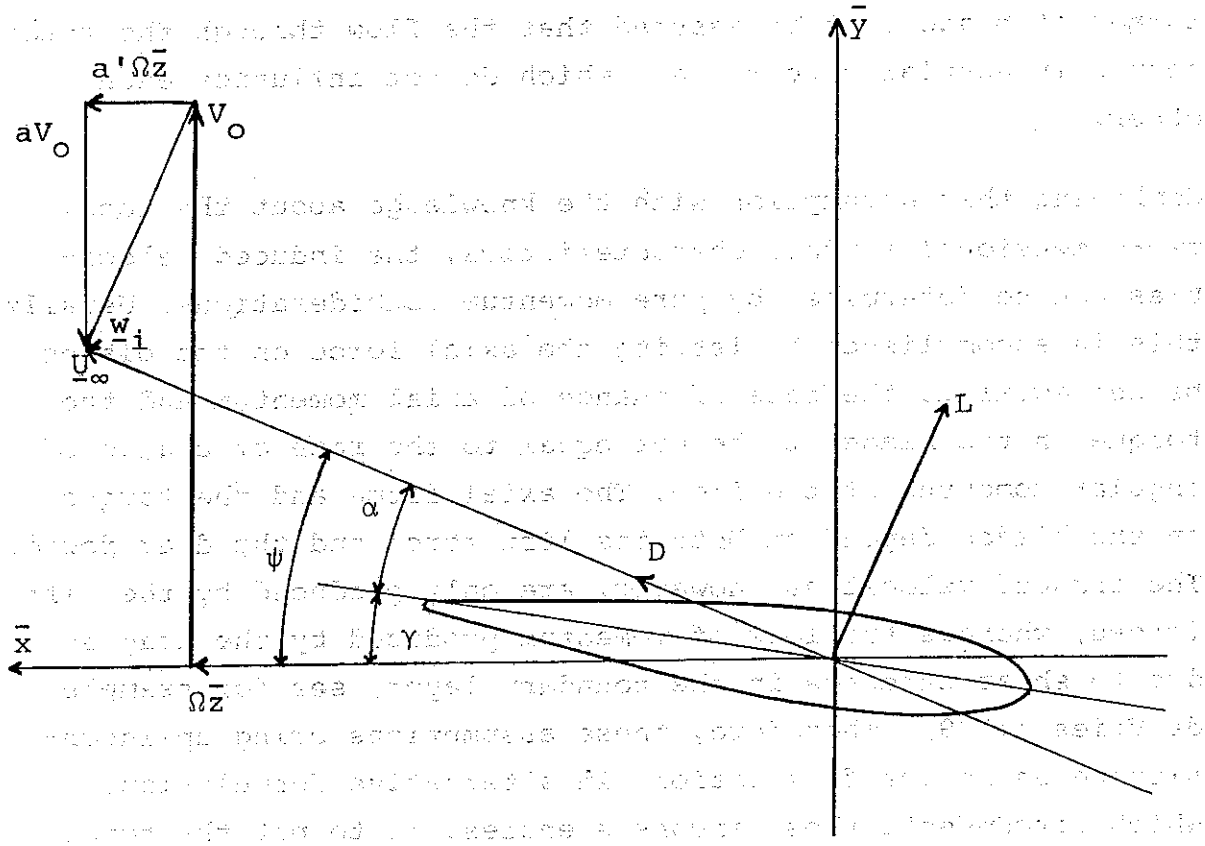

Fig. 3.6 Velocity triangle of blade element.

The lift force per unit length, normal to the direction of $\underline{U}_\infty$, is given by

$$L = \frac{1}{2} \rho U_\infty^2 c C_L \quad , \tag{3.32}$$

and the drag force per unit length, parallel to $\underline{U}_\infty$, is determined as

$$D = \frac{1}{2} \rho U_\infty^2 c C_D \quad , \tag{3.33}$$

where c is the length of the chord, C_L is the lift coefficient and C_D the drag coefficient of the airfoil considered.

As the change in linear momentum has to be in the direction of the applied force, the total induced velocity w_i is directed in the opposite direction to the lift. At the blade-element we have

$$w_i \sin\psi = a' \Omega \bar{z} \tag{3.34a}$$

$$w_i \cos\psi = a V_o \quad . \tag{3.34b}$$

According to eq.(3.19), the value of the axial induced velocity far downstream from the rotor is $V_\infty = (1-2a)V_o$, and, assuming no expansion of the wake, the tangential induced velocity is $V_t = 2 a' \Omega \bar{z}$, eq.(3.29). Therefore, the direction of the induced velocity is constant throughout the wake, whereas the magnitude is increased from w_i at the blade-element to $2 w_i$ far downstream of the rotor. Applying eq.(3.16) on a stream-tube, the pressure drop due to the rate of change of the total momentum is given by

$$\begin{aligned} \Delta p &= \rho(V_o - w_i\cos\psi)[V_o\cos\psi - (V_o\cos\psi - 2 w_i)] \\ &= 2 \rho w_i (V_o - w_i\cos\psi) \quad . \end{aligned} \tag{3.35}$$

Since the pressure drop corresponds to the lift force L, we get

$$B L \, d\bar{z} = \Delta p \, 2 \pi \bar{z} \, d\bar{z} \quad , \tag{3.36}$$

where B denotes the number of blades and $2\pi \bar{z}\, d\bar{z}$ is the area of the annular streamtube. Combining eq.(3.35) and eq.(3.36), we get

$$w_i = BL/4\,\pi\rho\bar{z}(V_o - w_i\cos\psi) \quad . \tag{3.37}$$

From geometrical considerations, see fig. 3.6, we have

$$\psi = \tan^{-1}\left(\frac{V_o}{\Omega\bar{z}}\right) - \tan^{-1}\left(\frac{w_i}{U_\infty}\right) \quad . \tag{3.38}$$

Combining eqs.(3.30)-(3.32) with eqs.(3.37)-(3.38), a solution may be established iteratively as follows:

1. Start with an initial guess of w_i (for example, $w_i=0$).
2. Calculate ψ from eq.(3.38).
3. Calculate α and U_∞ from eq.(3.30) and eq.(3.31), respectively.
4. Use eq.(3.32) to determine the lift force L.
5. Update w_i by using the updating formula (eq.3.37)

$$w_i^{(n)} = BL/4\,\pi\rho\bar{z}\left(V_o - w_i^{(n-1)}\cos\psi\right)$$

where (n) denotes the iteration count.

6. Go back to point 2 and continue the iteration until convergence is obtained.

Usually the airfoil coefficients, C_L and C_D, are obtained from tabulated two-dimensional, measured data. The main purpose of the present work, however, is to determine the flow properties about the blades numerically. Therefore, in order to accomplish a complete three-dimensional solution, the described procedure has to be coupled to a viscous-inviscid interaction model.

After a complete solution has been obtained, the normal and tangential forces on a blade element are determined as

$$dF_x = (D\cos\psi - L\sin\psi)d\bar{z} \tag{3.39}$$

$$dF_y = (L\cos\psi + D\sin\psi)d\bar{z} \quad . \tag{3.40}$$

The total axial force, i.e. the thrust T, and the power P are calculated from

$$T = B\int_o^R dF_y \tag{3.41}$$

and

$$P = -B\Omega\int_o^R \bar{z}dF_x \quad . \tag{3.42}$$

3.3 The inviscid near-field: Interactive potential flow theory

The inviscid near-field denotes the inviscid flow field external to the boundary layer of the blade. This is calculated using a strip-theory in which the inviscid spanwise velocity component at a given cross-section, is treated as being independent of the flow at the remaining cross-sections. Assuming the inviscid flow to be irrotational, the inviscid near-field is described by a set of two-dimensional potential flow equations.

3.3.1 The onset flow

To determine the inviscid flow about a rotating blade, Sears (1950) elegantly derived a relation between the potential flow past a blade in a uniform, two-dimensional stream and the inviscid flow over the same airfoil steadily rotating. Sears considered the problem of an infinite cylinder of arbitrary cross-section rotating at angular velocity Ω about an axis normal to it, and found that the inviscid velocity components in the rotating Cartesian coordinate system (recall fig. 3.1) could be expressed as

$$\bar{U}_I = \Omega\, \bar{z}\, \frac{\partial \bar{\phi}}{\partial \bar{x}} \quad , \tag{3.43a}$$

$$\bar{V}_I = \Omega\, \bar{z}\, \frac{\partial \bar{\phi}}{\partial \bar{y}} \quad , \tag{3.43b}$$

and

$$\bar{W}_I = \Omega(\bar{\phi} - 2\,\bar{x}) \quad , \tag{3.43c}$$

where ϕ denotes the potential for a plane flow past the same cylinder placed in a parallel stream of unit speed in the direction of the $\bar{x}$-axis.

It is readily seen, that the velocity components $\bar{U}_I$ and $\bar{V}_I$ are given in a form which is also expected from a purely two-dimensional analysis. It is surprising, however, that it is possibly to express the spanwise velocity component $\bar{W}_I$ in a simple formula which only depends on the potential of the equivalent plane flow.

In a later study, Fogarty & Sears (1950) showed that, if the blade advances in the direction of the $\bar{y}$-axis (the axis of rotation), the expression for the spanwise velocity component eq.(3.43c) is unaltered, and the total circulation about the blade is obtained by superposing the partial solutions from the rotating and translating motion of the blade.

Thus, in view of the analysis of Sears, the chordwise inviscid velocity distribution of a specific cross-section is determined from two-dimensional potential flow theory using the resultant relative velocity $\underline{U}_\infty$, eq.(3.31), as the onset flow.

The corresponding inviscid spanwise velocity distribution is determined by first using a parallel flow of unit speed in the positive $\bar{x}$-direction (recall fig. 3.6) as the onset flow to calculate a velocity distribution $\bar{U}_I(\bar{x})$ about the airfoil. $\bar{U}_I(\bar{x})$ is here measured in the direction of the $\bar{x}$-axis. The corresponding velocity potential is obtained by

$$\bar{\phi}(\bar{x}) = \int_{\bar{x}_{stag}}^{\bar{x}} \bar{U}_I(\bar{x})\, d\bar{x} \quad , \tag{3.44}$$

where $\bar{x}_{stag}$ denotes the $\bar{x}$-component of the position of the stagnation point. Thus, according to eq.(3.43c), the inviscid spanwise velocity component is given as

$$\bar{W}_I(\bar{x}) = (1 + a')\, \Omega\, (\bar{\phi}(\bar{x}) - 2\,\bar{x}) \quad , \tag{3.45}$$

where the induction factor a' has been introduced in order to account for induced effects of the trailing wake.

Here it shall be noted, that eq.(3.45) only defines an exact expression for the spanwise inviscid velocity distribution in the case where the generators of the blade are parallel to the $\bar{z}$-axis. A real blade configuration, however, exhibits both variations in the distribution of chord length and thickness. Thus, in praxis, eq.(3.45) serves only as an approximation to the true three-dimensional flow.

3.3.2 Modelling of the potential flow problem

The solution of the potential flow is basically carried out by using a distribution of singularities placed on the surface contour. The concepts of this method has been given by Hess (1971) and (1973).

Consider an incompressible potential flow about a surface S. On a point P in the flow domain it is convenient to express the velocity of the flow as

$$\underline{U} = \underline{U}_\infty + \underline{u} \quad , \tag{3.46}$$

where $\underline{U}_\infty$ denotes the undisturbed onset flow, which would exist if the surface S was transparent, and $\underline{u}$ is the disturbance velocity field induced by the presence of S. As it is assumed that $\underline{u}$ is irrotational, it can be expressed as the negative gradient of a potential function ϕ,

$$\underline{u} = -\,\mathrm{grad}\,\phi \quad , \tag{3.47}$$

where the potential satisfies Laplace's equation,

$$\nabla^2 \phi = 0 \quad . \tag{3.48}$$

If the surface S is impervious the normal component of velocity must vanish at S , that is

$$\frac{\partial \phi}{\partial n} = \text{grad } \phi \cdot \underline{n} = \underline{U}_\infty \cdot \underline{n} \quad \text{on} \quad S \quad , \tag{3.49}$$

where $\underline{n}$ is the unit normal vector to the surface.

Furthermore, $\underline{u}$ goes to zero as the distance between the point P and the surface S goes to infinity, that is

$$|\text{grad } \phi| \to 0 \quad \text{for} \quad r \to \infty \quad . \tag{3.50}$$

Totally, eqs.(3.48)-(3.50) define a Neumann problem.
By using Greens third identity, the solution of Laplace's equation is carried out by superposition of fundamental solutions of sources. The sources are distributed on the surface, hence the velocity potential at a panel control point p is given as

$$\phi(p) = \iint_S \frac{1}{r(p,q)} \sigma(q) \, dS \quad , \tag{3.51}$$

where $r(p,q)$ is the distance between two control points p and q , and $\sigma(q)$ denotes the source density at the point q.

In order to fulfil the boundary condition at the surface, the normal derivative of ϕ must satisfy eq.(3.49). This gives the following integral equation for the source density distribution

$$\frac{\partial \phi}{\partial n} = -2\pi\sigma(p) + \iint_S \frac{\partial}{\partial n} \frac{1}{r(p,q)} \sigma(q) \, dS = \underline{U}_\infty \cdot \underline{n} \quad . \tag{3.52}$$

This expression is a Fredholm equation of second kind and it defines a well-posed diagonal dominant problem.

If the surface S is permeable a normal velocity corresponding to the flow rate permeating the surface must be added to the right-hand side of eq.(3.52). This is in particular useful when taking into account the influence of the boundary layer on the inviscid flow. In this case a normal transpiration velocity V_{Iw} is added to the right-hand side of eq. (3.52).

3.3.3 Discretization of the potential flow problem

The solution of the integral equation (3.52) is carried out by replacing the airfoil contour S with a singularity distribution consisting of flat panel elements (see fig. 3.7). On each element the surface source density is taken to be constant and the control point, in which the boundary condition eq.(3.49) is to be satisfied, is chosen as the element midpoint. Consequently, the continous potential flow problem is reduced to that of determining the source density of each panel element.

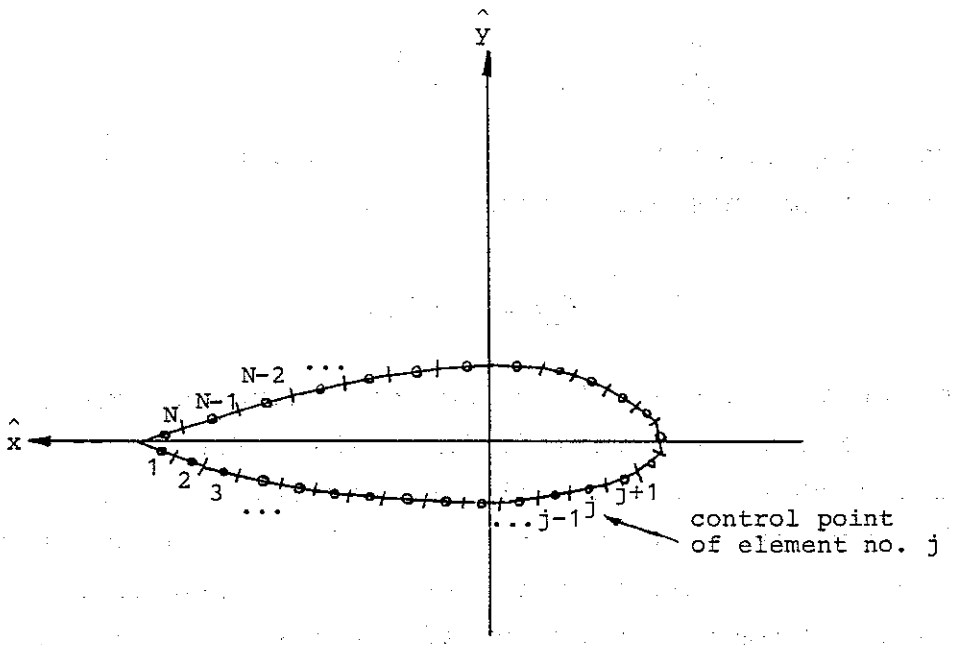

Fig. 3.7 Airfoil contour replaced by flat panel elements.

The surface contour is divided in N elements where the end points of each element are located on the contour. On each element is placed a source with constant density σ_j ($j = 1, 2, \ldots, N$) with $j = 1$ at the lower surface and $j = n$ at the upper surface nearest the trailing edge.

The velocity induced at the control point of element no. i by a unit source distribution of element no. j is denoted $\underline{v}_{ij}$. The component normal to the surface of this velocity is denoted by A_{ij} and is given as

$$A_{ij} = \underline{n}_i \cdot \underline{v}_{ij} \quad , \tag{3.53}$$

where $\underline{n}_i$ is the unit normal vector at element no. i .

The corresponding velocity component parallel to the surface is given as

$$B_{ij} = \underline{t}_i \cdot \underline{v}_{ij} \quad , \tag{3.54}$$

where $\underline{t}_i$ is the unit tangent vector at element no. i .

The boundary condition stating that the flow in the normal direction to the surface must be zero (i.e. eq.3.52) yields

$$\sum_{j=1}^{N} A_{ij}\sigma_j = - \underline{n}_i \cdot \underline{U}_\infty \quad . \tag{3.55}$$

This system is solved for σ_j and the tangential velocities in the control points are determined by

$$U_i = \sum_{j=1}^{N} B_{ij}\sigma_j + \underline{t}_i \cdot \underline{U}_\infty \quad . \tag{3.56}$$

The discretized potential flow problem defined by eqs.(3.55) and (3.56) results in a flow field in which the velocity around the trailing edge of the airfoil becomes infinite. To avoid this behaviour, which is clearly unphysical, it must be required that there is a stagnation point at the trailing edge. In practice, this is accomplished by satisfying the Kutta condition, which states that the pressures in the control points nearest to the trailing edge at the lower and upper surface, respectively, must be equal.

To fulfil the Kutta condition it is appropriate to introduce a rotating onset flow $\underline{U}_i^{\infty r}$ (i = 1, 2, ... , N) into the describing equations. This is most easily accomplished by forming a vortex distribution γ_j on the airfoil contour, in which the vorticity is constant on each element and varied parabolically along the surface, with zero strength at the two control points nearest the trailing edge.

Thus, the vortex distribution is defined as

$$\gamma_j = \Gamma \frac{(j-1)(N-j)}{\sum_{k=1}^{N} (k-1)(N-k)\Delta s_k} \quad , \tag{3.57}$$

where Δs_k denotes the length of element no. k .

The factor Γ determines the total vortex strength on the airfoil,

$$\Gamma = \sum_{k=1}^{N} \gamma_k \Delta s_k \quad . \tag{3.58}$$

Since a vortex induces the same numerical velocity in a point as a source of the same intensity but with a direction turned 90° , one gets the following expressions for the rotating onset flow in the normal and tangential direction, respectively

$$\underline{U}_i^{\infty r} \cdot \underline{n}_i = \sum_{j=1}^{N} (-B_{ij}) \gamma_j \quad , \tag{3.59}$$

and

$$\underline{U}_i^{\infty r} \cdot \underline{t}_i = \sum_{j=1}^{N} A_{ij} \gamma_j \quad . \tag{3.60}$$

To satisfy the boundary condition, stating that the airfoil contour is imperveous, eq.(3.55) is solved with the rotating onset flow of eq.(3.59) as the right-hand side,

$$\sum_{j=1}^{N} A_{ij} \sigma_j^r = \sum_{j=1}^{N} B_{ij} \gamma_j \quad . \tag{3.61}$$

This equation is solved for the unknown source densities σ_j^r (j = 1, 2, ... , N) and the tangential velocities are determined by

$$U_i^r = \sum_{j=1}^{N} B_{ij} \sigma_j^r + \sum_{j=1}^{N} A_{ij} \gamma_j \quad . \tag{3.62}$$

By adjusting Γ to satisfy the Kutta condition, the resulting tangential velocity distribution is determined by writing the solution as a linear combination of eqs.(3.56) and (3.62).

3.3.4 The velocity induced by a surface element

To obtain the velocity induced by a surface element, it is appropriate to introduce an element coordinate system. Such a coordinate system is shown in fig. 3.8.

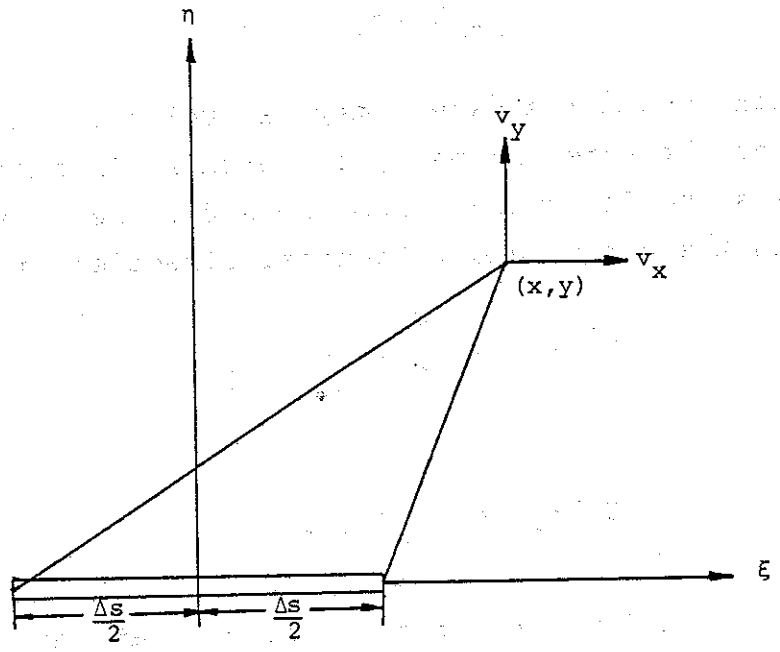

Fig. 3.8 Induced velocity of surface element.

Here the ξ-axis is directed in the direction of the tangent vector of the surface element and the η-axis is directed outward in the direction of the normal vector to the element.

In this coordinate system, according to Hess (1971), the components of the velocity vector $\underline{v}_{ij}$, induced by a constant rectlinear source element of density σ on a point (x,y), is given by

$$v_x = \sigma \cdot \ell n \left[\frac{\left(x+\frac{\Delta s}{2}\right)^2 + y^2}{\left(x-\frac{\Delta s}{2}\right)^2 + y^2} \right] \tag{3.63}$$

and

$$v_y = \sigma \cdot 2 \left[\tan^{-1} \left(\frac{x+\frac{\Delta s}{2}}{y} \right) - \tan^{-1} \left(\frac{x-\frac{\Delta s}{2}}{y} \right) \right] \quad , \tag{3.64}$$

where Δs denotes the length of the element.

It is readily seen that

$$\lim_{y \to \pm 0} v_y = \pm 2 \pi \sigma \quad \text{for} \quad |x| < \frac{\Delta s}{2} \tag{3.65}$$

and

$$\lim_{y \to \pm 0} v_y = 0 \quad \text{for} \quad |x| > \frac{\Delta s}{2} \quad . \tag{3.66}$$

If the element control point coincides with the element mid-point, the velocity induced by the element on its own control point is given as $v_y = 2 \pi \sigma$.

3.3.5 Utilization of the injection function

When solving an actual flow problem the viscous boundary layer alters the streamlines of the potential flow by an amount proportional to the displacement thickness. This effect can be accounted for by specifying an injection function F. This function simulates a normal velocity which is equivalent to the flow rate permeating the surface. Consider for example the influence of a two-dimensional boundary layer flow, at a specific boundary layer station, we get (recall eq.2.17)

$$F = \frac{d}{dx}(U_e \delta^*) \quad , \tag{3.67}$$

where $U_e = U_e(x)$ denotes the velocity at the edge of the boundary layer, $\delta^* = \delta^*(x)$ denotes the displacement thickness and x denotes the coordinate along the airfoil surface.

Putting the F-function on the right-hand side of eq.(3.55) yields

$$\sum_{j=1}^{N} A_{ij} \sigma_i^F = F_j \quad , \tag{3.68}$$

where σ^F is the sigma function connected with F .

Solving this equation for σ_i^F $(i = 1, 2, \ldots, N)$, the resulting tangential velocity distribution is obtained as

$$U_i^F = \sum_{j=1}^{N} B_{ij} \sigma_j^F \quad . \tag{3.69}$$

The advantage of using an injection function to simulate the influence of the boundary layer is that the matrices A_{ij} and B_{ij} and their inverse are found once and for all. Hence, U_i^F can be determined with very little extra effort.

Another important use of the injection function is to be found in its availability to solve the inverse airfoil problem. The inverse airfoil problem defines the case where one wants to determine an airfoil contour which is defined by a velocity distribution specified as a modification from a velocity distribution about another contour.
In such a case a vortex distribution γ_j is placed on the original airfoil contour. This distribution is used to simulate a tangential velocity deviation δU_j from the original velocity U_j as follows

$$\sum_{j=1}^{N} A_{ij} \gamma_j = \delta U_i \quad . \tag{3.70}$$

Solving eq.(3.70) for γ_j , the corresponding normal velocity defining the injection function is given as

$$F_i = - \sum_{j=1}^{N} B_{ij} \gamma_j \quad . \tag{3.71}$$

At a specific location, according to eq.(3.67), the injection function determines the displacement contour δy as

$$\frac{d}{dx}(U \cdot \delta y) = F \quad . \tag{3.72}$$

Integrating eq.(3.72), the modified geometry is obtained by adding δy to the original contour.

3.3.6 Description of the complete equivalent inviscid flow problem

To describe the complete flow field about an airfoil, the solution is build up by superposition of various classes of fundamental solutions comprising the influence of the translating onset flow, the rotating onset flow and the viscous shear layer. The influence of the viscous shear layer is divided into a contribution due to the surface boundary layer and a contribution due to the wake. Both will be simulated by a normal transpiration velocity.

For simplicity, a more convenient notation will be used in the following. In this notation the variables used previously with subscripts 'i' and 'j' are replaced by a conventional vector and matrix notation, i.e. $\sum_{j=1}^{N} A_{ij}\sigma_j$ is replaced by $\underline{\underline{A}}\,\underline{\sigma}$, etc.

The orientation of the panel elements on the airfoil contour is described by the components of the corresponding unit tangent vectors, where $\underline{t}_x$ denotes the first component and $\underline{t}_y$ the second component. The components of the vectors $\underline{t}_x$ and $\underline{t}_y$ are measured in the usual way with the first component referring to the element lying at the lower surface nearest the trailing edge and the remaining components measured around the contour.
When induced velocities are to be evaluated elsewhere than on the airfoil contour, say at a point (x^*, y^*), the matrices of influence are denoted by superscript '*' ; i.e. $\underline{\underline{A}}^*$ and $\underline{\underline{B}}^*$, respectively.

The translating onset flow

It is convenient to divide the translating onset flow $\underline{U}_\infty$ into a contribution, $U_{x\infty} = U_\infty \cos\alpha$, which is lying in the direction of the chord and a contribution, $U_{y\infty} = U_\infty \sin\alpha$, which is perpendicular on this.

Projecting $U_{x\infty}$ on the surface elements results in the local tangential velocities $U_\infty \cos\alpha \, \underline{t}_x$ and the local normal velocities $- U_\infty \cos\alpha \, \underline{t}_y$.

In order to satisfy the Neumann condition, a source distribution $\underline{\sigma}_x$ is introduced as (recall eq.3.55)

$$\underline{\sigma}_x = U_\infty \cos\alpha \, \underline{\underline{A}}^{-1} \, \underline{t}_y \quad . \tag{3.73}$$

Thus, the tangential and normal velocities at the surface contour are determined as

$$\underline{u}_x = \underline{\underline{B}} \, \underline{\sigma}_x + U_\infty \cos\alpha \, \underline{t}_x \quad , \tag{3.74a}$$

$$\underline{v}_x = 0 \quad . \tag{3.74b}$$

If we wish to evaluate the velocities outside the surface, the tangential and normal velocities are given by

$$\underline{u}_x^* = \underline{\underline{B}}^* \underline{\sigma}_x + U_\infty \cos\alpha \, \underline{t}_x \quad , \tag{3.75a}$$

$$\underline{v}_x^* = \underline{\underline{A}}^* \underline{\sigma}_x - U_\infty \cos\alpha \, \underline{t}_y \quad . \tag{3.75b}$$

Performing a similar procedure for the translating onset flow $U_{y\infty}$ yields the source distribution

$$\underline{\sigma}_y = - U_\infty \sin\alpha \, \underline{\underline{A}}^{-1} \, \underline{t}_x \quad , \tag{3.76}$$

with the corresponding tangential and normal velocities evaluated at the surface

$$\underline{u}_y = \underline{\underline{B}} \, \underline{\sigma}_y + U_\infty \sin\alpha \, \underline{t}_y \quad , \tag{3.77a}$$

$$\underline{v}_y = 0 \quad . \tag{3.77b}$$

Evaluating of the source distribution and the onset flow on the off-body location yields

$$\underline{u}_y^* = \underline{\underline{B}}^* \underline{\sigma}_y + U_\infty \sin\alpha \, \underline{t}_y \quad , \tag{3.78a}$$

$$\underline{v}_y^* = \underline{\underline{A}}^* \underline{\sigma}_y + U_\infty \sin\alpha \, \underline{t}_x \quad . \tag{3.78b}$$

The rotating onset flow

As mentioned, the rotating onset flow is produced by forming a parabolic vortex distribution $\underline{\gamma}$ on the airfoil contour. According to eqs.(3.59) and (3.60) the vortices induce a rotating onset flow as follows

$$\underline{U}_{R\infty} = - \underline{\underline{B}} \, \underline{\gamma} \quad , \tag{3.79a}$$

$$\underline{V}_{R\infty} = \underline{\underline{A}} \, \underline{\gamma} \quad , \tag{3.79b}$$

where $\underline{U}_{R\infty}$ denote the tangential component and $\underline{V}_{R\infty}$ the normal component of the rotating onset flow. Both are measured in the coordinate systems of the surface elements.

In order to satisfy the Neumann condition on the surface, a source distribution $\underline{\sigma}_R$ is established

$$\underline{\sigma}_R = \underline{\underline{A}}^{-1} \underline{\underline{B}} \, \underline{\gamma} \quad . \tag{3.80}$$

The resulting distribution of tangential and normal velocities at the surface is given as

$$\underline{u}_R = \underline{\underline{B}} \, \underline{\sigma}_R + \underline{\underline{A}} \, \underline{\gamma} \quad , \tag{3.81a}$$

$$\underline{v}_R = 0 \quad . \tag{3.81b}$$

Evaluating the velocities at the off-body locations yields

$$\underline{u}_R^* = \underline{\underline{B}}^* \, \underline{\sigma}_R + \underline{\underline{A}}^* \, \underline{\gamma} \quad , \tag{3.82a}$$

$$\underline{v}_R^* = \underline{\underline{A}}^* \, \underline{\sigma}_R - \underline{\underline{B}}^* \, \underline{\gamma} \quad . \tag{3.82b}$$

The influence of the boundary layer

In order to simulate the influence of the displacement thickness of the boundary layer, an injection function $\underline{F}$ is used to produce a normal transpiration velocity at the surface. At a specific boundary layer station the transpiration velocity is given by

$$V_w = \frac{1}{h_1 h_3 \sin\theta}\left[\frac{\partial}{\partial x}\left(U_e \delta^* h_3 \sin\theta\right) + \frac{\partial}{\partial z}\left(m_z h_1 \sin\theta\right)\right] \quad , \quad (3.83)$$

where

$$m_z = \int_o^\delta (W_e - w)\,dy \quad . \quad (3.84)$$

Note here, that all variables appearing in eqs.(3.83)-(3.84) are taken from a boundary layer calculation. More details will be given in a subsequent chapter.

According to eq.(3.68), the source distribution $\underline{\sigma}_F$ corresponding to $\underline{F}$ is given by

$$\underline{\sigma}_F = \underline{\underline{A}}^{-1}\,\underline{F} \quad . \quad (3.85)$$

Consequently, the resulting distribution of tangential and normal velocities is given by

$$\underline{u}_F = \underline{\underline{B}}\,\underline{\underline{A}}^{-1}\,\underline{F} \quad , \quad (3.86a)$$

$$\underline{v}_F = \underline{F} \quad . \quad (3.86b)$$

Evaluating the velocities at the off-body locations yields

$$\underline{u}_F^* = \underline{\underline{B}}^*\underline{\underline{A}}^{-1}\,\underline{F} \quad , \quad (3.87a)$$

$$\underline{v}_F^* = \underline{\underline{A}}^*\underline{\underline{A}}^{-1}\,\underline{F} \quad . \quad (3.87b)$$

The influence of the near-wake

In order to take into account the viscous influence from the decay of the displacement thickness in the near-wake, a number of source elements is located on the wake center-line. The strength of these sources is determined by using a normal injection velocity $\underline{F}_W$, according to eq.(3.83).
Here it is assumed that the solution of the wake sources $\underline{\sigma}_W$ is uninfluenced by the remaining sources. Hence the solution is established as being decoupled from the remaining equations. Denoting the local matrix of influence of normal velocities as $\underline{\underline{A}}_W$, we get the following expression for the distribution of the sources

$$\underline{\tilde{\sigma}}_W = \underline{\underline{A}}^{-1} \underline{F}_W \quad , \tag{3.88}$$

where $\underline{\underline{A}}_W$ is a M×M matrix, with M denoting the number of source elements in the wake.

At the body surface $\underline{\tilde{\sigma}}_W$ produces an onset flow as follows

$$\underline{U}_{W\infty} = \underline{\underline{\tilde{B}}}\, \underline{\tilde{\sigma}}_W \quad , \tag{3.89a}$$

$$\underline{V}_{W\infty} = \underline{\underline{\tilde{A}}}\, \underline{\tilde{\sigma}}_W \quad , \tag{3.89b}$$

where $\underline{U}_{W\infty}$ denotes the induced tangential onset flow and $\underline{V}_{W\infty}$ denotes the induced normal onset flow.

$\underline{\underline{\tilde{A}}}$ and $\underline{\underline{\tilde{B}}}$ is N×M matrices of influence giving the influence of the wake sources on the surface contour. In order to satisfy the Neumann condition at the surface, a source distribution $\underline{\sigma}_W$ is established on the contour as follows

$$\underline{\sigma}_W = - \underline{\underline{A}}^{-1} \underline{V}_{W\infty} \quad , \tag{3.90}$$

with the resulting distribution of tangential and normal velocities given by

$$\underline{u}_W = \underline{\underline{B}}\, \underline{\sigma}_W + \underline{U}_{W\infty} \quad , \tag{3.91a}$$

$$\underline{v}_W = 0 \quad . \tag{3.91b}$$

If the velocities are evaluated outside the body contour, the off-body onset velocities are established as follows

$$\underline{U}^*_{w\infty} = \tilde{\underline{\underline{B}}}^* \, \underline{\tilde{\sigma}}_w \quad , \tag{3.92a}$$

$$\underline{V}^*_{w\infty} = \tilde{\underline{\underline{A}}}^* \, \underline{\tilde{\sigma}}_w \quad , \tag{3.92b}$$

where $\tilde{\underline{\underline{A}}}^*$ and $\tilde{\underline{\underline{B}}}^*$ is N×M matrices of influence are on the off-body locations.

The resulting off-body tangential - and normal velocities are thus given as

$$\underline{u}^*_w = \underline{\underline{B}}^* \, \underline{\sigma}_w + \underline{U}^*_{w\infty} \quad , \tag{3.93a}$$

$$\underline{v}^*_w = \underline{\underline{A}}^* \, \underline{\sigma}_w + \underline{V}^*_{w\infty} \quad . \tag{3.93b}$$

Establishment of the solution of the full equivalent inviscid flow problem

The solution of the full equivalent inviscid flow is formed by superposition of the aforementioned fundamental solutions.

At the surface of the airfoil the distribution of tangential velocities is established as

$$\begin{aligned} \underline{U}_I = U_\infty \Big[& \cos\alpha \left(\underline{\underline{B}} \, \hat{\underline{\sigma}}_x + \underline{t}_x \right) + \sin\alpha \left(\underline{\underline{B}} \, \hat{\underline{\sigma}}_y + \underline{t}_y \right) \Big] \\ & + \Gamma \left(\underline{\underline{A}} \, \hat{\underline{\gamma}} + \underline{\underline{B}} \, \hat{\underline{\sigma}}_R \right) + \underline{\underline{B}} \, \underline{\underline{A}}^{-1} \, \underline{F} \\ & + \left(\tilde{\underline{\underline{B}}} \, \underline{\underline{A}}_w^{-1} - \underline{\underline{B}} \, \underline{\underline{A}}^{-1} \, \tilde{\underline{\underline{A}}} \, \underline{\underline{A}}_w^{-1} \right) \underline{F}_w \quad , \end{aligned} \tag{3.94}$$

where the source and vorticity distributions denoted by '~' are normalised as

$$\hat{\underline{\sigma}}_x = \underline{\sigma}_x / U_\infty \cos\alpha \quad , \tag{3.95a}$$

$$\hat{\underline{\sigma}}_y = \underline{\sigma}_y / U_\infty \sin\alpha \quad , \tag{3.95b}$$

$$\hat{\underline{\sigma}}_R = \underline{\sigma}_R / \Gamma \quad , \tag{3.95c}$$

$$\hat{\underline{\gamma}} = \underline{\gamma} / \Gamma \quad . \tag{3.95d}$$

These expressions plus the matrices of influence $\underline{\underline{A}}$ and $\underline{\underline{B}}$ depend only of the geometry of the surface, therefore they can be calculated once for all.

If it is assumed that the presence of the boundary layer does not alter the location of the center-line, $\underline{\underline{A}}^{-1}\,\underline{\underline{\tilde{A}}}\,\underline{\underline{A}}_w^{-1}$ and $\underline{\underline{\tilde{B}}}$ are also established once for all. Hence, it is appropriate to write eq.(3.94) as

$$\underline{U}_I = U_\infty(\cos\alpha\,\underline{U}_x + \sin\alpha\,\underline{U}_y) + \Gamma\,\underline{U}_R + \underline{\underline{C}}\,\underline{F} + \underline{\underline{C}}_w\,\underline{F}_w \quad , \tag{3.96}$$

where

$$\underline{U}_x = \underline{\underline{B}}\,\hat{\underline{\sigma}}_x + \underline{t}_x \quad , \tag{3.97a}$$

$$\underline{U}_y = \underline{\underline{B}}\,\hat{\underline{\sigma}}_y + \underline{t}_y \quad , \tag{3.97b}$$

$$\underline{U}_R = A\,\hat{\underline{\gamma}} + \underline{\underline{B}}\,\hat{\underline{\sigma}}_R \quad , \tag{3.97c}$$

$$\underline{\underline{C}} = \underline{\underline{B}}\,\underline{\underline{A}}^{-1} \quad , \tag{3.97d}$$

and

$$\underline{\underline{C}}_w = \underline{\underline{\tilde{B}}}\,\underline{\underline{A}}_w^{-1} - \underline{\underline{B}}\,\underline{\underline{A}}^{-1}\underline{\underline{\tilde{A}}}\,\underline{\underline{A}}_w^{-1} \quad , \tag{3.97e}$$

all are known quantities.

To accomplish the solution of eq.(3.96), the total vortex strength Γ is adjusted to satisfy the Kutta condition.

With the velocities evaluated at off-body locations, the distribution of tangential velocities is

$$\underline{U}_I^* = U_\infty \left[\cos\alpha \left(\underline{\underline{B}}^* \hat{\underline{\sigma}}_x + \underline{t}_x\right) + \sin\alpha \left(\underline{\underline{B}}^* \hat{\underline{\sigma}}_y + \underline{t}_y\right)\right]$$

$$+ \Gamma\left(\underline{\underline{A}}^* \hat{\underline{\gamma}} + \underline{\underline{B}}^* \hat{\underline{\sigma}}_R\right) + \underline{\underline{B}}^* \underline{\underline{A}}^{-1} \underline{F}$$

$$+ \left(\tilde{\underline{\underline{B}}}^* \underline{\underline{A}}_w^{-1} - \underline{\underline{B}}^* \underline{\underline{A}}^{-1} \tilde{\underline{\underline{A}}} \underline{\underline{A}}_w^{-1}\right) \underline{F}_w \quad , \tag{3.98}$$

and the corresponding distribution of normal velocities is written as

$$\underline{V}_I^* = U_\infty \left[\cos\alpha \left(\underline{\underline{A}}^* \hat{\underline{\sigma}}_x - \underline{t}_y\right) + \sin\alpha \left(\underline{\underline{A}}^* \hat{\underline{\sigma}}_y + \underline{t}_x\right)\right]$$

$$+ \Gamma\left(\underline{\underline{A}}^* \hat{\underline{\sigma}}_R - \underline{\underline{B}}^* \hat{\underline{\gamma}}\right) + \underline{\underline{A}}^* \underline{\underline{A}}^{-1} \underline{F}$$

$$+ \left(\underline{\underline{A}}^* \underline{\underline{A}}_w^{-1} - \underline{\underline{A}}^* \underline{\underline{A}}^{-1} \tilde{\underline{\underline{A}}} \underline{\underline{A}}_w^{-1}\right) \underline{F}_w \quad . \tag{3.99}$$

In eqs.(3.98) and (3.99), all the off-body matrices have to be calculated for each new location considered. It is seen, however, that there is no need for any further matrix inversion.

3.4 The viscous near-field: Interactive boundary layer theory

Since the beginning of the 70ties much effort has been put into the development of computer codes which cope with separated boundary layer flows. This trend has mainly been directed towards calculations of two-dimensional flows, whereas the development of general three-dimensional boundary layer codes has not been paid comparatively the same intensive attention.

To construct an efficient and general three-dimensional boundary layer code, it is required that it can be coupled iteratively to an inviscid flow solver and that it handles separated - as well as attached flows.

To the author's knowledge the only code which satisfies both requirements is the interactive integral formulation of Yoshihara and his collegues (Wai, Baillie & Yoshihara, 1985). Quite recently, however, Cebeci and co-workers have extended their two-dimensional interactive differential approach to a quasi three-dimensional formulation, in which the interaction is performed between a full three-dimensional potential flow solver and a set of equations refered to as the quasi-three-dimensional boundary layer equations (Cebeci, Chang, Clark, Mack & Schinke, 1986). In this approach the boundary layer is calculated by employing a strip-theory in which flow variations in the spanwise direction are neglected. It should be mentioned, however, that neither the method of Cebeci or of Yoshihara are directly applicable to flows where effects due to blade rotation are significant.

In the present work it was found that the use of a differential method is preferable to an integral one, because a differential method allows more general flows to be calculated without imposing any restrictions on the velocity profile assumptions. Several difference schemes can be used to discretize the boundary layer equations. Here we employ an approach based on the Keller-box scheme, which has proven to be efficient and accurate for many flow cases (see for example Bradshaw, Cebeci & Whitelaw, 1981).

The interaction between the potential flow and the boundary layer is carried out by use of a quasi-simultaneous interaction procedure, which is imposed on the boundary layer equations as an additional boundary condition. Based on thin-airfoil theory, in the two-dimensional flow case, this technique was originally formulated by Veldman (1981). In a previous work, Sørensen (1986) has extended the technique to be a part of the solution to the potential flow problem, and in the present work it is extended further into a complete three-dimensional formulation.

3.4.1 The boundary layer equations in primitive variables

As discussed in chapter 3.1 the boundary layer equations are expressed in a non-orthogonal, curvilinear and rotating coordinate system. In this coordinate system x and z denote the coordinates embedded on the surface of the blade and, to be consistent with the usual boundary layer concept, y defines the coordinate axis along the normal to the surface. The metric tensor defining the coordinate system is given as

$$g_{ij} = \begin{vmatrix} g_{11} & 0 & g_{13} \\ 0 & 1 & 0 \\ g_{31} & 0 & g_{33} \end{vmatrix} \quad . \tag{3.100}$$

Denoting the angle between the coordinates x and z as θ it is convenient to replace the g_{ij}'s as

$$g_{11}^{\frac{1}{2}} = h_1 \quad , \tag{3.101a}$$

$$g_{33}^{\frac{1}{2}} = h_3 \quad , \tag{3.101b}$$

and

$$g_{13} = g_{31} = h_1 h_3 \cos\theta \quad , \tag{3.101c}$$

where the expressions for h_1, h_3 and $\cos\theta$ are derived in chapter 3.1.

With this metric the length of a surface element ds is given by

$$ds^2 = h_1^2\,dx^2 + h_3^2\,dz^2 + 2\,h_1 h_3 \cos\theta\,dx\,dz \quad . \quad (3.102)$$

The boundary layer equations are obtained from the Navier-Stokes equations by assuming that the gradients of shear stresses parallel to the surface are negligible in comparison with the gradients of shear stresses normal to the surface. In addition, the normal pressure gradients induced by the rotation is neglected in accordance to first order boundary layer theory.

Assuming the flow to be incompressible and letting ν represent the kinematic viscosity, (u,v,w) the velocity components along the coordinate curves (x,y,z), R the length of the blade and Ω the angular velocity about the $\bar{z}$-axis, the boundary layer equations are written as (see appendix A for a general derivation)

Continuity

$$\frac{\partial}{\partial x}(uh_3\sin\theta) + \frac{\partial}{\partial y}(vh_1 h_3 \sin\theta) + \frac{\partial}{\partial z}(wh_1\sin\theta) = 0 \quad . \quad (3.103)$$

x-momentum

$$\frac{u}{h_1}\frac{\partial u}{\partial x} + v\frac{\partial u}{\partial y} + \frac{w}{h_3}\frac{\partial u}{\partial z} - \frac{2\,\Omega R\cos\theta}{h_1 h_3 \sin^2\theta}\frac{\partial \bar{x}}{\partial x}u - \frac{2\,\Omega R}{h_1 h_3 \sin^2\theta}\frac{\partial \bar{x}}{\partial x}w$$

$$- \cot\theta\,K_1 u^2 + K_{13}\,uw + \frac{K_3}{\sin\theta}w^2$$

$$= \frac{U_e}{h_1}\frac{\partial U_e}{\partial x} + \frac{W_e}{h_3}\frac{\partial U_e}{\partial z} - \frac{2\,\Omega R\cos\theta}{h_1 h_3 \sin^2\theta}\frac{\partial \bar{x}}{\partial x}U_e - \frac{2\,\Omega R}{h_1 h_3 \sin^2\theta}\frac{\partial \bar{x}}{\partial x}W_e$$

$$- \cot\theta\,K_1 U_e^2 + K_{13}\,U_e W_e + \frac{K_3}{\sin\theta}W_e^2 + \frac{\partial}{\partial y}\left(\nu\frac{\partial u}{\partial y} - \overline{u'v'}\right) \quad . \quad (3.104)$$

z-momentum

$$\frac{u}{h_1}\frac{\partial w}{\partial x} + v\frac{\partial w}{\partial y} + \frac{w}{h_3}\frac{\partial w}{\partial z} + \frac{2\,\Omega R}{h_1 h_3 \sin^2\theta}\frac{\partial \bar{x}}{\partial x}u + \frac{2\,\Omega R\cos\theta}{h_1 h_3 \sin^2\theta}\frac{\partial \bar{x}}{\partial x}w$$

$$+ \frac{K_1}{\sin\theta}u^2 + K_{31}uw - \cot\theta\, K_3 w^2$$

$$= \frac{U_e}{h_1}\frac{\partial W_e}{\partial x} + \frac{W_e}{h_3}\frac{\partial W_e}{\partial z} + \frac{2\,\Omega R}{h_1 h_3 \sin^2\theta}\frac{\partial \bar{x}}{\partial x}U_e + \frac{2\,\Omega R\cos\theta}{h_1 h_3 \sin^2\theta}\frac{\partial \bar{x}}{\partial x}W_e$$

$$+ \frac{K_1}{\sin\theta}U_e^2 + K_{31}U_e W_e - \cot\theta\, K_3 W_e^2 + \frac{\partial}{\partial y}\left(\nu\frac{\partial w}{\partial y} - \overline{v'w'}\right) \quad . \quad (3.105)$$

Here the curvature parameters K_1 , K_3 , K_{13} and K_{31} are given by

$$K_1 = \frac{1}{h_1 h_3 \sin\theta}\left[\frac{\partial}{\partial x}(h_3\cos\theta) - \frac{\partial h_1}{\partial z}\right] \quad , \quad (3.106a)$$

$$K_3 = \frac{1}{h_1 h_3 \sin\theta}\left[\frac{\partial}{\partial z}(h_1\cos\theta) - \frac{\partial h_3}{\partial z}\right] \quad , \quad (3.106b)$$

$$K_{13} = \frac{1}{\sin\theta}\left[\cos\theta\left(K_3 + \frac{1}{h_3}\frac{\partial\theta}{\partial z}\right) - K_1 - \frac{1}{h_1}\frac{\partial\theta}{\partial z}\right] \quad , \quad (3.106c)$$

$$K_{31} = \frac{1}{\sin\theta}\left[\cos\theta\left(K_1 + \frac{1}{h_1}\frac{\partial\theta}{\partial x}\right) - K_3 - \frac{1}{h_3}\frac{\partial\theta}{\partial z}\right] \quad , \quad (3.106d)$$

where K_1 and K_3 represent the geodesic curvatures of the z = constant curves and the x = constant curves, respectively.

The boundary conditions are given by

$$y = 0 \;:\; u = v = w = 0 \quad , \quad (3.107a)$$

$$y = \delta \;:\; u = U_e(x,z) \quad , \quad w = W_e(x,z) \quad , \quad (3.107b)$$

where subscript 'e' refers to values evaluated at the edge of the boundary layer.

In the momentum equations the pressure distribution $p(x,z)$ has been eliminated by imposing the two Euler equations at the edge of the boundary layer (see appendix A). These are given by

$$
\begin{aligned}
&- \frac{1}{h_1 \sin^2\theta}\,\frac{1}{\rho}\,\frac{\partial p}{\partial x} + \frac{\cos\theta}{h_3 \sin^2\theta}\,\frac{1}{\rho}\,\frac{\partial p}{\partial z} \\
&= \frac{U_e}{h_1}\,\frac{\partial U_e}{\partial x} + \frac{W_e}{h_3}\,\frac{\partial U_e}{\partial z} - \frac{2\,\Omega R\cos\theta}{h_1 h_3 \sin^2\theta}\,\frac{\partial \bar{x}}{\partial x}\,U_e - \frac{2\,\Omega R}{h_1 h_3 \sin^2\theta}\,\frac{\partial \bar{x}}{\partial x}\,W_e \\
&+ \frac{\Omega^2 \bar{r}}{\sin^2\theta}\left(\frac{\cos\theta}{h_3}\,\frac{\partial \bar{r}}{\partial z} - \frac{1}{h_1}\,\frac{\partial \bar{r}}{\partial x}\right) - \cot\theta\, K_1 U_e^2 + K_{13}\, U_e W_e + \frac{K_3}{\sin\theta}\, W_e^2
\end{aligned}
\tag{3.108a}
$$

and

$$
\begin{aligned}
&\frac{\cos\theta}{h_1 \sin^2\theta}\,\frac{1}{\rho}\,\frac{\partial p}{\partial x} - \frac{1}{h_3 \sin^2\theta}\,\frac{1}{\rho}\,\frac{\partial p}{\partial z} \\
&= \frac{U_e}{h_1}\,\frac{\partial W_e}{\partial x} + \frac{W_e}{h_3}\,\frac{\partial W_e}{\partial z} + \frac{2\,\Omega R}{h_1 h_3 \sin^2\theta}\,\frac{\partial \bar{x}}{\partial x}\,U_e + \frac{2\,\Omega R\cos\theta}{h_1 h_3 \sin^2\theta}\,\frac{\partial \bar{x}}{\partial x}\,W_e \\
&+ \frac{\Omega^2 \bar{r}}{\sin^2\theta}\left(\frac{\cos\theta}{h_1}\,\frac{\partial \bar{r}}{\partial x} - \frac{1}{h_3}\,\frac{\partial \bar{r}}{\partial z}\right) + \frac{K_1}{\sin\theta}\, U_e^2 + K_{31}\, U_e W_e - \cot\theta\, K_3 W_e^2 \,.
\end{aligned}
\tag{3.108b}
$$

Here $\bar{r}$ denotes the distance from the axis of rotation to a point on the blade; that is

$$
\bar{r} = (\bar{x}^2 + \bar{z}^2)^{\frac{1}{2}} \,. \tag{3.109}
$$

The terms containing $\bar{r}$ represent the contribution due to the centrifugal force field. According to the Euler equations these terms act like a hydrostatic pressure in the boundary layer, hence they do not appear explicitly in the present formulation of boundary layer equations.

Since the boundary layer equations are parabolic in both the x- and the z-direction, initial conditions are required at two intersecting planes. According to Cebeci, Kaups and Ramsey (1977) it is appropriate to let the plane given by the stagnation line and the normal to this define the initial conditions in the streamwise directions.

At the stagnation line $u = 0$, thus making the x-momentum equation singular. However, differentiating the x-momentum equation with x and taking advantage of the symmetri condition $\frac{\partial w}{\partial x} = \frac{\partial v}{\partial x} = \frac{\partial^2 u}{\partial x^2} = 0$, the stagnations line equations become nonsingular and are written as

continuity

$$h_3 \sin\theta \, u_x + \frac{\partial}{\partial y}(v h_1 h_3 \sin\theta) + \frac{\partial}{\partial z}(w h_1 \sin\theta) = 0 \qquad (3.110a)$$

x-momentum

$$\frac{u_x^2}{h_1} + v \frac{\partial u_x}{\partial y} + \frac{w}{h_3} \frac{\partial u_x}{\partial z} - \frac{2\,\Omega R \cos\theta}{h_1 h_3 \sin^2\theta} \frac{\partial \bar{x}}{\partial x} u_x + K_{13} w u_x =$$

$$\frac{U_{xe}^2}{h_1} + \frac{W_e}{h_3} \frac{\partial U_{xe}}{\partial z} + K_{13} W_e \cdot U_{xe} - \frac{2\,\Omega R \cos\theta}{h_1 h_3 \sin^2\theta} \frac{\partial \bar{x}}{\partial x} U_{xe}$$

$$+ \frac{\partial}{\partial y}\left(\nu \frac{\partial u_x}{\partial y}\right) \qquad (3.110b)$$

z-momentum

$$v \frac{\partial w}{\partial y} + \frac{w}{h_3} \frac{\partial w}{\partial z} + \frac{2\,\Omega R \cos\theta}{h_1 h_3 \sin^2\theta} \frac{\partial \bar{x}}{\partial x} w - \cot\theta \, K_3 w^2 =$$

$$\frac{W_e}{h_3} \frac{\partial W_e}{\partial z} + \frac{2\,\Omega R \cos\theta}{h_1 h_3 \sin^2\theta} \frac{\partial \bar{x}}{\partial x} W_e - \cot\theta \, K_3 W_e^2 + \frac{\partial}{\partial y}\left(\nu \frac{\partial w}{\partial y}\right) \qquad (3.110c)$$

Here $u_x = \frac{\partial u}{\partial x}$ and $U_{xe} = \frac{\partial U_e}{\partial x}$.

The boundary conditions are given by

$$y = 0 \quad : \quad u_x = v = w = 0 \tag{3.111a}$$

$$y = \delta \quad : \quad u_x = U_{xe}(x,z) \quad , \quad w = W_e(x,z) \quad . \tag{3.111b}$$

When starting the calculations at the root end of the blade the equations are approximated by the infinite-swept-wing assumption. Usually this assumption is obtained by neglecting the spanwise variations of u , v and w . Some of these terms, however, are approximately known from the inviscid flow. Here we assume that $\frac{\partial w}{\partial z} = \frac{\partial}{\partial z}\left(\frac{u}{U_e}\right) = 0$, whereas the term $\frac{\partial U_e}{\partial z} \neq 0$, and take advantage of the following relationship

$$\frac{\partial u}{\partial z} = \frac{\partial}{\partial z}\left(\frac{u}{U_e} U_e\right) = \frac{u}{U_e} \frac{\partial U_e}{\partial z} \quad . \tag{3.112}$$

From the inviscid flow we have

$$U_{Ie} = U_\infty \frac{\partial \phi}{\partial x} = \left(V_o^2 + \Omega^2 R^2 z^2 - w_i^2\right)^{\frac{1}{2}} \frac{\partial \phi}{\partial x} \quad . \tag{3.113}$$

Here ϕ denotes the velocity potential from a unit onset flow in the free-stream direction and U_∞ denotes the magnitude of the onset flow (recall eq.3.31).

Differentiating eq.(3.113) with respect to z , $\frac{\partial U_e}{\partial z}$ is approximated as

$$\frac{\partial U_e}{\partial z} \cong \frac{\partial U_{Ie}}{\partial z} = \frac{\Omega^2 R^2 z}{U_\infty} \frac{\partial \phi}{\partial x} \quad . \tag{3.114}$$

Thus, in a rotating frame of reference, the <u>infinite-swept-wing equations</u> are written as

continuity

$$\frac{\partial}{\partial x}(u h_3 \sin\theta) + \frac{\partial}{\partial y}(v h_1 h_3 \sin\theta) = 0 \tag{3.115a}$$

x-momentum

$$\frac{u}{h_1}\frac{\partial u}{\partial x} + v\frac{\partial u}{\partial y} + \frac{w}{h_3}\left(\frac{u}{U_e}\right)\frac{\partial U_e}{\partial z} - \frac{2\,\Omega R\cos\theta}{h_1 h_3 \sin^2\theta}\frac{\partial \bar{x}}{\partial x}u$$

$$- \frac{2\,\Omega R}{h_1 h_3 \sin^2\theta}\frac{\partial \bar{x}}{\partial x}w - \cot\theta\, K_1 u^2 + K_{13}\,uw + \frac{K_3}{\sin\theta}w^2$$

$$= \frac{U_e}{h_1}\frac{\partial U_e}{\partial x} + \frac{W_e}{h_3}\frac{\partial U_e}{\partial z} - \frac{2\,\Omega R\cos\theta}{h_1 h_3 \sin^2\theta}\frac{\partial \bar{x}}{\partial x}U_e$$

$$- \frac{2\,\Omega R}{h_1 h_3 \sin^2\theta}\frac{\partial \bar{x}}{\partial x}W_e - \cot\theta\, K_1 U_e^2 + K_{13}\,U_e W_e + \frac{K_3}{\sin\theta}W_e^2$$

$$+ \frac{\partial}{\partial y}\left(\nu\frac{\partial u}{\partial y} - \overline{u'v'}\right) \qquad (3.115b)$$

z-momentum

$$\frac{u}{h_1}\frac{\partial w}{\partial x} + v\frac{\partial w}{\partial y} + \frac{2\,\Omega R}{h_1 h_3 \sin^2\theta}\frac{\partial \bar{x}}{\partial x}u + \frac{2\,\Omega R\cos\theta}{h_1 h_3 \sin^2\theta}\frac{\partial \bar{x}}{\partial x}w$$

$$+ \frac{K_1}{\sin\theta}u^2 + K_{13}\,uw - \cot\theta\, K_3 w^2$$

$$= \frac{U_e}{h_1}\frac{\partial W_e}{\partial x} + \frac{2\,\Omega R}{h_1 h_3 \sin^2\theta}\frac{\partial \bar{x}}{\partial x}U_e + \frac{2\,\Omega R\cos\theta}{h_1 h_3 \sin^2\theta}\frac{\partial \bar{x}}{\partial x}W_e$$

$$+ \frac{K_1}{\sin\theta}U_e^2 + K_{31}\,U_e W_e - \cot\theta\, K_3 W_e^2 + \frac{\partial}{\partial y}\left(\nu\frac{\partial w}{\partial y} - \overline{v'w'}\right) \qquad (3.115c)$$

These equations are subject to the boundary conditions

$$y = 0 \;:\; u = v = w = 0 \qquad (3.116a)$$

$$y = \delta \;:\; u = U_e(x,z) \;,\; w = W_e(x,z) \qquad (3.116b)$$

In order to start the calculations at the intersecting line between the first calculated cross-section and the plane defined by the stagnation line, the stagnation line equations are approximated by the infinite-swept wing assumption. This yields a set of ordinary differential equations, which here is referred to as the initial line equations. They are given by

continuity

$$h_3 \sin\theta \, u_x + \frac{\partial}{\partial y}(v h_1 h_3 \sin\theta) = 0 \qquad (3.117a)$$

x-momentum

$$\frac{u_x^2}{h_1} + v \frac{\partial u_x}{\partial y} - \frac{2\,\Omega R \cos}{h_1 h_3 \sin^2\theta} \frac{\partial \bar{x}}{\partial x} u_x + K_{13} w u_x$$

$$= \frac{U_{xe}^2}{h_1} - \frac{2\,\Omega R \cos\theta}{h_1 h_3 \sin^2\theta} \frac{\partial \bar{x}}{\partial x} U_{xe} + K_{13} W_e U_{xe} + \frac{\partial}{\partial y}\left(\nu \frac{\partial u_x}{\partial y}\right) \qquad (3.117b)$$

z-momentum

$$v \frac{\partial w}{\partial y} + \frac{2\,\Omega R \cos\theta}{h_1 h_3 \sin^2\theta} \frac{\partial \bar{x}}{\partial x} w - \cot\theta \, K_3 w^2$$

$$= \frac{2\,\Omega R \cos\theta}{h_1 h_3 \sin^2\theta} \frac{\partial \bar{x}}{\partial x} W_e - \cot\theta \, K_3 W_e^2 + \frac{\partial}{\partial y}\left(\nu \frac{\partial w}{\partial y}\right) \qquad (3.117c)$$

The boundary conditions are given by

$$y = 0 \; : \; u_x = v = w = 0 \qquad (3.118a)$$

$$y = \delta \; : \; u_x = U_{xe}(x,z) \quad , \quad w = W_e(x,z) \qquad (3.118b)$$

3.4.2 Turbulence modelling

For calculations of turbulent flows, it is necessary to model the Reynolds stress terms $-\overline{u'v'}$ and $-\overline{v'w'}$. The approach employed in the present study is to use the Cebeci-Smith two-layer eddy-viscosity model extended to three-dimensional flows (see for example Cebeci, Kaups & Ramsey, 1977). In this approach the Reynolds stresses are related to the mean velocity profiles as follows

$$-\overline{u'v'} = \nu^t \frac{\partial u}{\partial y} \quad , \tag{3.119a}$$

$$-\overline{v'w'} = \nu^t \frac{\partial w}{\partial y} \quad . \tag{3.119b}$$

The eddy-viscosity ν^t is defined by two separate formulaes. In the inner region of the boundary layer, ν^t is given by

$$\nu_i^t = L^2\left[\left(\frac{\partial u}{\partial y}\right)^2 + \left(\frac{\partial w}{\partial y}\right)^2 + 2\cos\theta\left(\frac{\partial u}{\partial y}\right)\left(\frac{\partial w}{\partial y}\right)\right]^{\frac{1}{2}} \quad , \tag{3.120}$$

where the mixing length L is given by

$$L = 0.4\, y[1 - \exp(-y/A)] \quad . \tag{3.121}$$

The damping constant A is expressed as

$$A = 26\, \nu/u_\tau \quad . \tag{3.122}$$

The wall-friction velocity u_τ is defined as

$$u_\tau = (\tau_{tw}/\rho)^{\frac{1}{2}} \quad , \tag{3.123}$$

with the total wall-friction τ_{tw} given by

$$\tau_{tw} = \mu\left[\left(\frac{\partial u}{\partial y}\right)_w^2 + \left(\frac{\partial w}{\partial y}\right)_w^2 + 2\cos\theta\left(\frac{\partial u}{\partial y}\right)_w\left(\frac{\partial w}{\partial y}\right)_w\right]^{\frac{1}{2}} \quad . \tag{3.124}$$

Subscript 'w' denotes values at the wall and $\mu = \rho\nu$ is the viscosity.

In the outer region of the boundary layer ν_o^t is given as

$$\nu_o^t = 0.0168 \left| \int_o^\infty (U_{te} - u_t)\, dy \right| \quad , \qquad (3.125)$$

where u_t is the total tangential velocity

$$u_t = (u^2 + w^2 + 2\cos\theta\, uw)^{\frac{1}{2}} \quad , \qquad (3.126)$$

and U_{te} is the corresponding velocity evaluated at the edge of the boundary layer

$$U_{te} = \left(U_e^2 + W_e^2 + 2\cos\theta\, U_e W_e\right)^{\frac{1}{2}} \quad . \qquad (3.127)$$

When starting the calculations at the wall, the inner formulation is employed until ν_i^t equals ν_o^t. Thereafter, the calculations are continued using ν_o^t until the edge of the boundary layer is reached.

3.4.3 Transformation of the boundary layer equations

For the external flow about a body exposed to an adverse pressure gradient, the growth of the boundary layer becomes significant. Usually it is therefore necessary to transform the governing equations in order to establish a suitable grid, which follows the physics of the flow. A commonly used transformation is the two-dimensional Falker-Skan transformation (or, for a compressible flow, the Levy-Lees tranformation) which is easily extended to three demensions. This transformation is found, however, not to work satisfactorily for turbulent boundary layer flows developing under strong pressure gradients, as is the case for the present investigation.

Instead, we employ a transformation in which the normal coordinate is non-dimensionalised by the streamwise displacement thickness δ^*. In two dimensions this transformation has been employed by Drela & Thompkins (1984) and later by Sørensen (1986). This type of transform was originally formulated by Carter (1975).

The transformed coordinates are defined by

$$x = x \quad , \quad \eta = \frac{y}{\delta^*} \quad , \quad z = z \quad , \tag{3.128}$$

where the streamwise displacement thickness is given by

$$\delta^* = \int_0^\delta \left(1 - \frac{u}{U_e}\right) dy \quad . \tag{3.129}$$

A two-component vector potential (Φ,Ψ) is introduced by

$$uh_3 \sin\theta = \frac{\partial \Psi}{\partial y} \quad , \tag{3.130a}$$

$$wh_1 \sin\theta = \frac{\partial \Phi}{\partial y} \quad , \tag{3.130b}$$

where

$$vh_1 h_3 \sin\theta = -\left(\frac{\partial \Psi}{\partial x} + \frac{\partial \Phi}{\partial z}\right) \quad . \tag{3.130c}$$

At the stagnation line the governing equations are singular. The singularity, however, is removed by introducing the following similarity variables

$$F = \Psi / U_e \delta^* h_3 \sin\theta \quad , \tag{3.131a}$$

$$G = \Phi / W_{ref} \delta^* h_1 \sin\theta \quad , \tag{3.131b}$$

where W_{ref} is a crosswise reference velocity.

Using the chain rule of differentiation we have that

$$\frac{\partial}{\partial x} = \frac{\partial}{\partial x} + \left(\frac{\partial \eta}{\partial x}\right)\frac{\partial}{\partial \eta} \quad , \tag{3.132a}$$

$$\frac{\partial}{\partial y} = \left(\frac{\partial \eta}{\partial y}\right)\frac{\partial}{\partial \eta} \quad , \tag{3.132b}$$

$$\frac{\partial}{\partial z} = \frac{\partial}{\partial z} + \left(\frac{\partial \eta}{\partial z}\right)\frac{\partial}{\partial \eta} \quad , \tag{3.132c}$$

where the derivatives at the left-hand sides are given in old coordinates. Using the definition eq.(3.128), we get

$$\frac{\partial \eta}{\partial x} = -\frac{\eta}{\delta^*}\frac{\partial \delta^*}{\partial x} \quad , \tag{3.133a}$$

$$\frac{\partial \eta}{\partial y} = \frac{1}{\delta^*} \quad , \tag{3.133b}$$

$$\frac{\partial \eta}{\partial z} = -\frac{\eta}{\delta^*}\frac{\partial \delta^*}{\partial z} \quad . \tag{3.133c}$$

Combining eqs.(3.130 - (3.133) yields

$$u = U_e F' \quad , \tag{3.134a}$$

$$w = W_{ref} G' \quad , \tag{3.134b}$$

$$v = -\frac{U_e \delta^*}{h_1}\frac{\partial F}{\partial x} - F\left(\frac{U_e \delta^*}{h_1 h_3 \sin\theta}\frac{\partial}{\partial x}(h_3 \sin\theta) + \frac{1}{h_1}\frac{\partial}{\partial x}(U_e \delta^*)\right)$$

$$+ \frac{U_e \eta}{h_1}\frac{\partial \delta^*}{\partial x} F' + \frac{W_{ref}\eta}{h_3}\frac{\partial \delta^*}{\partial z} G' - \frac{W_{ref}\delta^*}{h_3}\frac{\partial G}{\partial z}$$

$$- G\left(\frac{W_{ref}\delta^*}{h_1 h_3 \sin\theta}\frac{\partial}{\partial z}(h_1 \sin\theta) + \frac{W_{ref}}{h_3}\frac{\partial \delta^*}{\partial z}\right) \quad , \tag{3.134c}$$

$$\frac{\partial u}{\partial x} = U_e \frac{\partial F'}{\partial x} + F' \frac{\partial U_e}{\partial x} - \frac{\eta}{\delta^*}\frac{\partial \delta^*}{\partial x} U_e F'' \quad , \tag{3.134d}$$

$$\frac{\partial u}{\partial y} = \frac{U_e}{\delta^*} F'' \tag{3.134e}$$

$$\frac{\partial u}{\partial z} = U_e \frac{\partial F'}{\partial x} + F' \frac{\partial U_e}{\partial z} - \frac{\eta}{\delta^*}\frac{\partial \delta^*}{\partial z} U_e F'' \tag{3.134f}$$

$$\frac{\partial w}{\partial x} = W_{ref}\frac{\partial G'}{\partial x} - \frac{\eta}{\delta^*}\frac{\partial \delta^*}{\partial x} W_{ref} G'' \tag{3.134g}$$

$$\frac{\partial w}{\partial y} = \frac{W_{ref}}{\delta^*} G'' \tag{3.134h}$$

$$\frac{\partial w}{\partial z} = W_{ref}\frac{\partial G'}{\partial z} - \frac{\eta}{\delta^*}\frac{\partial \delta^*}{\partial z} W_{ref} G'' \tag{3.134i}$$

Here $(\,)'$ denotes variables differentiated with respect to η.

Transformation of eq.(3.129) yields

$$F_e = \eta_e - 1 \quad . \tag{3.135}$$

When solving the boundary layer equations, Bradshaw, Cebeci & Whitelaw (1981) have shown that special treatment of the normal velocity component is required if oscillations in the solution are to be avoided. Therefore we introduce a variable, which is related to the normal velocity, as

$$E = - v + \frac{\eta}{h_1} \frac{\partial \delta^*}{\partial x} U_e F' + \frac{\eta}{h_3} \frac{\partial \delta^*}{\partial z} W_{ref} G' \quad . \tag{3.136}$$

Furthermore, in order to write the governing equations as a set of first-order equations, new variables are introduced as

$$U = F' \quad , \tag{3.137a}$$

$$W = G' \quad , \tag{3.137b}$$

$$V = U' \quad , \tag{3.137c}$$

$$T = W' \quad . \tag{3.137d}$$

Transformation: General case

Combining eqs.(3.134) - (3.137) with eqs.(3.103) - (3.107) yields the transformed three-dimensional boundary layer equations

$$(bV)' + EV + \left(m_1 U_e - m_2 \frac{\partial U_e}{\partial x}\right)U^2 - \left(K_{13} + m_3 \frac{1}{U_e}\frac{\partial U_e}{\partial z}\right)UW$$

$$- m_4 \frac{1}{U_e} W^2 + m_5 U + m_6 \frac{1}{U_e} W - m_2 U_e U \frac{\partial U}{\partial x} - m_3 W \frac{\partial U}{\partial z}$$

$$- m_1 U_e + m_2 \frac{\partial U_e}{\partial x} + \left(K_{13} + m_3 \frac{1}{U_e}\frac{\partial U_e}{\partial z}\right)\frac{W_e}{W_{ref}} + \frac{m_4}{W_{ref}^2}\frac{W_e^2}{U_e}$$

$$- m_5 - \frac{m_6}{W_{ref}}\frac{W_e}{U_e} = 0 \quad , \tag{3.138a}$$

$$(bT)' + ET - m_7 U_e UW + m_8 W^2 - m_9 U_e^2 U^2 - m_{10} U_e U - m_{11} W$$

$$- m_2 U_e U \frac{\partial W}{\partial x} - m_3 W \frac{\partial W}{\partial z} + \frac{m_7}{W_{ref}} U_e W_e - \frac{m_8}{W_{ref}^2} W_e^2 + m_9 U_e^2$$

$$+ m_{10} U_e + \frac{m_{11}}{W_{ref}} W_e + \frac{m_2}{W_{ref}} U_e \frac{\partial W_e}{\partial x} + \frac{m_3}{W_{ref}^2} W_e \frac{\partial W_e}{\partial z} = 0, \tag{3.138b}$$

$$E' - \left(m_{12} U_e + m_2 \frac{1}{\delta^*}\frac{\partial (U_e \delta^*)}{\partial x}\right) U$$

$$- \left(m_{13} + m_3 \frac{1}{\delta^*}\frac{\partial \delta^*}{\partial z}\right) W - m_2 U_e \frac{\partial U}{\partial x} - m_3 \frac{\partial W}{\partial z} = 0 \tag{3.138c}$$

With the external velocity distribution specified as a boundary condition, we get

$$\eta = 0 \quad : \quad U = W = E = 0 \tag{3.139a}$$

$$\eta = \eta_e \quad : \quad U = 1 \quad , \quad W = \frac{W_e}{W_{ref}} \quad , \quad F_e = \eta_e - 1 \tag{3.139b}$$

Here the viscosity parameter b and the coefficients m_1 to m_{13} are given by

$$b = \frac{\nu+\nu^t}{W_{ref}\delta^{*2}} \quad , \tag{3.140a}$$

$$m_1 = \cot\theta \frac{K_1}{W_{ref}} \quad , \tag{3.140b}$$

$$m_2 = \frac{1}{h_1 W_{ref}} \quad , \tag{3.140c}$$

$$m_3 = \frac{1}{h_3} \quad , \tag{3.140d}$$

$$m_4 = \frac{K_3 W_{ref}}{\sin\theta} \quad , \tag{3.140e}$$

$$m_5 = \frac{2\,\Omega R\cos\theta}{h_1 h_3 \sin^2\theta} \frac{\partial\bar{x}}{\partial x} \frac{1}{W_{ref}} \quad , \tag{3.140f}$$

$$m_6 = \frac{2\,\Omega R}{h_1 h_3 \sin^2\theta} \frac{\partial\bar{x}}{\partial x} \quad , \tag{3.140g}$$

$$m_7 = \frac{K_{31}}{W_{ref}} \quad , \tag{3.140h}$$

$$m_8 = \cot\theta\, K_3 \quad , \tag{3.140i}$$

$$m_9 = \frac{K_1}{\sin\theta\, W_{ref}^2} \quad , \tag{3.140j}$$

$$m_{10} = \frac{2\,\Omega R}{h_1 h_3 \sin^2\theta} \frac{\partial\bar{x}}{\partial x} \frac{1}{W_{ref}^2} \quad , \tag{3.140k}$$

$$m_{11} = \frac{2\,\Omega R\cos\theta}{h_1 h_3 \sin^2\theta} \frac{\partial\bar{x}}{\partial x} \frac{1}{W_{ref}} \quad , \tag{3.140ℓ}$$

$$m_{12} = \frac{1}{h_1 h_3 \sin\theta} \frac{\partial}{\partial x}(h_3\sin\theta) \frac{1}{W_{ref}} \quad , \tag{3.140m}$$

$$m_{13} = \frac{1}{h_1 h_3 \sin\theta} \frac{\partial}{\partial z}(h_1\sin\theta) \quad . \tag{3.140n}$$

Transformation: Stagnation line equations

To transform the governing stagnation line equations, a two-component vector potential is introduced

$$u_x h_3 \sin\theta = \frac{\partial \Psi}{\partial y} \quad , \tag{3.141a}$$

$$w h_1 \sin\theta = \frac{\partial \Phi}{\partial y} \quad , \tag{3.141b}$$

from which it follows

$$v h_1 h_3 \sin\theta = -\left(\Psi + \frac{\partial \Phi}{\partial z}\right) \quad . \tag{3.141c}$$

The dimensionless potentials are defined as

$$F = \Psi / U_{xe} \delta^* h_3 \sin\theta \quad , \tag{3.142a}$$

$$G = \Phi / W_{ref} \delta^* h_1 \sin\theta \quad . \tag{3.142b}$$

Assuming the flow to be laminar, the stagnation line equations are written as

$$(bV)' + EV - m_2 U_{xe} U^2 - \left(K_{13} + \frac{m_3}{U_{xe}} \frac{\partial U_{xe}}{\partial z}\right) UW$$

$$+ m_5 U - m_3 W \frac{\partial U}{\partial z} + m_2 U_{xe} + \left(K_{13} + \frac{m_3}{U_{xe}} \frac{\partial U_{xe}}{\partial z}\right) \frac{W_e}{W_{ref}} - m_5 = 0 \quad , \tag{3.143a}$$

$$(bT)' + ET + m_8 W^2 - m_{11} W - m_3 W \frac{\partial W}{\partial z}$$

$$- \frac{m_8}{W_{ref}^2} W_e^2 + \frac{m_{11}}{W_{ref}} W_e + \frac{m_3}{W_{ref}^2} W_e \frac{\partial W_e}{\partial z} = 0 \quad , \tag{3.143b}$$

$$E' - m_2 U_{xe} U - \left(m_{13} + m_3 \frac{1}{\delta^*} \frac{\partial \delta^*}{\partial z}\right) W - m_3 \frac{\partial W}{\partial z} = 0 \quad . \tag{3.143c}$$

The boundary conditions are given as

$$\eta = 0 \quad : \quad U = W = E = 0 \quad , \tag{3.144a}$$

$$\eta = \eta_e \quad : \quad U = 1 \quad , \quad W = \frac{W_e}{W_{ref}} \quad , \quad F_e = \eta_e - 1 \quad . \tag{3.144b}$$

Transformation: Infinite-swept-wing equations

Combining eqs.(3.134) - (3.137) with eqs.(3.115) - (3.116) yields the transformed infinite-swept-wing equations

$$(bV)' + EV + \left(m_1 U_e - m_2 \frac{\partial U_e}{\partial x}\right)U^2 - \left(K_{13} + m_3 \frac{1}{U_e}\frac{\partial U_e}{\partial z}\right)UW$$

$$- m_4 \frac{1}{U_e} W^2 + m_5 U + m_6 \frac{1}{U_e} W - m_2 U_e U \frac{\partial U}{\partial x} - m_1 U_e + m_2 \frac{\partial U_e}{\partial x}$$

$$+ \left(K_{13} + m_3 \frac{1}{U_e}\frac{\partial U_e}{\partial z}\right)\frac{W_e}{W_{ref}} + \frac{m_4}{W_{ref}^2}\frac{W_e^2}{U_e} - m_5 - \frac{m_6}{W_{ref}}\frac{W_e}{U_e} = 0 \quad . \tag{3.145a}$$

$$(bT)' + ET - m_7 U_e UW + m_8 W^2 - m_9 U_e^2 U^2 - m_{10} U_e U - m_{11} W$$

$$- m_2 U_e U \frac{\partial W}{\partial x} + \frac{m_7}{W_{ref}} U_e W_e - \frac{m_8}{W_{ref}^2} W_e^2 + m_9 U_e^2 + m_{10} U_e$$

$$+ \frac{m_{11}}{W_{ref}} W_e + \frac{m_2}{W_{ref}} U_e \frac{\partial W_e}{\partial x} = 0 \quad , \tag{3.145b}$$

$$E' - \left(m_{12} U_e + m_2 \frac{1}{\delta^*}\frac{\partial (U_e \delta^*)}{\partial x}\right)U - m_{13} W - m_2 U_e \frac{\partial U}{\partial x} = 0 . \tag{3.145c}$$

The boundary conditions are given as

$$\eta = 0 \quad : \quad U = W = E = 0 \quad , \tag{3.146a}$$

$$\eta = \eta_e \quad : \quad U = 1 \quad , \quad W = \frac{W_e}{W_{ref}} \quad , \quad F_e = \eta_e - 1 \quad . \tag{3.146b}$$

Transformation: Initial line equations

Combining eqs.(3.134) - (3.137) with eqs.(3.117) - (3.118), we get the transformed initial line equations as follows

$$(bV)' + EV - m_2 U_{xe} U^2 - K_{13} UW + m_5 U$$

$$+ m_2 U_{xe} + \frac{K_{13}}{W_{ref}} W_e - m_5 = 0 \quad , \tag{3.147a}$$

$$(bT)' + ET + m_8 W^2 - m_{11} W$$

$$- \frac{m_8}{W_{ref}^2} W_e^2 + \frac{m_{11}}{W_{ref}} W_e = 0 \quad , \tag{3.147b}$$

$$E' - m_2 U_{xe} U - m_{13} W = 0 \quad . \tag{3.147c}$$

Here the boundary conditions are given by

$$\eta = 0 \quad : \quad U = W = E = 0 \quad , \tag{3.148a}$$

$$\eta = \eta_e \quad : \quad U = 1 \quad , \quad W = \frac{W_e}{W_{ref}} \quad , \quad F_e = \eta_e - 1 \quad . \tag{3.148b}$$

Transformation: The eddy-viscosity

Combining eqs.(3.120) - (3.124) with the transformation formulaes eqs.(3.134) - (3.137) yields the transformed expression for the mixing length

$$L = 0.4\, \eta\delta^* \left\{ 1 - \exp\left[- \frac{\eta}{26} \left(\frac{W_{ref}\delta^*}{\nu} \right)^{\frac{1}{2}} \left[\left(\frac{U_e}{W_{ref}} \right)^2 V_w^2 + T_w^2 + 2\cos\theta \left(\frac{U_e}{W_{ref}} \right) V_w T_w \right]^{1/4} \right] \right\} . \tag{3.149}$$

Here subscript 'w' denotes values at the wall.

The formula for the transformed eddy-viscosity in the inner region of the boundary layer is given by

$$\nu_i^t = L^2 \frac{W_{ref}}{\delta^*}\left[\left(\frac{U_e}{W_{ref}}\right)^2 V^2 + T^2 + 2\cos\theta\left(\frac{U_e}{W_{ref}}\right) V T\right]^{\frac{1}{2}} . \quad (3.150)$$

The corresponding formula in the outer region of the boundary layer is here written as

$$\nu_o^t = 0.0168\, U_e \delta^* C_\nu \quad , \quad (3.151)$$

where

$$C_\nu = \left|\int_o^{\eta_e}\left[\left(1 + \left(\frac{W_e}{U_e}\right)^2 + 2\cos\theta\,\frac{W_e}{U_e}\right)^{\frac{1}{2}} - \left(U^2 + \left(\frac{W_{ref}}{U_e}\right)^2 W^2 + 2\cos\theta\left(\frac{W_{ref}}{U_e}\right)UW\right)^{\frac{1}{2}}\right] d\eta\right| . \quad (3.152)$$

Transformation: Miscellaneous boundary layer parameters

After the solution has been accomplished, we calculate miscellaneous boundary layer parameters.

Denoting the skin-friction along the coordinate lines x and z as τ_{xw} and τ_{zw}, respectively, in transformed variables we get

$$\tau_{xw} = \mu \left.\frac{\partial u}{\partial y}\right|_w = \mu \frac{U_e}{\delta^*} V_w \quad , \quad (3.153a)$$

$$\tau_{zw} = \mu \left.\frac{\partial w}{\partial y}\right|_w = \mu \frac{W_{ref}}{\delta^*} T_w \quad . \quad (3.153b)$$

Dissolving the components of the skin-friction in a chordwise component τ_{cw} and a spanwise component τ_{sw}, yields (see fig. 3.9)

$$\tau_{cw} = \tau_{xw} + \tau_{zw}\cos\theta \quad , \quad (3.154a)$$

$$\tau_{sw} = \tau_{zw}\sin\theta \quad , \quad (3.154b)$$

with the resulting skin-friction given as

$$\tau_w = (\tau_{cw}^2 + \tau_{sw}^2)^{\frac{1}{2}} = (\tau_{xw}^2 + \tau_{zw}^2 + 2\cos\theta\ \tau_{xw}\tau_{zw})^{\frac{1}{2}}. \tag{3.155}$$

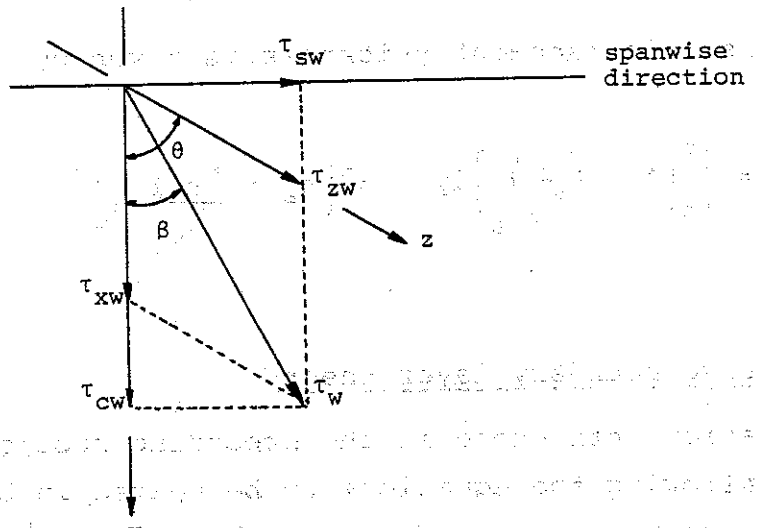

Fig. 3.9 Components of the skin-friction.

Combining this expression with eqs.(3.153) - (3.154), the cross-flow angle β in transformed variables is expressed as

$$\cos\beta = \frac{\tau_{cw}}{\tau_w} = \frac{U_e V_w + W_{ref}\cos\theta\ T_w}{\left(U_e^2 V_w^2 + W_{ref}^2 T_w^2 + 2\cos\theta\ U_e W_{ref} V_w T_w\right)^{\frac{1}{2}}}\ . \tag{3.156}$$

The non-dimensionalised chordwise and spanwise components of the velocity profiles $\left(\frac{u}{U_e}\right)_c$ and $\left(\frac{w}{W_e}\right)_s$, respectively, are given by

$$\left(\frac{u}{U_e}\right)_c = \frac{u + w\cos\theta}{U_e + W_e\cos\theta} = \frac{F' + \frac{W_{ref}}{U_e}\cos\theta\ G'}{1 + \frac{W_e}{U_e}\cos\theta}\ , \tag{3.157a}$$

and

$$\left(\frac{w}{W_e}\right)_s = \frac{w\sin\theta}{W_e\sin\theta} = \frac{W_{ref}}{W_e}\ G'\ . \tag{3.157b}$$

The chordwise displacement thickness is given as

$$\delta_c^* = \int_o^\delta \left[1 - \left(\frac{u}{U_e}\right)_c\right] dy = \delta^* \left[\eta_e - \frac{F_e + \frac{W_{ref}}{U_e} \cos\theta \, G_e}{1 + \frac{W_e}{U_e} \cos\theta}\right], \quad (3.158a)$$

and the spanwise displacement thickness is given by

$$\delta_s^* = \int_o^\delta \left[1 - \left(\frac{w}{W_e}\right)_s\right] dy = \delta^* \left[\eta_e - \frac{W_{ref}}{W_e} G_e\right] \quad . (3.158b)$$

3.4.4 Interactive boundary layer theory

The transformation introduced in the preceding section has the advantage of allowing the equations to be solved in both the direct manner, with U_e specified as a boundary condition, and in the inverse manner, with δ^* specified as a boundary condition, without imposing any further modifications.

In an interactive boundary layer calculation, however, both U_e and δ^* are treated as unknowns. Therefore an extra equation, which couples U_e and δ^*, is required. In the case of a two-dimensional flow, such a relation was first formulated by Veldman (1979). He employed an expression in which the external velocity $U_e(x)$ was written as the sum of the inviscid velocity $U_I(x)$ and a perturbation velocity $\delta U_e(x)$, that is (recall section 2.2.2)

$$U_e(x) = U_I(x) + \delta U_e(x) \quad , \quad (3.159)$$

where the perturbation is an approximate expression, derived from thin-airfoil theory, given by

$$U_e(x) = \int_{x_A}^{x_B} \frac{\frac{d(U_e^*)}{dx}}{x - \xi} \, d\xi \quad . \quad (3.160)$$

Discretization of eq.(3.160) gives together with eq.(3.159) a relation between U_e and δ^*, which is solved simultaneously together with the boundary layer equations in successive sweeps over the airfoil surface.

In an investigation performed by Sørensen (1986), however, it was found more convenient to derive the link between U_e and δ^* by way of the actual potential flow equations. This has furthermore the advantage of being easy to extend into three dimensions, as will be demonstrated in the following.

Consider the inviscid velocity external to the boundary layer, eq.(3.96) of section 3.3.6; by using a compact notation it can be written as

$$\underline{U}_I = \underline{U}_T + \Gamma \underline{U}_R + \underline{U}_{wake} + \underline{\underline{C}}\, \underline{V}_w \qquad (3.161)$$

where $\underline{U}_T$ = the contribution due to the translating onset flow,

$\underline{U}_R$ = the contribution due to the rotating onset flow,

$\underline{U}_{wake}$ = the contribution due to the wake,

$\underline{\underline{C}}$ = the influence matrix of the transpiration velocity,

$\underline{V}_w$ = the transpiration velocity.

Integrating the equation of continuity (3.103) across the boundary layer, at a specific boundary layer station the transpiration velocity is given by (recall section 2.1.2)

$$V_w = \frac{1}{h_1 h_3 \sin\theta}\left[\frac{\partial}{\partial x}(U_e \delta^* h_3 \sin\theta) + \frac{\partial}{\partial z}(m_z h_1 \sin\theta)\right], \qquad (3.162)$$

where

$$m_z = \int_0^{\delta} (W_e - w)\, dy \quad . \qquad (3.163)$$

Note here that

$$m_z = W_e \delta_z^* \quad , \tag{3.164}$$

where

$$\delta_z^* = \int_o^\delta \left(1 - \frac{w}{W_e}\right) dy \quad . \tag{3.165}$$

We employ m_z as a variable instead of W_e and δ_z^*, because W_e locally may vanish, with the result that δ_z^* becomes singular.

In transformed variables eq.(3.163) yields

$$m_z = \delta^* \left(\eta_e W_e - G_e W_{ref}\right) \quad . \tag{3.166}$$

In order to solve the interactive problem, we have to go through several viscous/inviscid sweeps before convergence is achieved. Assuming that eq.(3.161) is identical satisfied at sweep nr.(p-1), we want to solve the boundary layer equations in sweep nr.(p) together with an updated version of eq.(3.161), in which $\underline{U}_I$ is replaced by $\underline{U}_e$, that is

$$\underline{U}_e^{(p)} = \underline{U}_T^{(p-1)} + \Gamma^{(p-1)}\, \underline{U}_R^{(p-1)} + \underline{U}_{wake}^{(p-1)} + \underline{\underline{C}}\, \underline{V}_w^{(p)} \quad . \tag{3.167}$$

Subtracting eq.(3.161) from eq.(3.167), we obtain

$$\underline{U}_e^{(p)} = \underline{U}_I^{(p-1)} + \underline{\underline{C}}\left(\underline{V}_w^{(p)} - \underline{V}_w^{(p-1)}\right) \quad . \tag{3.168}$$

In order to discretize eq.(3.168), we employ a three-point central differencing for the x-derivatives and a three-point backward difference formula for the z-derivatives.
Thus, considering a point $Q(x_n, z_i)$ on the surface, the derivatives are written as

$$\left[\frac{\partial(\ )}{\partial x}\right]_Q = \alpha_{n,1}(\ )_{n-1,i} + \alpha_{n,2}(\ )_{n,i} + \alpha_{n,3}(\ )_{n+1,i} \tag{3.169}$$

and

$$\left[\frac{\partial(\ )}{\partial z}\right]_Q = \beta_{i,1}(\ )_{n,i-2} + \beta_{i,2}(\ )_{n,i-1} + \beta_{i,3}(\ )_{n,i} \tag{3.170}$$

where $\alpha_{n,k}$ and $\beta_{i,k}$ denote the coefficients of a three-point Lagrange interpolation.

Employing eqs.(3.169) and (3.170), the discretized form of the transpiration velocity at point $Q(x_n,z_i)$ is written as

$$\left[V_w\right]_Q = (m_2)_{n,i}\left(\alpha_{n,1}\, U_{e_{n-1,i}}\, \delta^*_{n-i,i} + \alpha_{n,2}\, U_{e_{n,i}}\, \delta^*_{n,i} + \alpha_{n,3}\, U_{e_{n+1,i}}\, \delta^*_{n+1,i}\right)$$

$$+ (m_3)_{n,i}\left(\beta_{i,1}\, m_{z_{n,i-2}} + \beta_{i,2}\, m_{z_{n,i-1}} + \beta_{i,3}\, m_{z_{n,i}}\right)$$

$$+ (m_{12})_{n,i}\, U_{e_{n,i}}\, \delta^*_{n,i} + (m_{13})_{n,i}\, m_{z_{n,i}} \quad , \tag{3.171}$$

where m_2, m_3, m_{12} and m_{13} are given by eq.(3.140).

The solution of eq.(3.168) is accomplished in a Gauss-Seidel manner, such that variables upstream of $Q(x_n,z_i)$ are updated. Hence, by inserting eq.(3.171), eq.(3.168) can be written as

$$U^{(p)}_{e_n} = U^{(p-1)}_{I_n} + \sum_{k=1}^{n} d_{n,k}\left[U^{(p)}_{e_k}\,\delta^{*(p)}_k - U^{(p-1)}_{e_k}\,\delta^{*(p-1)}_k\right]$$

$$+ \sum_{k=1}^{n} e_{n,k}\left[m^{(p)}_{z_k} - m^{(p-1)}_{z_k}\right] \quad , \tag{3.172}$$

where

$$d_{n,k} = c_{n,k-1}\,\alpha_{k-1,3}\,(m_2)_{k-1} + c_{n,k}\left[(m_2)_k\,\alpha_{k,2} + (m_{12})_k\right] + c_{n,k+1}\,\alpha_{k+1,1}\,(m_2)_{k+1} \quad , \tag{3.173}$$

and

$$e_{n,k} = c_{n,k}\left[(m_3)_k\,\beta_{i,3} + (m_{13})_k\right] \quad . \tag{3.174}$$

Here $c_{n,k}$ denotes the element at n'th row and k'th column of $\underline{\underline{C}}$.
For simplicity, subscript 'i' has been omitted from the variables.
Eq.(3.172) can be rearranged as

$$U_{e_n}(1 - d_{n,n}\delta_n^*) - e_{n,n}\delta_n^*(\eta_e W_{e_n} - G_{e_n} W_{ref}) = K_n \quad , \quad (3.175)$$

where

$$K_n = \sum_{k=1}^{n-1} d_{n,k}\left[U_{e_k}^{(p)} \delta_k^{*(p)} - U_{e_k}^{(p-1)} \delta_k^{*(p-1)}\right]$$

$$+ \sum_{k=1}^{n-1} e_{n,k}\left[m_{z_k}^{(p)} - m_{z_k}^{(p-1)}\right]$$

$$- d_{n,n}\, U_{e_n}^{(p-1)} \delta_n^{*(p-1)} - e_{n,n}\, m_{z_n}^{(p-1)} + U_{I_n}^{(p-1)} \quad . \quad (3.176)$$

To perform an interactive boundary layer calculation, eq.(3.175) is employed as a boundary condition in addition to those given by eqs.(3.139a) and (3.139b).
This type of interaction is usually referred to as a quasi-simultaneous interaction procedure.

3.4.5 Numerical treatment of the boundary layer equations

As the boundary layer momentum equations are purely convective in planes parallel to the surface, the information of the flow propagates along the local stream directions. It is therefore required that the discretization scheme assures, that the information which yields the solution is taken from a domain, that has influence on the point calculated. Otherwise the so-called Courant-Friederichs-Lewey (CFL) condition may be violated with stability problems as a consequence.

Several numerical schemes can be used to solve the boundary layer equations, see for example the survey by Smith (1982), and in general it is necessary to use more than one scheme because of the stability restrictions. Furthermore, the CFL condition may restrict the size of the grid employed.

To overcome these limitations, Cebeci (1986) advocates the use of the characteristic difference scheme which is based on solving the governing equations along local streamlines. This scheme, however, is found to require three times as much computing time as a conventional Keller-box scheme (Smith, 1982).

In the present investigation minimizing the computing cost has been of crucial interest, therefore, despite its obvious advantages, the characteristic scheme was found to be too costly. Instead, depending on the flow properties considered, the solution will be based upon various versions of the box scheme. As compared with most other schemes, this scheme has the advantage of being second order accurate for arbitrarily varying step sizes.

In order to improve the solution procedure of the resulting non-linear difference equations, Newton's method is employed to make a full linearized formulation, which assures quadratic convergence of the iterations.

Discretization of the boundary layer equations

For conciseness only a brief discussion of the discretization procedures will be given here, whereas a detailed description, which covers the expressions of the fully discretized equations, are given in appendix B.

Here the mesh is defined by the nodepoints

$$x_n = x_{n-1} + k_{n-1} \quad , \quad n = 1,2, \ldots , N \quad , \qquad (3.177a)$$

$$\eta_j = \eta_{j-1} + h_{j-1} \quad , \quad j = 1,2, \ldots , J \quad , \qquad (3.177b)$$

$$z_i = z_{i-1} + r_{i-1} \quad , \quad i = 1,2, \ldots , I \quad , \qquad (3.177c)$$

where k_{n-1} , h_{j-1} and r_{i-1} denote the mesh sizes, and we seek the solution at (x_n,η_j,z_i) .

If the flow is attached, that is if $U > 0$, the standard Keller-box scheme is employed to approximate the equations. At a plane $\eta = \eta_{j-\frac{1}{2}}$ this is shown in fig. 3.10.

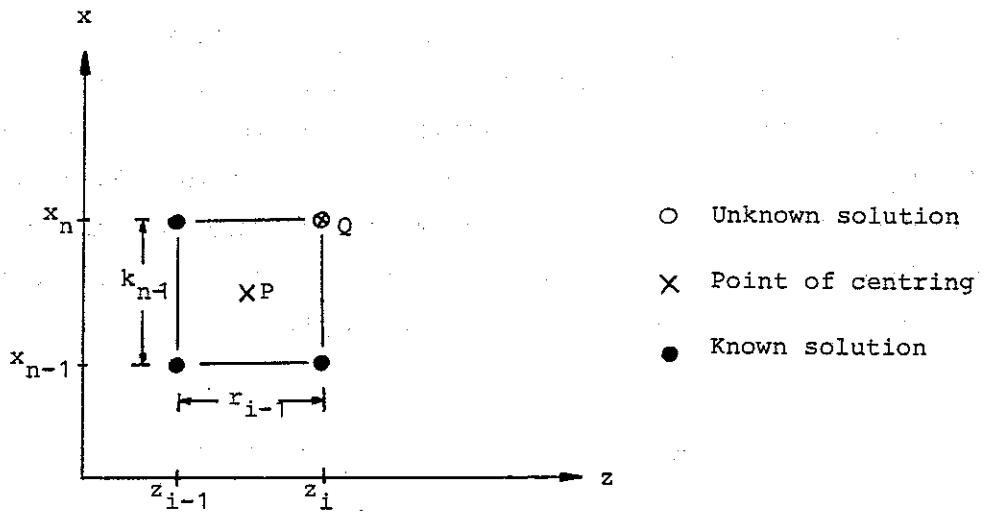

Fig. 3.10 Keller-box scheme at $\eta=\eta_{j-\frac{1}{2}}$

The boundary layer momentum equations are centred at $P(x_{n-\frac{1}{2}},\ \eta_{j-\frac{1}{2}},\ z_{i-\frac{1}{2}})$ and the derivatives are written as

$$\left[\frac{\partial(\ )}{\partial x}\right]_P = \frac{1}{2}\,k_{n-1}^{-1}\left[(\ )^{n,i} + (\ )^{n,i-1} - (\ )^{n-1,i} - (\ )^{n-1,i-1}\right]_{j-\frac{1}{2}}, \tag{3.178}$$

$$\left[\frac{\partial(\ )}{\partial z}\right]_P = \frac{1}{2}\,r_{i-1}^{-1}\left[(\ )^{n,i} + (\ )^{n-1,i} - (\ )^{n,i-1} - (\ )^{n-1,i-1}\right]_{j-\frac{1}{2}}, \tag{3.179}$$

$$\left[\frac{\partial(\ )}{\partial \eta}\right]_P = \frac{1}{2}\,h_{j-1}^{-1}\left[\frac{1}{2}(\ )_j^{n,i} + \frac{1}{2}(\ )_j^{n-1,i} + (\ )_j^{n-\frac{1}{2},i-1} - \frac{1}{2}(\ )_{j-1}^{n,i} - \frac{1}{2}(\ )_{j-1}^{n-1,i} - (\ )_{j-1}^{n-\frac{1}{2},i-1}\right], \tag{3.180}$$

and $(\ )_{j-\frac{1}{2}}^{n-\frac{1}{2},i-\frac{1}{2}}$ is taken as the average of the eight corner values.

The definition equations (3.137a) - (3.137d) are discretized by averaging about $Q(x_n, \eta_{j-\frac{1}{2}}, z_i)$. Thus, for example, eq.(3.137a) is written as

$$F_j^{n,i} - F_{j-1}^{n,i} - \frac{1}{2}\,h_{j-1}\left(U_j^{n,i} + U_{j-1}^{n,i}\right) = 0 \quad . \tag{3.181}$$

In order to avoid oscillations in the normal direction the variable E, which is related to the normal velocity component, is expressed in terms of its values at the four corner points of the η-plane (Bradshaw, Cebeci & Whitelaw, 1981). Thus $E_j^{n-\frac{1}{2},i-\frac{1}{2}} \equiv \frac{1}{4}\left(E_j^{n,i} + E_j^{n,i-1} + E_j^{n-1,i} + E_j^{n-1,i-1}\right)$ is taken as the unknown.

In the case of separated flows, i.e. for $U < 0$, it is required that the discretized equations contain information from downstream, since the marching direction is against the streamwise velocity. Therefore, in this case, we employ the zig-zag scheme which is shown in fig. 3.11.

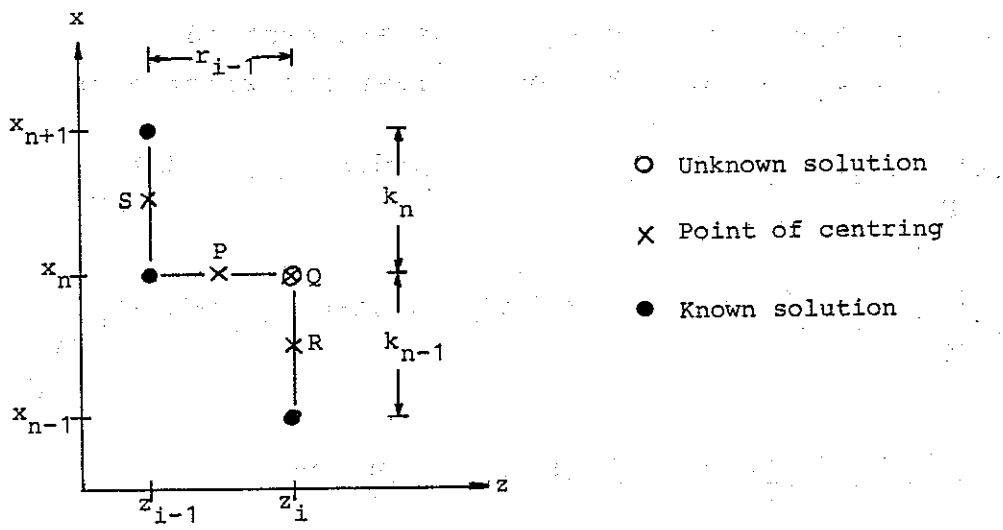

Fig. 3.11 Zig-zag scheme at $\eta=\eta_{j-\frac{1}{2}}$

As in the case of the Keller-box scheme the definition equations (3.137a) - (3.137d) are averaged about $Q(x_n,\eta_{j-\frac{1}{2}},z_i)$, whereas the remaining equations (3.138a) - (3.138c) are centred at $P(x_n,\eta_{j-\frac{1}{2}},z_{i-\frac{1}{2}})$. Here derivatives with respect to η and z are written as

$$\left[\frac{\partial(\ )}{\partial\eta}\right]_P = \frac{1}{2}\,h_{j-1}^{-1}\left[(\ )_j^{n,i} - (\ )_{j-1}^{n,i} + (\ )_j^{n,i-1} - (\ )_{j-1}^{n,i-1}\right] \tag{3.182}$$

and

$$\left[\frac{\partial(\ )}{\partial z}\right]_P = \frac{1}{2}\,r_{i-1}^{-1}\left[(\ )_j^{n,i} + (\ )_{j-1}^{n,i} - (\ )_j^{n,i-1} - (\ )_{j-1}^{n,i-1}\right] \tag{3.183}$$

In order to assure upstream influence the derivatives with respect to x at point $P(x_n,\eta_{j-\frac{1}{2}},z_{i-\frac{1}{2}})$ are taken as the weighted averages of the derivatives at $S(x_{n+\frac{1}{2}},\eta_{j-\frac{1}{2}},z_{i-1})$ and $R(x_{n-\frac{1}{2}},\eta_{j-\frac{1}{2}},z_i)$. That is, we take

$$\left[\frac{\partial(\ )}{\partial x}\right]_P = \theta_1\left[\frac{\partial(\ )}{\partial x}\right]_S + \theta_2\left[\frac{\partial(\ )}{\partial x}\right]_R \quad , \qquad (3.184a)$$

where

$$\left[\frac{\partial(\ )}{\partial x}\right]_S = k_n^{-1}\left[(\ )^{n+1,i-1} - (\ )^{n,i-1}\right]_{j-\frac{1}{2}}, \qquad (3.184b)$$

and

$$\left[\frac{\partial(\ )}{\partial x}\right]_R = k_{n-1}^{-1}\left[(\ )^{n,i} - (\ )^{n-1,i}\right]_{j-\frac{1}{2}} \quad . \qquad (3.184c)$$

The weighting coefficients are given as

$$\theta_1 = \frac{x_n - x_{n-1}}{x_{n+1} - x_{n-1}} \quad , \qquad (1.385a)$$

and

$$\theta_2 = \frac{x_{n+1} - x_n}{x_{n+1} - x_{n-1}} \quad . \qquad (3.185b)$$

As in the case of the standard box scheme the variable E is expressed in terms of its values at the corner points; i.e. $E_j^{n,i-\frac{1}{2}} = \frac{1}{2}\left(E_j^{n,i} + E_j^{n,i-1}\right)$ is taken as the unknown.

Cast into a compact notation, it is appropriate to write the discretized equations as

$$F_j - F_{j-1} - \frac{1}{2}\,h_{j-1}(U_j + U_{j-1}) = 0 \quad , \qquad (3.186a)$$

$$G_j - G_{j-1} - \frac{1}{2}\,h_{j-1}(W_j + W_{j-1}) = 0 \quad , \qquad (3.186b)$$

$$P_{j-\frac{1}{2}}^{n-\frac{1}{2},i-\frac{1}{2}}\left(U_j,U_{j-1},W_j,W_{j-1},V_j,V_{j-1},T_j,T_{j-1},E_j,E_{j-1},U_e,\delta^*,T_w,V_w\right) = 0 \quad , \qquad (3.186c)$$

$$Q_{j-\frac{1}{2}}^{n-\frac{1}{2},i-\frac{1}{2}}\left(U_j,U_{j-1},W_j,W_{j-1},V_j,V_{j-1},T_j,T_{j-1},E_j,E_{j-1},U_e,\delta^*,T_w,V_w\right) = 0 \quad , \qquad (3.186d)$$

$$S_{j-\frac{1}{2}}^{n-\frac{1}{2},i-\frac{1}{2}}\left(U_j,U_{j-1},W_j,W_{j-1},E_j,E_{j-1},U_e,\delta^*\right) = 0 \quad , \qquad (3.186e)$$

$$U_j - U_{j-1} - \frac{1}{2} h_{j-1}\left(V_j + V_{j-1}\right) = 0 \quad , \qquad (3.186f)$$

$$W_j - W_{j-1} - \frac{1}{2} h_{j-1}\left(T_j + T_{j-1}\right) = 0 \quad , \qquad (3.186g)$$

where $P_{j-\frac{1}{2}}^{n-\frac{1}{2},i-\frac{1}{2}}$, $Q_{j-\frac{1}{2}}^{n-\frac{1}{2},i-\frac{1}{2}}$, and $S_{j-\frac{1}{2}}^{n-\frac{1}{2},i-\frac{1}{2}}$ denote the difference operators of the discretized momentum equations (3.138a), (3.138b), and (3.138c), respectively, and eqs. (3.186a) - (3.186b) and eqs. (3.186f) - (3.186g) define the approximated definition equations (3.137a) - (3.137d).

Solved by a direct or inverse method the equations are subject to the boundary conditions

$$\eta = 0 \quad : F_o = G_o = U_o = W_o = E_o = 0, \; T_w = T_o, \; V_w = V_o \; . \qquad (3.187a)$$

$$\eta = \eta_J \; : \quad U_J = 1 \quad , \quad W_j = \frac{W_e}{W_{ref}} \quad , \quad F_J = \eta_j - 1 \; . \qquad (3.187b)$$

To perform a quasi-simultaneous boundary layer calculation, both U_e and δ^* are taken as unknowns and an additional boundary condition is introduced as

$$U_e\left(1 - d_{n,n}\delta^*\right) - e_{n,n}\delta^*\left(\eta_J W_e - G_J W_{ref}\right) = K_n \quad , \qquad (3.187c)$$

where $d_{n,n}$, $e_{n,n}$ and K_n are defined by eqs. (3.173), (3.174) and (3.176), respectively.

At a specific boundary layer station, (x_n, z_i), eqs. (3.186a) - (3.186g) and eqs. (3.187a) - (3.187c) define a non-linear two-point boundary value problem with the unknown boundary layer variables F_j, G_j, U_j, W_j, V_j, T_j and E_j, $j = 1,2, \ldots , J$, and the unknown global variables U_e, δ^*, T_w and V_w . Note that the wall shear parameters T_w and V_w appear explicitly in the momentum equations because we want to linearize the discretized equations with Newton's method.

Linearization: Newton's method

The solution of eqs. (3.186) - (3.187) is carried out iteratevely by employing Newton's method to linearize the equations. This method, which has the advantage of assuring quadratic convergence, proceeds in general as follows:

Let $\underline{\Gamma} = (\gamma_1, \gamma_2, \ldots, \gamma_N)$ at N node points represent the difference approximations to a non-linear differential equation, we then seek a vector $\omega = (\omega_1, \omega_2, \ldots, \omega_N)$ which satisfies the difference approximations. Thus, we seek a solution to the non-linear problem

$$\underline{\Gamma}(\underline{\omega}) = \underline{0} \quad , \tag{3.188}$$

and we want, based on an initial approximation $\underline{\omega}^{(o)}$ to the sought solution $\underline{\omega}$, to determine a convergence serie $\underline{\omega}^{(o)}, \underline{\omega}^{(1)}, \ldots, \underline{\omega}^{(\nu)}$ which is stationary for $\nu \to \infty$, and which satisfies the expression

$$\underline{\Gamma}(\underline{\omega}^{(\nu)}) = \underline{0} \quad \text{for} \quad \nu \to \infty \quad . \tag{3.189}$$

If the initial guess $\underline{\omega}^{(o)}$ is within the convergence radius, it can be demonstrated that quadratic convergence is obtained if eq.(3.189) is replaced by the linear system of equations

$$\underline{\underline{J}}_{\Gamma}^{(\nu)} \Delta\underline{\omega}^{(\nu)} = - \underline{\Gamma}^{(\nu)} \quad , \tag{3.190}$$

where the iterate $\Delta\underline{\omega}^{(\nu)}$ denotes the solution step and $\underline{\underline{J}}_{\Gamma}^{(\nu)}$ defines the jacobian for the system, and the next iterand is given by

$$\underline{\omega}^{(\nu+1)} = \underline{\omega}^{(\nu)} + \Delta\underline{\omega}^{(\nu)} \quad . \tag{3.191}$$

The jacobian is obtained by differentiating the components of the residue vector $\underline{\Gamma}^{(\nu)}$ with respect to each component of the solution vector $\underline{\omega}^{(\nu)}$.

Employing Newton's method on the present problem, at a specific boundary layer station the approximated equations are written as

$$\Delta F_j - \Delta F_{j-1} - \frac{1}{2} h_{j-1}(\Delta U_j + \Delta U_{j-1}) = (r_1)_j \quad , \quad (3.192a)$$

$$\Delta G_j - \Delta G_{j-1} - \frac{1}{2} h_{j-1}(\Delta W_j + \Delta W_{j-1}) = (r_2)_j \quad , \quad (3.192b)$$

$$(s_1)_j \Delta U_j + (s_2)_j \Delta U_{j-1} + (s_3)_j \Delta W_j + (s_4)_j \Delta W_{j-1} + (s_5)_j \Delta V_j$$
$$+ (s_6)_j \Delta V_{j-1} + (s_7)_j \Delta T_j + (s_8)_j \Delta T_{j-1} + (s_9)_j \Delta E_j + (s_{10})_j \Delta E_{j-1}$$
$$= (r_3)_j - (p_3)_j \Delta U_e - (q_3)_j \Delta\delta^* - (v_3)_j \Delta V_w - (t_3)_j \Delta T_w \quad , \quad (3.192c)$$

$$(s_{11})_j \Delta U_j + (s_{12})_j \Delta U_{j-1} + (s_{13})_j \Delta W_j + (s_{14})_j \Delta W_{j-1} + (s_{15})_j \Delta V_j$$
$$+ (s_{16})_j \Delta V_{j-1} + (s_{17})_j \Delta T_j + (s_{18})_j \Delta T_{j-1} + (s_{19})_j \Delta E_j + (s_{20})_j \Delta E_{j-1}$$
$$= (r_4)_j - (p_4)_j \Delta U_e - (q_4)_j \Delta\delta^* - (v_4)_j \Delta V_w - (t_4)_j \Delta T_w \quad , \quad (3.192d)$$

$$(s_{21})_j \Delta U_j + (s_{22})_j \Delta U_{j-1} + (s_{23})_j \Delta W_j + (s_{24})_j \Delta W_{j-1}$$
$$+ (s_{25})_j \Delta E_j + (s_{26})_j \Delta E_{j-1} = (r_5)_j - (p_5)_j \Delta U_e - (q_5)_j \Delta\delta^* \quad , \quad (3.192e)$$

$$\Delta U_j - \Delta U_{j-1} - \frac{1}{2} h_{j-1}(\Delta V_j + \Delta V_{j-1}) = (r_6)_{j-1} \quad , \quad (3.192f)$$

$$\Delta W_j - \Delta W_{j-1} - \frac{1}{2} h_{j-1}(\Delta T_j + \Delta T_{j-1}) = (r_7)_{j-1} \quad . \quad (3.192g)$$

Here for convenience the superscript ν in Δ quantities have been omitted.

The coefficients $(s_1)_j - (_{26})_j$, $(p_3)_j - (p_5)_j$, $(q_3)_j - (q_5)_j$, $(v_3)_j - (v_4)_j$ and $(t_3)_j - (t_4)_j$ represent the non-zero elements of the jacobian. Thus, for example,

$$(s_1)_j = \frac{\partial P_{j-\frac{1}{2}}^{n-\frac{1}{2},i-\frac{1}{2}}}{\partial U_j} \quad , \quad (s_2)_j = \frac{\partial P_{j-\frac{1}{2}}^{n-\frac{1}{2},i-\frac{1}{2}}}{\partial U_{j-1}} \quad , \quad (p_3)_j = \frac{\partial P_{j-\frac{1}{2}}^{n-\frac{1}{2},i-\frac{1}{2}}}{\partial U_e} \quad ,$$

$$(v_4)_j = \frac{\partial Q_{j-\frac{1}{2}}^{n-\frac{1}{2},i-\frac{1}{2}}}{\partial V_w} \quad , \text{ etc.}$$

The residues $(r_1)_j - (r_7)_j$ are defined by

$$(r_1)_j = F_{j-1} - F_j + \frac{1}{2} h_{j-1}(U_j + U_{j-1}) \quad , \quad (3.193a)$$

$$(r_2)_j = G_{j-1} - G_j + \frac{1}{2} h_{j-1}(W_j + W_{j-1}) \quad , \quad (3.193b)$$

$$(r_3)_j = - P^{n-\frac{1}{2},i-\frac{1}{2}}_{j-\frac{1}{2}} \quad , \quad (3.193c)$$

$$(r_4)_j = - Q^{n-\frac{1}{2},i-\frac{1}{2}}_{j-\frac{1}{2}} \quad , \quad (3.193d)$$

$$(r_5)_j = - S^{n-\frac{1}{2},i-\frac{1}{2}}_{j-\frac{1}{2}} \quad , \quad (3.193e)$$

$$(r_6)_{j-1} = U_{j-1} - U_j + \frac{1}{2} h_{j-1}(V_j + V_{j-1}) \quad , \quad (3.193f)$$

$$(r_7)_{j-1} = W_{j-1} - W_j + \frac{1}{2} h_{j-1}(T_j + T_{j-1}) \quad . \quad (3.193g)$$

The boundary conditions eq.(3.187) become

$$\Delta F_o = \Delta G_o = \Delta U_o = \Delta W_o = \Delta E_o = 0 \quad , \quad (3.194a)$$

$$\Delta U_J = 0 \quad , \quad \Delta W_j = \frac{W_e}{W_{ref}} - W_J \quad , \quad (3.194b)$$

$$\Delta F_J = \eta_J - 1 - F_J \quad , \quad (3.194c)$$

$$\Delta T_w = T_o - T_w \quad , \quad \Delta V_w = V_o - V_w \quad , \quad (3.194d)$$

and, if a quasi-simultaneous boundary layer calculation is being performed,

$$[1 - d_{n,n}\delta^*]\Delta U_e - [d_{n,n}U_e + e_{n,n}(\eta_J W_e - G_J W_{ref})]\Delta\delta^* + e_{n,n}W_{ref}\delta^*\Delta G_j = - U_e(1 - d_{n,n}\delta^*) - e_{n,n}m_z + K_n \quad . \quad (3.194e)$$

To solve the linear system of equations, it is useful to observe that it can be put into a block tridiagonal form:

$$\underline{\underline{A}}_o\underline{\delta}_o + \underline{\underline{C}}_o\underline{\delta}_1 = \underline{r}_o \quad ,$$

$$\underline{\underline{B}}_j\underline{\delta}_{j-1} + \underline{\underline{A}}_j\underline{\delta}_j + \underline{\underline{C}}_j\underline{\delta}_{j+1} = \underline{r}_j - \underline{p}_j\Delta U_e - \underline{q}_j\Delta\delta^* - \underline{v}_j\Delta V_w - \underline{t}_j\Delta T_w \quad ,$$

$$j = 1,2, \ldots , N-1$$

$$\underline{\underline{B}}_J\underline{\delta}_{J-1} + \underline{\underline{A}}_J\underline{\delta}_J = \underline{r}_J - \underline{p}_J\Delta U_e - \underline{q}_J\Delta\delta^* - \underline{v}_J\Delta V_w - \underline{t}_J\Delta T_w \quad ,$$

(3.195a)-(3.195c)

where the boundary layer iterates are given as

$$\underline{\delta}_j = [\Delta F_j, \Delta G_j, \Delta U_j, \Delta W_j, \Delta E_j, \Delta V_j, \Delta T_j] \quad , \quad j = 0,1,2, \ldots , J \, . \tag{3.196}$$

The influence coefficients to the global iterates are written as

$$\underline{p}_j = [0,0,(p_3)_j,(p_4)_j,(p_5)_j,0,0], \; j = 1,2, \ldots ,J,$$

$$\underline{q}_j = [0,0,(q_3)_j,(q_4)_j,(q_5)_j,0,0], \; j = 1,2, \ldots ,J,$$

$$\underline{v}_j = [0,0,(v_3)_j,(v_4)_j,0,0,0] \quad , \; j = 1,2, \ldots ,J$$

$$\underline{t}_j = [0,0,(t_3)_j,(t_4)_j,0,0,0] \quad , \; j = 1,2, \ldots ,J,$$

(3.197a)-(3.197d)

and the residue vector as

$$\underline{r}_j = [(r_1)_j,(r_2)_j,(r_3)_j,(r_4)_j,(r_5)_j,(r_6)_j,(r_7)_j] \, , \quad j = 0,1,2, \ldots , J \, . \tag{3.198}$$

The components of the 7×7 matrices $[\underline{\underline{A}}_j,\underline{\underline{B}}_j,\underline{\underline{C}}_j]$ are readily obtained by inspection of the equations. They are given explictly in Appendix C.

Note here that the boundary conditions at the wall eq.(3.194a) are imposed directly into the equations as the first five rows of eq.(3.195a), and, similarily, the boundary conditions at the edge of the boundary layer eq.(3.194b) define the last two rows of eq.(3.195c).

$$
\begin{bmatrix}
\underline{\underline{A}}_0 & \underline{\underline{C}}_0 & & & & \\
\underline{\underline{B}}_1 & \underline{\underline{A}}_1 & \underline{\underline{C}}_1 & & & \\
 & \ddots & \ddots & \ddots & & \\
 & & \underline{\underline{B}}_j & \underline{\underline{A}}_j & \underline{\underline{C}}_j & \\
 & & & \ddots & \ddots & \ddots \\
 & & & & \underline{\underline{B}}_{J-1} & \underline{\underline{A}}_{J-1} & \underline{\underline{C}}_{J-1} \\
 & & & & & \underline{\underline{B}}_J & \underline{\underline{A}}_J
\end{bmatrix}
\begin{Bmatrix}
\underline{\delta}_0 \\ \underline{\delta}_1 \\ \vdots \\ \underline{\delta}_j \\ \vdots \\ \underline{\delta}_{J-1} \\ \underline{\delta}_J
\end{Bmatrix} =
$$

$$
\begin{Bmatrix}
\underline{r}_0 \\ \underline{r}_1 \\ \vdots \\ \underline{r}_j \\ \vdots \\ \underline{r}_{J-1} \\ \underline{r}_J
\end{Bmatrix}
- \Delta U_e
\begin{Bmatrix}
\underline{p}_0 \\ \underline{p}_1 \\ \vdots \\ \underline{p}_j \\ \vdots \\ \underline{p}_{J-1} \\ \underline{p}_J
\end{Bmatrix}
- \Delta\delta^*
\begin{Bmatrix}
\underline{q}_0 \\ \underline{q}_1 \\ \vdots \\ \underline{q}_j \\ \vdots \\ \underline{q}_{J-1} \\ \underline{q}_J
\end{Bmatrix}
- \Delta V_w
\begin{Bmatrix}
\underline{v}_0 \\ \underline{v}_1 \\ \vdots \\ \underline{v}_j \\ \vdots \\ v_{J-1} \\ \underline{v}_J
\end{Bmatrix}
- \Delta T_w
\begin{Bmatrix}
\underline{t}_0 \\ \underline{t}_1 \\ \vdots \\ \underline{t}_j \\ \vdots \\ t_{J-1} \\ \underline{t}_J
\end{Bmatrix}
\qquad (3.199)
$$

Thus, it is seen that the system of linearized equations (3.199) define a multiple eigenvalue problem which has a block tridiagonal structure.

Block_elimination_procedure

For each vector on the right-hand side of eq.(3.199) the solution is obtained by a block elimination method. Thus, for a given right-hand side vector $\underline{Y} = [\underline{Y}_o, \underline{Y}_1, \ldots, \underline{Y}_J]$, eq.(3.199) is written as

$$[\underline{\underline{B}}_j , \underline{\underline{A}}_j , \underline{\underline{C}}_j]\underline{\Delta} = \underline{Y} \quad , \tag{3.200}$$

where the solution vector $\underline{\Delta} = [\underline{\delta}_o, \underline{\delta}_1, \ldots, \underline{\delta}_J]$, and we seek a factorization of the form

$$[\underline{\underline{B}}_j , \underline{\underline{A}}_j , \underline{\underline{C}}_j] = \underline{\underline{L}}\ \underline{\underline{U}} \quad , \tag{3.201a}$$

where
$$\underline{\underline{L}} = [\underline{\underline{\Omega}}_j , \underline{\underline{\Psi}} , \underline{\underline{0}}] \tag{3.201b}$$

is a block-lower triangular matrix

and
$$\underline{\underline{U}} = [\underline{\underline{0}} , \underline{\underline{\Lambda}}_j , \underline{\underline{\Gamma}}_j] \tag{3.201c}$$

is a block-upper triangular matrix.

As discussed by Keller (1974) the factorization is not uniquely determined by eqs.(3.201a) - (3.201c).
However, a factorization scheme, which in all cases has existence and is unique, is obtained by letting

$$\underline{\underline{\Psi}}_j = \underline{\underline{I}} \quad , \tag{3.202a}$$

and
$$\underline{\underline{\Gamma}}_j = \underline{\underline{C}}_j \quad , \tag{3.202b}$$

Hence we get

$$\underline{\underline{L}} = [\underline{\underline{\Omega}}_j , \underline{\underline{I}} , \underline{\underline{0}}] \tag{3.203a}$$

$$\underline{\underline{U}} = [\underline{\underline{0}} , \underline{\underline{\Lambda}}_j , \underline{\underline{C}}_j] \tag{3.203b}$$

By inspection of eq.(3.201a) and eqs.(3.203a) - (3.203b) the factorization is given by the following recursion formulas

$$\underline{\underline{\Lambda}}_o = \underline{\underline{A}}_o \quad , \tag{3.204a}$$

$$\underline{\underline{\Omega}}_j \underline{\underline{\Lambda}}_{j-1} = \underline{\underline{B}}_j \quad , \quad 1 \leq j \leq J \tag{3.204b}$$

$$\underline{\underline{\Lambda}}_j = \underline{\underline{A}}_j - \underline{\underline{\Omega}}_j \underline{\underline{C}}_{j-1} \quad , \quad 1 \leq j \leq J \tag{3.204c}$$

From eq.(3.204b) it follows that the first two columns and the last two rows of $\underline{\underline{\Omega}}_j$ are identical to the ones of $\underline{\underline{B}}_j$, and from eq.(3.204c) it is seen that the elements of the first two columns and the last two rows of $\underline{\underline{\Lambda}}_j$ correspond to the ones of $\underline{\underline{A}}_j$. Consequently the factorization is accomplished by solving eqs.(3.204a) - (3.204b) for the $2\times(5\times5)\times J$ unknown elements of $\underline{\underline{\Lambda}}_j$ and $\underline{\underline{\Omega}}_j$, $1 \leq j \leq J$.

The solution of eq.(3.200) is obtained in two steps. The first, referred to as the forward sweep, is given by the solution of the system of equations

$$\underline{\underline{L}}\ \underline{Z} = \underline{Y} \quad , \tag{3.205a}$$

where $\underline{Z} = [\underline{z}_o, \underline{z}_1, \ \cdots\ , \underline{z}_J]$, and the second step, referred to as the backward sweep, defines the resulting solution as

$$\underline{\underline{U}}\ \underline{\Delta} = \underline{Z} \quad . \tag{3.205b}$$

Inserting eq.(3.203a) into eq.(3.205a), in the forward sweep, $\underline{Z}$ is computed from the following recursion formulas

$$\underline{z}_o = \underline{Y}_o \quad , \tag{3.206a}$$

$$\underline{z}_j = \underline{Y}_j - \underline{\underline{\Omega}}_j \underline{z}_{j-1} \quad , \quad 1 \leq j \leq J \ . \tag{3.206b}$$

Combining eq.(3.203b) and eq.(3.205b), the sought solution $\underline{\delta}_j$ is in the backward sweep obtained from the recursion formulas

$$\underline{\underline{\Lambda}}_J \underline{\delta}_J = \underline{z}_J \tag{3.207a}$$

$$\underline{\underline{\Lambda}}_j \underline{\delta}_j = \underline{z}_j - \underline{\underline{C}}_j \underline{\delta}_{j+1}, \quad J-1 \geq j \geq 0 \ . \tag{3.207b}$$

Solution of the multiple eigenvalue problem and the corresponding boundary conditions

After eq.(3.199) is solved with the block factorization algorithm, the multiple eigenvalue problem is written as

$$\underline{\delta}_j = \hat{\underline{r}}_j - \Delta U_e \hat{\underline{p}}_j - \Delta\delta^* \hat{\underline{q}}_j - \Delta V_w \hat{\underline{v}}_j - \Delta T_w \hat{\underline{t}}_j \quad , \quad 0 \leq j \leq J \quad , \tag{3.208}$$

where vectors denoted by $(\hat{})$ refer to the solution of the right-hand side vectors of eq.(3.199). To obtain the four global unknown iterates ΔU_e , $\Delta\delta^*$, ΔV_w and ΔT_w , eq.(3.208) is combined with the boundary conditions eqs.(3.194c) - (3.194e). Thus we get

$$\Delta F_J = (\hat{r}_1)_J - \Delta U_e(\hat{p}_1)_J - \Delta\delta^*(\hat{q}_1)_J - \Delta V_w(\hat{v}_1)_J - \Delta T_w(\hat{t}_1)_J \quad , \tag{3.209a}$$

$$\Delta G_J = (\hat{r}_2)_J - \Delta U_e(\hat{p}_2)_J - \Delta\delta^*(\hat{q}_2)_J - \Delta V_w(\hat{v}_2)_J - \Delta T_w(\hat{t}_2)_J \quad , \tag{3.209b}$$

$$\Delta V_o = (\hat{r}_6)_o - \Delta U_e(\hat{p}_6)_o - \Delta\delta^*(\hat{q}_6)_o - \Delta V_w(\hat{v}_6)_o - \Delta T_w(\hat{t}_6)_o \quad , \tag{3.209c}$$

$$\Delta T_o = (\hat{r}_7)_o - \Delta U_e(\hat{p}_7)_o - \Delta\delta^*(\hat{q}_7)_o - \Delta V_w(\hat{v}_7)_o - \Delta T_w(\hat{t}_7)_o \quad , \tag{3.209d}$$

$$\Delta F_J = \eta_J - 1 - F_J \quad , \tag{3.209e}$$

$$\Delta V_o = \Delta V_w \quad , \tag{3.209f}$$

$$\Delta T_o = \Delta T_w \quad , \tag{3.209g}$$

$$a_1 \Delta U_e + a_2 \Delta\delta^* + a_3 \Delta G_J = a_4 \quad , \tag{3.209h}$$

where

$$a_1 = 1 - d_{n,n}\delta^* \quad , \tag{3.210a}$$

$$a_2 = -[d_{n,n}U_e + e_{n,n}(\eta_J W_e - G_J W_{ref})\beta] \quad , \tag{3.210b}$$

$$a_3 = e_{n,n} W_{ref} \delta^* \beta \quad , \tag{3.210c}$$

$$a_4 = -U_e(1 - d_{n,n}\delta^*) + K_n - e_{n,n} m_z \beta \quad , \tag{3.210d}$$

where β is a coefficient which takes the value $\beta = 0$ if the infinite-swept-wing equations are being solved and $\beta = 1$ if the general three-dimensional equations are being solved.

Combining eqs.(3.209a) - (3.209h) yields

$$(\hat{p}_1)_J \Delta U_e + (\hat{q}_1)_J \Delta\delta^* + (\hat{v}_1)_J \Delta V_w + (\hat{t}_1)_J \Delta T_w = (\hat{r}_1)_J - \eta_J + 1 + F_J,$$

$$(\hat{p}_6)_o \Delta U_e + (\hat{q}_6)_o \Delta\delta^* + [1 + (\hat{v}_6)_o] \Delta V_w + (\hat{t}_6)_o \Delta T_w = (\hat{r}_6)_o ,$$

$$(\hat{p}_7)_o \Delta U_e + (\hat{q}_7)_o \Delta\delta^* + (\hat{v}_7)_o \Delta V_w + [1 + (\hat{t}_7)_o] \Delta T_w = (\hat{r}_7)_o ,$$

$$[a_1 - a_3(\hat{p}_2)_J] \Delta U_e + [a_2 - a_3(\hat{q}_2)_J] \Delta\delta^* - a_3(\hat{v}_2)_J \Delta V_w - a_3(\hat{t}_2)_J \Delta T_w = a_4 - a_3(\hat{r}_2)_J$$

(3.211a) - (3.211d)

If a turbulent boundary layer flow is solved by a quasi-simultaneous method, the global unknown iterates are obtained by solving the complete system of equations (3.211a) - (3.211d). If the flow is laminar, however, $\Delta V_w = \Delta T_w = 0$ and the solution is obtained by neglecting eqs.(3.211b) - (3.211c) and solving eqs.(3.211a) and (3.211d) for ΔU_e and $\Delta\delta^*$. Furthermore, if a direct method or an inverse method is employed, eq.(3.211d) is neglected and the remaining equations are solved for $\Delta\delta^*$ in the direct method and for ΔU_e in the inverse method. In the former we put $\Delta U_e = 0$ and in the latter we set $\Delta\delta^* = 0$.

After solving eqs. (3.211a)-(3.211d), the boundary layer iterates are obtained by inserting the global iterates in eq. (3.208). Updated iterates are given by eq. (3.191). A measure of the convergence progress is obtained by the relative stepsize, which here is taken as the ratio between the 2-norms of the boundary layer iterates and the boundary layer iterates. Thus for a specific boundary layer variable, for example F, the relative stepsize is given as

$$R_F = \left[\sum_{j=1}^{J} (\Delta F_j)^2 / \sum_{j=1}^{J} F_j^2 \right]^{\frac{1}{2}} \quad . \qquad (3.212)$$

Calculating the corresponding relative stepsizes for the remaining variables, convergence is said to be obtained when

$$\max\{R_F, R_G, R_u, R_w, R_E, R_v, R_T\} \leq \varepsilon \quad . \qquad (3.213)$$

Here ε is taken as $\varepsilon = 10^{-6}$.

Upwinding and FLARE

As the boundary layer equations are of the parabolic type one encounters numerical problems when marching against the streamwise velocity. These problems occur in regions with separated flows where it is required that information is transferred from downstream in order to accomplish a proper solution. In the two-dimensional case these problems are usually circumvented by employing the FLARE approximation (Reyhner & Flügge-Lotz, 1968), which is made by neglecting the streamwise convective term in the z-momentum equation. In the case of the infinite-swept-wing equations, it is furthermore found necessary to employ the FLARE approximation on the streamwise term of the z-momentum equation, if stable solutions are to be obtained. Consequently, the streamwise convective terms of eq.(3.115b) and eq.(3.115c) are replaced by $\lambda \frac{u}{h_1} \frac{\partial u}{\partial x}$ and $\lambda \frac{u}{h_1} \frac{\partial w}{\partial x}$, where

$$\lambda = \begin{cases} 1 & \text{for } u \geq 0 \\ 0 & \text{for } u < 0 \end{cases} \qquad (3.214)$$

As discussed by Cebeci (1986), in the three-dimensional case, it is required that the information is taken from a domain which has an influence on the point calculated. Otherwise the CFL condition may be violated. In general, when using the box scheme or the zig-zag scheme, this demand can only be satisfied in regions of separated flows if a very fine spacing of the z = constant coordinates is employed. As such a fine spacing would imply that the computing cost would be

prohibitively expensive, the FLARE approximation was also employed in the three-dimensional boundary layer equations. Consequently, the box scheme is used when calculating attached flows, and the zig-zag scheme subject to the FLARE approximation is employed when calculating separated flows. Even when using a relatively coarse z-spacing, no numerical problems encountered using this procedure.

When performing an interactive viscous/inviscid procedure, the use of the box scheme has a serious drawback in that it permits the occurence of streamwise wiggles with little tendency to damp out. Therefore an upwind correction is introduced to suppres the oscillations. According to Radwan & Lekondis (1984), such a correction may work as follows: If we call B the station where the boundary-layer quantities are known, C the station before it, and A the station we are solving for, the box scheme approximates the equations by using the midpoint between A and B. In the modified scheme, however, the boundary layer quantities, say q, at B are replaced by

$$q_B = r\, q_C + (1-r)\, q_B \quad , \tag{3.215}$$

where r is an upwinding parameter between zero and one. It should be noted, however, that the use of eq.(3.215) makes the scheme formally first-order accurate and a three-point scheme in the marching direction (Radwan & Lekoudis, 1984). When solving the infinite-swept-wing equations a value of $r = 0.3$ was employed and in the general three-dimensional case $r = 0.2$ was used.

3.5 Solution procedure of the complete interactive problem

As mentioned in the introduction to this section the developed computational model describes the complete flow field in three levels or zones. In the previous subsections a detailed description of the numerical treatment of the equations governing each zone has been presented.

As these equations mutually influence each other through the boundary conditions, the overall solution has to be established iteratively. Ideally, a iterative procedure may proceed as follows.

First, the distribution of induced velocities w_i , for example, are determined from eq.(3.37) by using tabulated empirical airfoil data. This distribution is then employed to determine the distribution of onset flow velocities and the angles of attack which define the inflow conditions to the inviscid near-field. Next, eq.(3.94) is employed to determine the velocities of the inviscid flow field. These velocities, in turn, are taken as the boundary condition to the boundary layer equations, and, after performing a complete iterative cycle between the interactive boundary layer equations and the inviscid flow equations, a new distribution of induced velocities are obtained from eq.(3.37).
An iterative procedure like that, however, would be very computing consuming. As a consequence the calculation of the induced velocities are decoupled from the overall iteration and as such are calculated once for all from empirical two-dimensional airfoil data.

At small wind velocities it is expected that the difference between the loading from the empirical two-dimensional data and the actual calculated loading is small. With the rotor running at high wind velocities, where the difference between the two-dimensional loading and the calculated loading is expected to be large, the induced velocities are small, due to the rapid shedding of the wake vorticies. Consequently, it is expected that the decoupling does not alter the accuracy of the overall calculation noticeably.

3.5.1 The grid

It is of crucial importance that the grid employed resolves the main characteristics of the solution which is to be obtained. Thus, it is clear that a fine grid spacing is provided in regions where the gradients of the variables are large.

In the η-direction, normal to the surface, a nonuniform grid is generated as suggested by Bradshaw, Cebeci and Whitelaw (1981). This grid is made up of a geometric progression with the property that the ratio of lengths of any two adjacent interval is constant. Thus the step length at $\eta = \eta_j$ is given as

$$\Delta\eta_j = K\,\Delta\eta_{j-1} \quad , \tag{3.216}$$

where $K > 1$ is the ratio of two succesive steps.

The grid is completely defined when the length of the first step $\Delta\eta_1$ is determined.

The total number of grid points are calculated as

$$J = \ell n[1 + (K-1)\eta_e/\Delta\eta_1]/\ell nK \quad , \tag{3.217}$$

and the distance to the j^{th} line is given by

$$\eta_j = \Delta\eta_1 (K^j - 1)/(K-1) \quad . \tag{3.218}$$

In fig.3.12, eqs.(3.217) and (3.218) are represented as curves.

In the present case the calculation of the boundary layer proceeded up to $\eta_e = 12$. Chosing the values $\Delta\eta_1 = 0.002$ and $K = 1.12$ a total number of 60 grid points was employed.

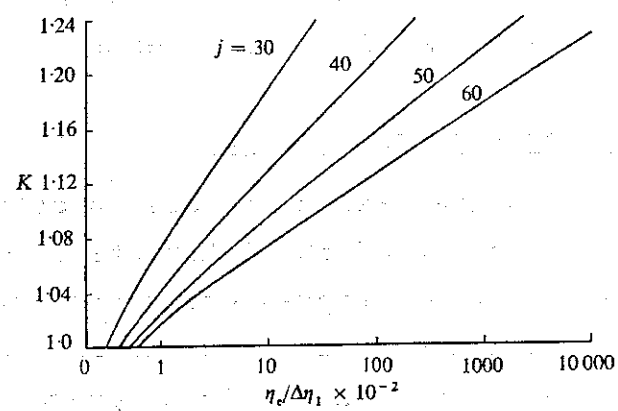

Fig. 3.12 Variation of K with $\Delta\eta_1$ for different η_e-values. (taken from Bradshaw, Cebeci & Whitelaw, 1981).

In the x-direction an amount of 160 coordinate points were used, with 100 on the upper surface and 60 on the lower surface of an airfoil cross-section. If fewer points were employed on the upper surface, oscillations in the solution occured in the neighbourhood of the separation point. The points on the airfoil were distributed with a fine spacing near the leading and trailing edges, and somewhat coarse in between.

For the spacing of the grid in the spanwise z-direction it may seem reasonable to take the distribution of the angles of attack as a guide. By doing this one would obtain a fine grid in regions where the variation of the angle of attack is large and a more coarse grid where the variation is small. However, it was found that such a spacing would demand a new grid to be generated for each wind velocity calculated, due to the nonlinearity of the induced velocities. Therefore an equidistant grid spacing was employed. Using an amount of 70 cross-sections it was assured that the variation of the angle of attack, when marching from one cross-section to the next, never exceeded a half degree.

Totally, the grid consists of $160 \times 60 \times 70 = 672000$ grid points.

To determine the geometric coefficients, eqs.(3.140b)-(3.140n), the wing surface was fitted with cubic splines. These were used to interpolate the values of the coordinates and the derivates necessary to determine the geometric coefficients.

3.5.2 Viscous-inviscid interaction procedure

As discussed in section 2 a quasi-simultaneous interaction consists of a cyclic calculation of the interactive boundary layer equations and the equations representing the inviscid domain. In order to increase the rate of convergence an over-relaxation scheme has been incorporated. This scheme uses a formula of the type as employed by Lee & Pletcher (1985).

The updating procedure takes the form

$$v_{Iw}^{(n)} = v_{Iw}^{(n-1)}\left\{1 + \omega\left[\left(\frac{q_e^{(n)}}{q_{Ie}^{(n-1)}}\right)^b - 1\right]\right\} \quad , \qquad (3.219)$$

where v_{Iw} is the surface transpiration velocity, (n) is the iteration count and q denotes the total tangential velocity

$$q_e = (U_e + W_e)^{\frac{1}{2}} \quad . \qquad (3.220)$$

The parameters ω and b are relaxation factors. Depending on the flow properties calculated, these factors are adjusted to fasten the convergence without destroying the stability. Typically, b takes values between 1.0 and 1.5 and ω may be varied between 1.0 and 2.0 . Practically, b was put equal to 1.2 and ω was taken to vary between 1.0 and 2.0 as a function of the local angle of attack.

In order to take into account the variation of the equivalent inviscid velocities in the boundary layer, the inviscid velocities are evaluated at the displacement surface. This is an alternative to the more computing consuming calculation of the actual distribution of velocities across the boundary layer. Thus, instead of applying the actual distribution of equivalent inviscid velocities to determine the displacement thicknesses, eqs.(2.23)-(2.24), a mean value taken at δ^* was used.

3.5.3 Marching procedure

A main feature of the boundary layer equations is that they are parabolic in both the streamwise and crosswise direction. Due to the independence principle of the spanwise component of the inviscid flow, the overall problem is elliptic in the streamwise direction and parabolic along the span of the wing. Taking advantage of this property most computing time is saved by completing the solution at one cross-section before marching to the next. At the first cross-section the infinite-swept-wing equations are solved iteratively together with the inviscid equations to obtain a proper initial condition to the full

three-dimensional interaction problem. Marching to the next cross-section, the global variables of the solution of the previous cross-section are employed as a first estimate to the new solution. This marching procedure assures that convergence is obtained in relatively few viscous-inviscid iteration cycles. Here we take the quantity

$$\Delta U_{max} = \max\left\{ \frac{U_{Ie}-U_e}{U_{Ie}} \right\} \qquad (3.221)$$

as a measure of the iteration history.

A typical iteration history is shown in fig.3.13.

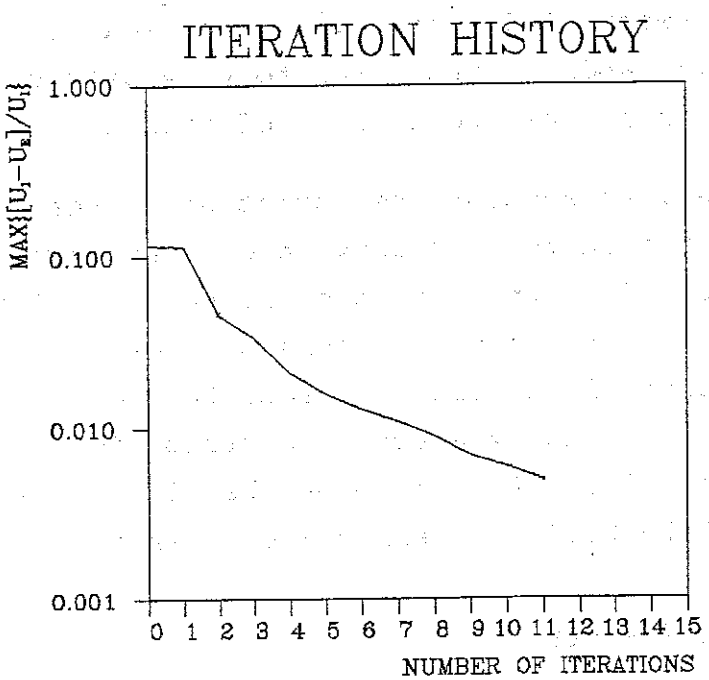

Fig. 3.13 Iteration history of a cross-sectional calculation.

Using a stop criterion of $5 \cdot 10^{-3}$, convergence was usually obtained within 10 - 15 iterations. When calculating cross-sections with large areas of separated flows it was not always possible to satisfy this criterion. The solution stalled at higher values of ΔU_{max} and consequently it was necessary

to relax the convergence criterion in order to obtain a solution. However, for local angles of attack less than 16 degrees a proper solution history was always achieved.

Furthermore, difficulties were experienced in performing the calculations beyond 20 degrees angle of attack for thick airfoil sections near the hub. In general, however, solutions were obtainable up to about 22° incidence.

The computing cost amounts to about 20 cpusec. per sweep on a conventional IBM main-frame computer. Thus, a solution of a complete wing consisting of 70 cross-sections is obtainable within 5 cpuhrs.

4. DISCUSSION AND RESULTS

A broad picture of the characteristic of three-dimensional stall on rotary wings was given in the introduction. From this it was found that the actual influence of the rotation on the flow in regions with separation still is uncertain. However, it is known from measurements that the use of a blade-element approach underpredicts the performance in the stalled condition. To clarify these uncertainties and to make a validation of the developed computer code, a comparison is made between measurements and calculations of the aerodynamic blade loads for a 7.5 m Aerostar wind turbine blade. Three blades of this type were installed on a 55-kW VESTAS windturbine, which was tested at the Test Plant for Small Windmills, Risø National Laboratory by Rasmussen (1983). The wind turbine, which is stall-regulated, was running with a rotational speed of 50.3 r.p.m. and a pitch angle of the tip at -2^{o}. The blade geometry consists of a NACA 4416-4424 profile series.
The main data for the blades are given in table 4.1.

Table 4.1 Main data for 7.5 m Aerostar wind turbine blade.

Radius (m)	Chord (m)	Twist (deg)	Thickness (% chord)
1.0	1.24	8.1	24.0
2.0	1.15	7.0	24.0
3.0	1.04	5.9	22.0
4.0	0.93	4.5	20.0
5.0	0.82	3.0	18.5
6.0	0.71	1.5	17.0
7.0	0.60	0.4	16.0
7.5	0.52	0.1	16.0
7.7	0.20	0.0	16.0

The calculations were carried out with the roter running at three different wind velocities, namely 10 m/s, 12 m/s and 14 m/s. As discussed previously,the computer code is not capable of solving flows where the local angle attack is higher than 22 degrees. To make sure that no numerical instabilities would occur during the calculation proces, the calculations started at the first cross-section which had an angle of attack less than or equal to 20 degrees. Consequently, the area calculated diminishes as the wind velocity is increased.
On figs. 4.1a-4.1c the surface flow pattern on the upper surface of the wing is shown at the three wind velocities. It shall be noted that the streamlines are determined by an Euler shooting method and therefore they do not represent equi-streamfunction lines. Rather they are to be considered as the paths of massless particles distributed uniformly along the edges of the wing.
In all the figures the separation line is indicated by a clear distinct line.
If a particle is followed from the leading edge, it is seen that it is nearly uninfluenced by the rotational effects, and that it mainly follows the direction of the chord. Due to the adverse pressure gradient in the streamwise direction, the flow separates at some distance downstream from the leading edge. When the separation line is reached the centrifugal forces significantly moves the fluid outward. A similar property for laminar separation bubbles has been experimentally visualised by McCroskey (1971). In the separated region the flow in large areas is strongly radial. Increasing the angles of attack by increasing the wind velocity, it is seen that the separated region increases in size and that the radial flow component becomes more dominant. This indicates that at sufficiently high wind velocities the flow in the separated region moves completely in the radial direction. Note here that the word 'separation' is somewhat misleading as, in three-dimensions, the flow can detach from the wall without the skin-friction becoming zero. However, the separation line in the present case clearly indicates a line separating two flows proceeding from different regions and, of practical reasons, the flow downstream from

this line is termed separated. In a visualisation study performed by Savino & Nyland (1985) a similar behaviour of the flow pattern as that shown in figs. 4.1a-4.1c was indicated. Employing balanced wind vanes located on the surface of a NACA 23024 airfoil section, they observed that the flow upstream from the separation line was directed along the chord line, whereas the direction of the separated flow was strongly radial. Thus, qualitatively, the calculated streamlines seem to be in agreement with these studies.

In figs. 4.2a-4.2c the distribution of lift coefficients C_L along the wing span is compared with corresponding two-dimensional calculated values.
Fig. 4.2c shows that for a wind velocity at 10 m/s it was possible to calculate nearly 60% of the wing surface. Some very interesting features arise from the figure. Firstly, it is seen that the three-dimensionally calculated lift coefficient is in close agreement to the two-dimensional non-rotating one on the outer 40% of the wing span. Secondly, in the inner 15% of the calculated wing span, the two-dimensional and the three-dimensional C_L-values differ considerably. Thus, at the first calculated cross-section, $Z/R = 0.43$, the lift coefficient is increased by more than 30% as compared to the two-dimensional value. Furthermore, it is seen that, when going from $Z/R = 0.6$ towards the hub, the three-dimensional lift coefficient is highly increased, whereas the two-dimensional C_L-value slightly decreases. Comparing the spanwise positions with the corresponding angles of attack, one finds that at $Z/R = 0.6$, the position where the two curves start to deviate from each other, the angle of attack has a value of 13°. This corresponds exactly to the angle of incidence at which C_L has its maximum value for the considered airfoil. Evaluating fig. 4.2b a similar behaviour is noticed. Here, the two curves start to deviate at $Z/R = 0.9$, which corresponds to the angle of attack at which $C_L = C_{L,max}$ for the two-dimensional airfoil.
In a wind tunnel study on a model rotor carried out by Milborrow & Ross (1984), the lift coefficient versus incidence was in good agreement with the two-dimensional data below stall, but higher lift coefficients was obtained above stall.

Thus, there is strong evidence that high C_L-values are obtainable in the stall-regime of the rotor.

On figs. 4.3a - 4.3c the drag coefficient C_D along the wing span is shown as function of the wind velocity. Only a slight deviation of the three-dimensional C_D-values compared to the two-dimensional values is to be seen. However, the three-dimensional values are always lower than the two-dimensional ones, suggesting that the rotational effects in general lower the drag coefficients. From both C_L- and C_D-calculations some oscillations are encountered at the first calculated cross-sections. These oscillations are probably due to the infinite-swept-wing equations being too crude an approximation to the true three-dimensional flow. Representing the physics of the flow, this would be an indication of the three-dimensional effects of the flow being of significant importance.

In figs. 4.4a - 4.4c the position of the separation line is sketched. In general the two-dimensional and the three-dimensional separation lines are in close agreement to each other at moderate angles of attack. At relatively high angles of attack, typically $\alpha > 16^o$, the rotation seems to delay the onset of the separation. From the figures it is seen that the stall may be delayed by an amount corresponding to about 10% of a chord length as compared to two-dimensional data. It shall be noted, that the two-dimensional values are obtained numerically by employing the computational model described by Sørensen (1986).

In figs. 4.5 - 4.7 the pressure-distribution on the wing surface is shown at the three wind velocities. It is a characteristic of these curves, that qualitatively they have a shape that usually are experienced from two-dimensional calculations. Thus, at relatively small angles of attack the curves form a triangle at the suction side of the blade and typically the chordwise pressure gradient diminishes in regions of separated flow.

In fig. 4.8 is shown the performance characteristic and in fig. 4.9 the flap-wise blade-root moment as function of wind velocity is given. It is seen that for wind velocities less than 10 m/s, both the blade-element theory and the three-dimensional interactive approach are in good agreement with the measurements. When increasing the wind velocity, however, the two-dimensional blade-element theory underpredicts both performance and the flap-wise moment.

In general, the three-dimensional interactive model is in good agreement with measurements also at high wind velocities. From fig. 4.8 it is seen that it exhibits a maximum performance value which is close to the measured. Although, in considerable better agreement with measurements than the blade-element theory, the flap-wise moment is not represented satisfactorily for $v_{wind} = 14$ m/s. It should be reminded, however, that due to the numerical limitations, i.e. α has to be less than 20^{o}, only a part of the blade has been calculated. When increasing the wind velocity to more than 15 m/s, the angles of attack are everywhere greater, indicating that the developed model in its present formulation fails to predict the fully stall. Thus, in order to predict the post-stall behaviour of the rotor, it is required that the computational model employed will be able to perform calculations at massive separation up to, say, 30^{o} incidence. Hopefully, future refinements will make it possible to accomodate this.

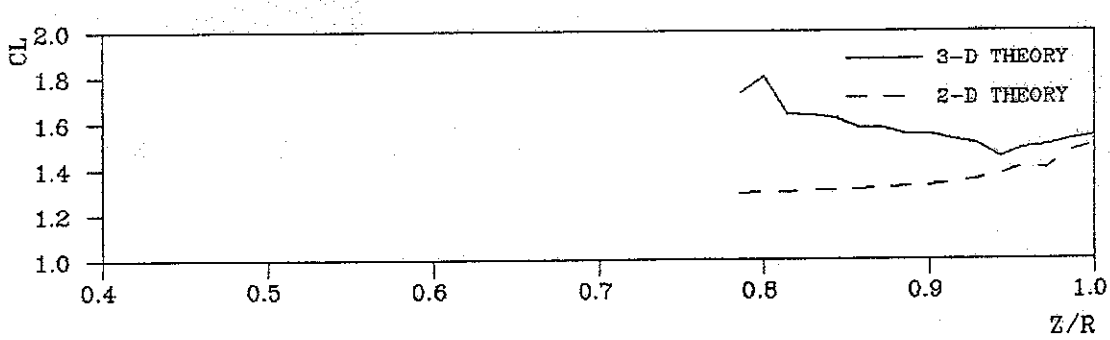

Fig. 4.2a C_L-distribution along wing span. Comparison of two- and three-dimensional calculation. V_{wind}=14 m/s.

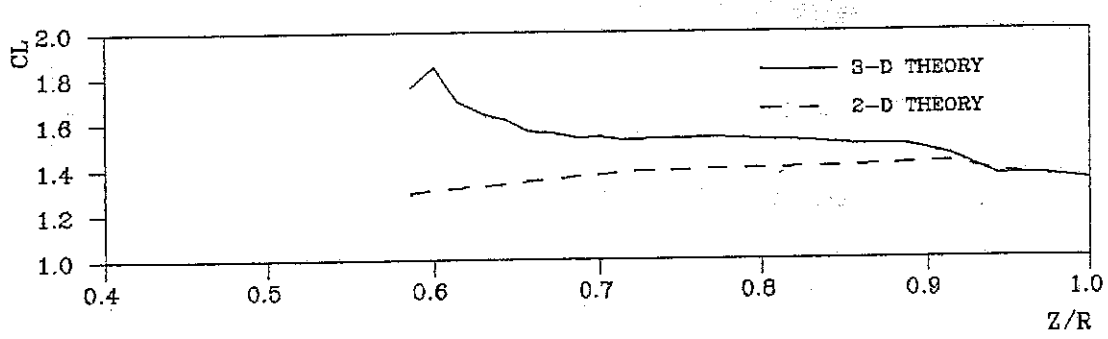

Fig. 4.2b C_L-distribution along wing span. Comparison of two- and three-dimensional calculation. V_{wind}=12 m/s.

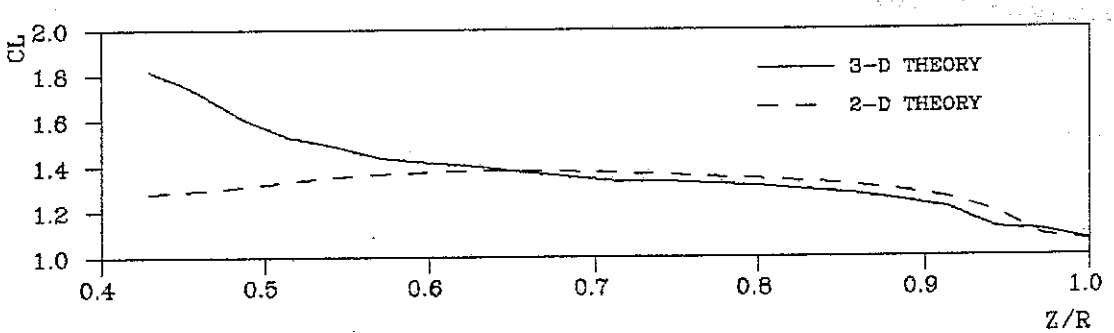

Fig. 4.2c C_L-distribution along wing span. Comparison of two- and three-dimensional calculation. V_{wind}=10 m/s.

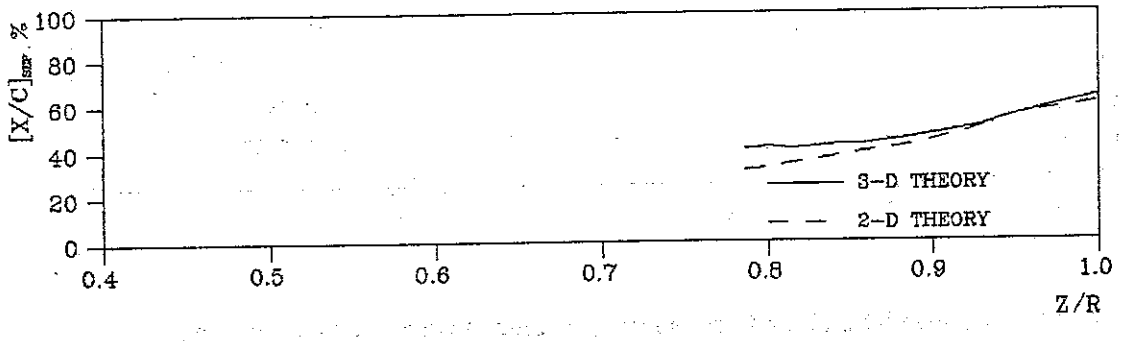

Fig. 4.4a Position of separation line. Comparison of two- and three-dimensional calculations. V_{wind}=14 m/s.

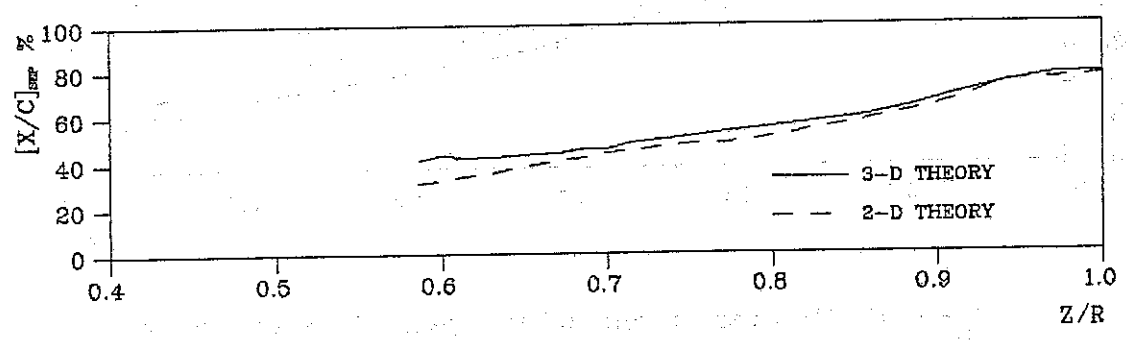

Fig. 4.4b Position of separation line. Comparison of two- and three-dimensional calculations. V_{wind}=12 m/s.

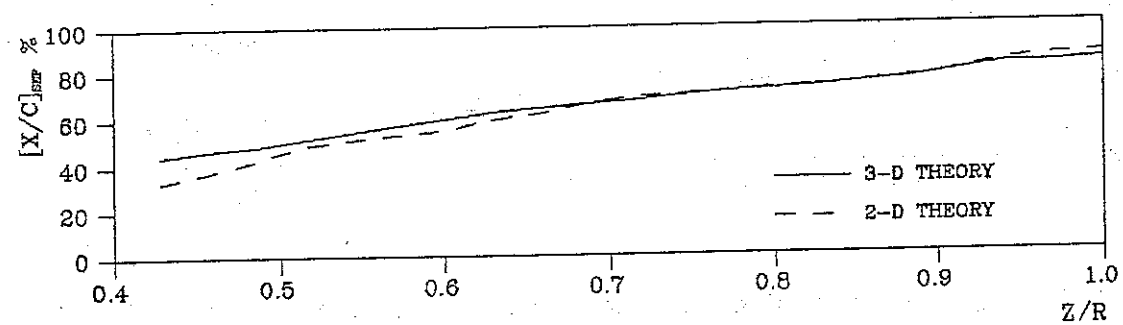

Fig. 4.4c Position of separation line. Comparison of two- and three-dimensional calculations. V_{wind}=10 m/s.

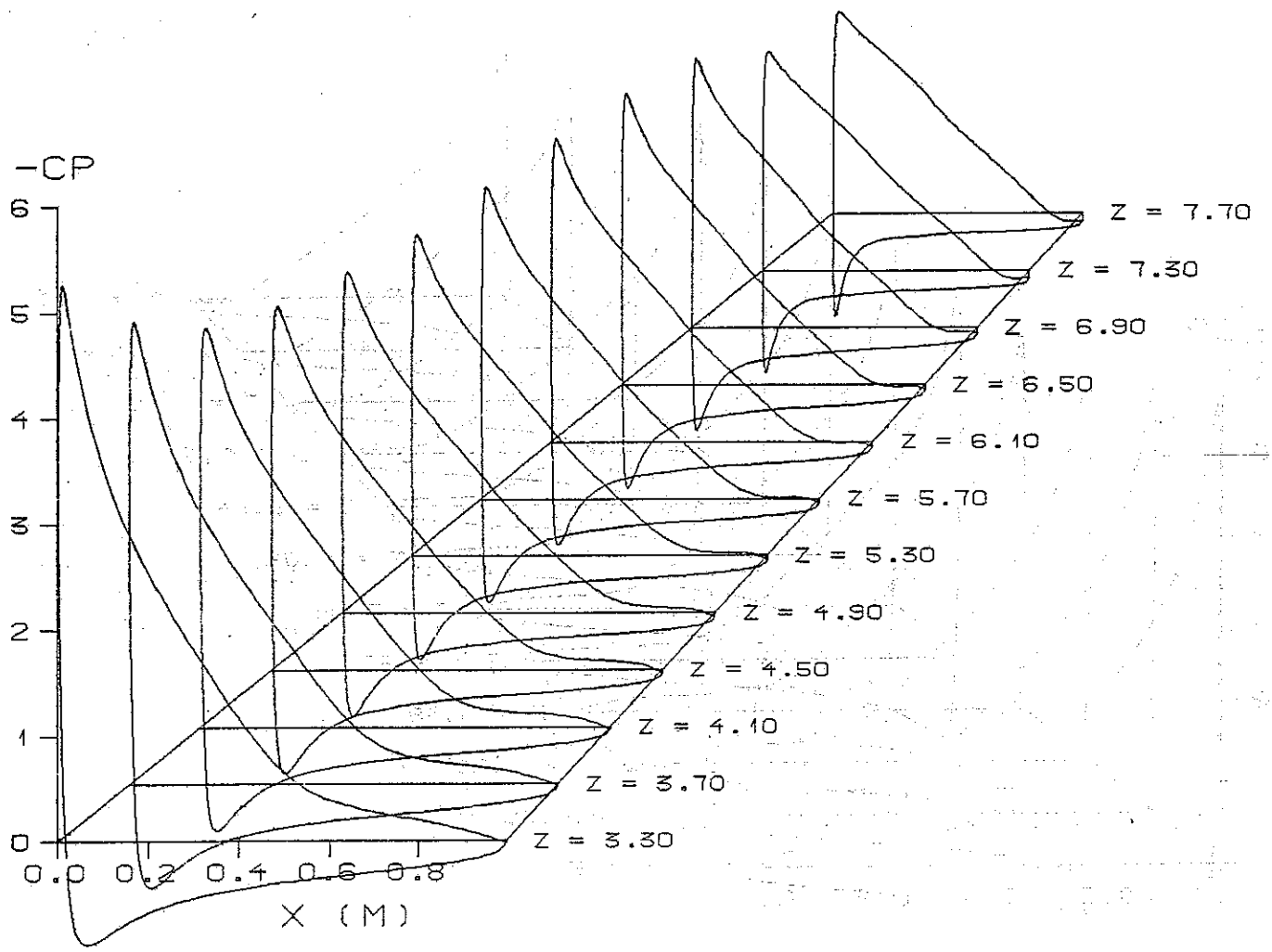

Fig. 4.5 Pressure-distribution on the wing surface. V_{wind}=10 m/s.

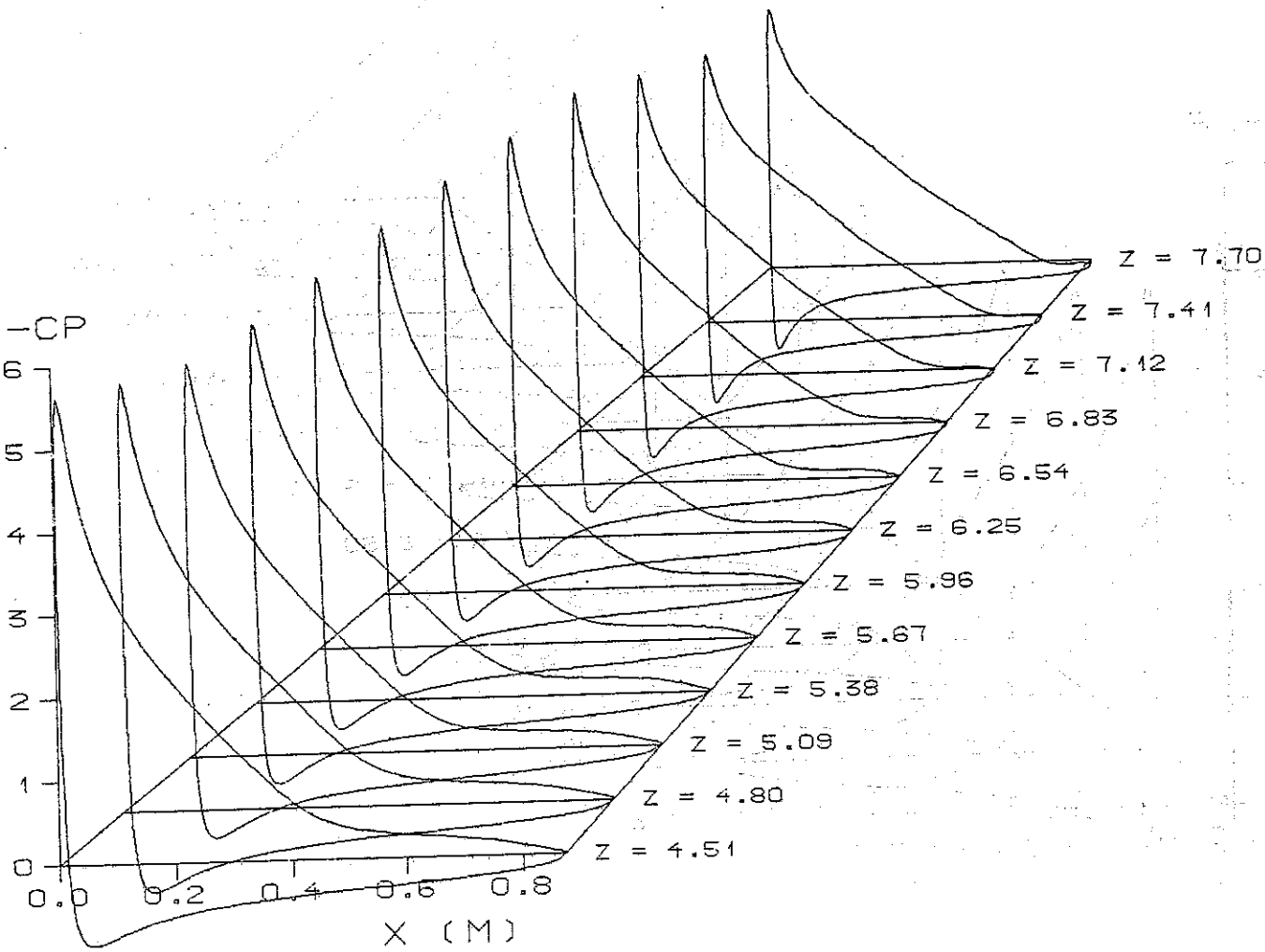

Fig. 4.6 Pressure-distribution on the wing surface. V_{wind}=12 m/s.

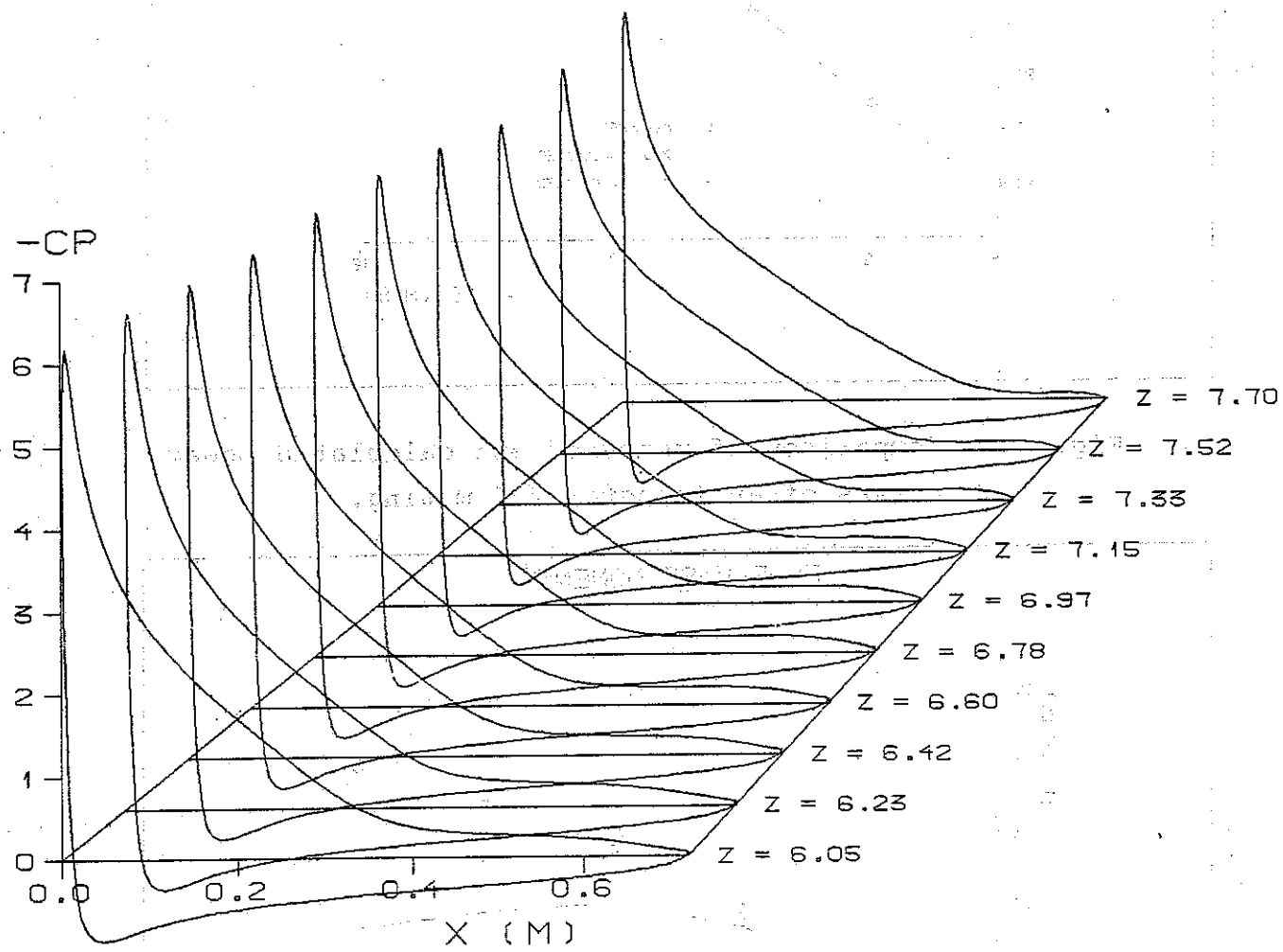

Fig. 4.7 Pressure-distribution on the wing surface. V_{wind}=14 m/s.

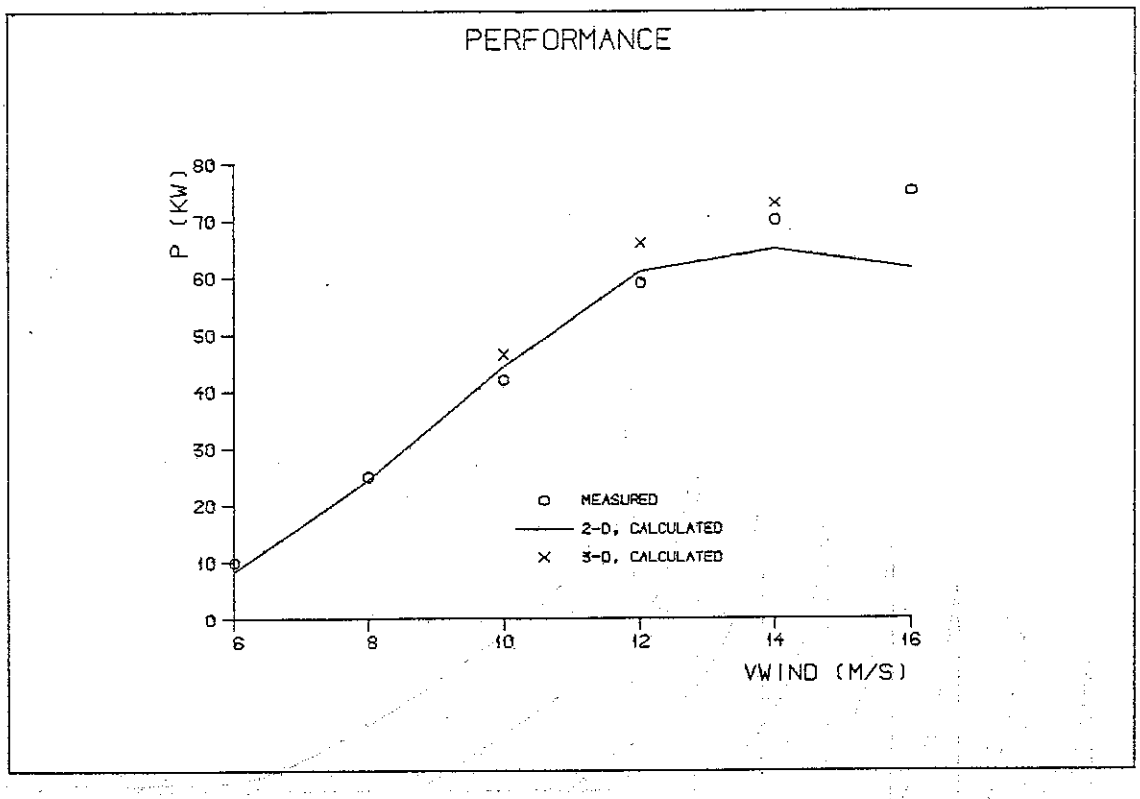

Fig. 4.8 Comparison of measured and calculated power curves of an Aerostar 7.5 m wing.

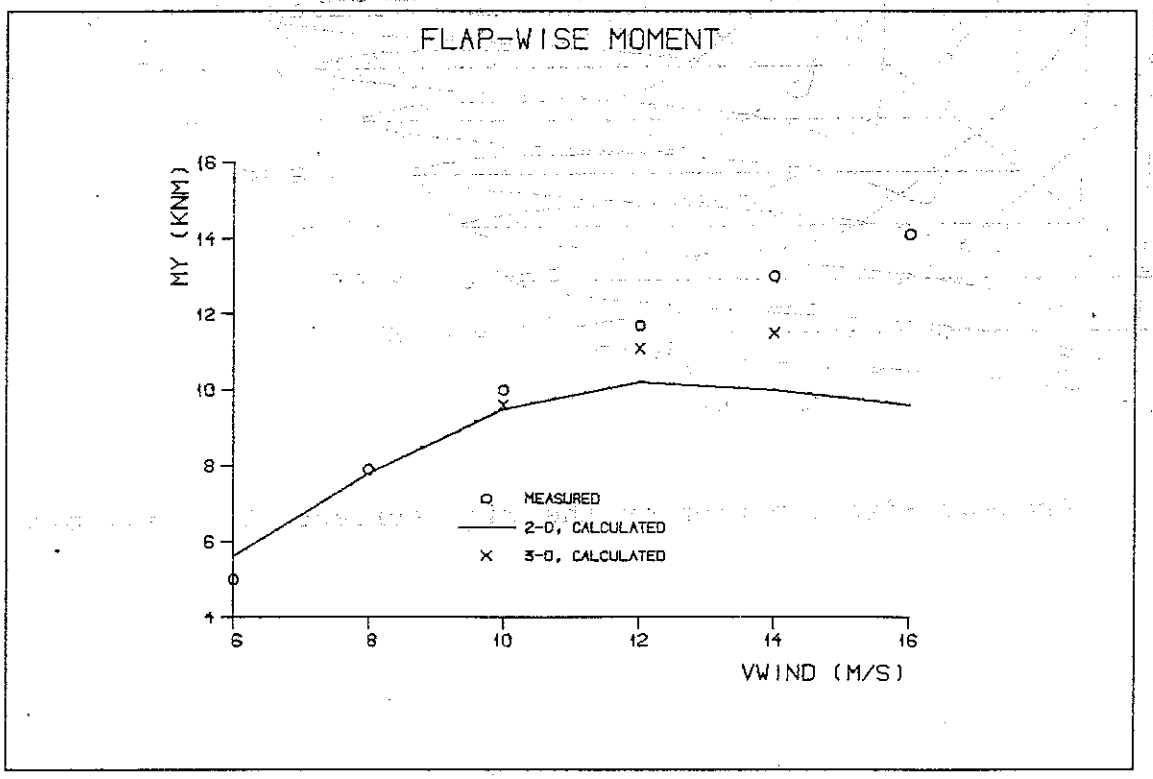

Fig. 4.9 Comparison of measured and calculated flap-wise blade-root moment curves of an Aerostar 7.5 m wing.

5. CONCLUSION

The use of an zonal approach in combination with a viscous-inviscid interaction procedure represents an elaborate and cpu-time saving alternative to the solution of the computing costly Navier-Stokes equations. Employing a grid of 642000 nodepoints a solution was obtained within 5 cpuhrs. on a conventional IBM main-frame computer.

Using a FLARE approximation and an upwinding correction scheme combined with the Keller-box - and the zig-zag scheme, assures the solution to be obtained without getting instability problems, even for cases with large areas of flow separation. Thus, it was possible to obtain solutions for local angles of attack up to 20^{o}.

Compared to measurements of a 7.5 m Aerostar wind turbine blade, the developed model is found to work well for the cases tested. However, due to the numerical limitations, i.e. α has to be less than 20^{o}, solutions was only obtained for wind velocities less than 15 m/s.

Using computational surface stream-lines to visualize the flow past the rotor, some interesting features of boundary layer flows on rotating wings are made visible. The separation line is indicated by a clearly distinct line separating two flows proceeding from different regions. Upstream of the separation line, the flow is nearly uninfluenced by the rotational effects, whereas the separated flow downstream from the separation line is highly radial.

As compared to two-dimensional blade-element calculations, the lift coefficient may be increased by more than 30%, yielding values as high as $C_L = 1.8$. Furthermore, it is indicated that the lift coefficient only increases for incidence angles greater than the one corresponding to $C_L = C_{L_{max}}$. The drag coefficients were found to be only slightly affected by the rotational effects.

The effect of the rotation seems only to delay the onset of the stall at angles of attack greater than 16^{o}. However, it is found that the separation line may be delayed by an amount corresponding to more than 10% of a chord length as compared to two-dimensional data.

Hopefully, future refinements of the model will enable us to compute the post-stall behaviour of the rotor.

REFERENCES

Aris, R. (1965)
Vectors, Tensors, and the basic equations of Fluid Mechanics.
Prentice-Hall, Inc.

Le Balleur, J.C. (1978)
Couplage visqueux non visqueux: Metode numerique et applications aux ecoulements bidimensionals transoniques et supersoniques.
La Recherche Aerospatial, N° 1978-2, pp.67-76.

Blaser, D.A. & Velkoff, H.R. (1973)
A preliminary analytical and experimental investigation of helicopter rotor boundary layers.
AIAA J., vol.11, No.12, pp.1660-1665.

Bradshaw, P., Cebeci, T. & Whitelaw, J.H. (1981)
Engineering calculation methods for turbulent flow.
Academic Press.

Carter, J.E. (1975)
Inverse solutions for laminar boundary-layer flows with separation and reattachment.
NASA TR R-447.

Carter, J.E. (1979)
A new boundary-layer inviscid interaction technique for separated flow.
AIAA Paper 79-1450.

Carter, J.E. & Wornom, S.F. (1975)
Solutions for incompressible separated boundary layers including viscous-inviscid interaction.
NASA SP-347, part I, pp.125-150.

Catherall, D. & Mangler, K.W. (1966)
The integration of the two-dimensional laminar boundary-layer equations past a point of vanishing skin friction.
J.of Fluid Mech., vol.26, pp. 163-182.

Cebeci, T. (1986)
An approach to practical aerodynamic calculations.
AGARD-FDP-VKI Special course on "Computation of three-dimensional boundary layers including separation".
Brussels, April 14-18.

Cebeci, T., Kaups, K. & Ramsey, J.A. (1977)
A general method for calculating three-dimensional compressible laminar and turbulent boundary layers on arbitrary wings.
NASA CR-2777.

Cebeci, T., Keller, H.B. & Williams, P.G. (1979)
Separating boundary-layer calculations.
J.Comp.Phys. 31, pp.363-378.

Cebeci, T., Clark, R.W., Chang, K.C. Halsey, N.D. & Lee, K. (1985)
Airfoils with separation and the resulting wakes.
3rd Sumposium on Numerical and Physical Aspects of Aerodynamic Flows, pp.2-13 - 2-25,
Long Beach.

Drela, M. & Thompkins Jr., W.T. (1984)
Investigation of compressible laminar boundary-layer solution behaviour at separation using a displacement thickness-based normal scaling.
2nd Symposium on Numerical and Physical Aspects of Aerodynamic Flows,
Long Beach.

Dwyer, H.A. & McCroskey, W.H. (1970)
Crossflow and unsteady boundary-layer effects on rotating blades.
AIAA Paper No.70-50.

Edwards, D.E. & Carter, J.E. (1985)
A quasi-simultaneous finite difference approach for strongly interacting flow.
3rd Symposium on Numerical and Physical Aspects of Aerodynamic Flows, pp.1-63 - 1-73,
Long Beach.

Fogarty, L.E. (1951)
The laminar boundary layer on a rotating blade.
J.Aero.Sci., vol.18, no.4, pp.247-252.

Fogarty, L.E. & Sears, W.R. (1950)
Potential flow around a rotating, advancing cylindrical blade.
J.Aero.Sci., vol.17, no.9, p.599.

Glauert, H. (1963)
Airplane propellers.
In: Durand, W.F. (ed.). Aerodynamic theory.
vol.IV, Division L.
Dover Publications, Inc. New York.

Goldstein, S. (1948)
On laminar boundary-layer flow near a position of separation.
Q.J.Mech.Appl.Math. 1, pp.43-69.

Grundmann, R. (1984)
Grenzschicht- und grenzschichtänliche Strömunger.
DFVLR-FB 84-46, Institut für Strömungsmechanik.
Göttingen.

Harris, F.D. (1966)
Preliminary study of radial flow effects on rotor blades.
J.of the Americal Helicopter Society.
vol.11, no.3, pp.1-21.

Hawkins, G.A. (1963)
Multilinear Analysis for Students in Engineering and Science.
John Wiley and Sons, Inc.

Hess, J.L. (1971)
Numerical solution of inviscid subsonic flows.
von Karman Institute for Fluid Dynamics.
Lecture Series 34, Belgium.

Hess, J.L. (1973)
Higher order numerical solution of the integral equation for the two-dimensional Neumann problem.
Comp.Meth.Appl.Mech.Eng., vol.2, pp.1-15.

Hicks, J.G. & Nash, J.F. (1971)
The calculation of three-dimensional turbulent boundary layers on helicopter rotors.
NASA CR-1845.

Himmelskamp, H. (1945)
Profile investigations on a rotating airscrew.
Ph.D. Dissertation, Göttingen.

Jameel, H.M. (1972)
Study of rotating arifoil.
J.Aircraft, vol.9, no.4, pp.314-316.

Keller, H.B. (1974)
Accurate difference methods for nonlinear two-point boundary value problems.
SIAM J.Numer.Anal. vol.11, no.2, pp.305-320.

Klineberg, J.M. & Steger, J.L. (1974)
On laminar boundary-layer separation.
AIAA paper 74-94.

Kwon, O.K. & Pletcher, R.H. (1979)
Prediction of incompressible separated boundary layers including viscous-inviscid interaction.
J.Fluids Eng., vol.101, pp.466-472.

Lee, D.S. & Pletcher, R.H. (1985)
Application of a viscous-inviscid interaction method to predict transonic separated flows.
3rd Symposium on Numerical and Physical Aspects of Aerodynamic Flows, pp.1-75 - 1-85,
Long Beach.

Lighthill, M.J. (1958)
On displacement thickness.
J.of Fluid Mech., vol.4, part 4, pp.383-392.

Lock, R.C. (1980)
A review of methods for predicting viscous effects on aerofoils and wings at transonic speeds.
AGARD CP 291, paper 2.

Lock, R.C. (1985)
Prediction of the drag of wings at subsonic speeds by viscous/inviscid interaction techniques.
AGARD Report No. 723, paper 10.

Mahgoub, H.E.H. & Bradshaw, P. (1979)
Calculation of turbulent-inviscid flow interactions with large normal pressure gradients.
AIAA Journal, vol.17, no.10, pp.1025-1029.

McCroskey, W.J. (1971)
Measurements of boundary layer transition, separation and streamline direction on rotating blades.
NASA TN D-6321.

McCroskey, W.J. & Dwyer, H.A. (1969)
Methods of analyzing propeller and rotor boundary layers.
NASA SP-228.

McCroskey, W.J. & Fisher, Jr., R.K. (1972)
Detailed aerodynamic measurements on a model rotor in the blade stall regime.
J.of the American Helicopter Society,
vol.17, no.1, pp.20-30.

McCroskey, W.J. & Yaggy, P.F. (1968)
Laminar boundary layers on helicopter rotors in forward flight.
AIAA J., vol.10, no.6, pp.1919-1926.

McCroskey, W.J., Nash, J.F. & Hicks, J.G. (1971)
Turbulent boundary-layer flow over a rotating flat-plate blade.
AIAA J., vol.9, no.1, pp.188-189.

Milborrow, D.J. & Ross, J.N. (1984)
Airfoils characteristics of rotating blades.
IEA LS-WECS, 12th Meeting of Experts, Copenhagen.

Moore, F.K. (1953)
Displacement effect of a three-dimensional boundary layer.
NACA Report 1124.

Nakayama, A. (1983)
Measurements of attached and separated turbulent flows in the trailing-edge regions of airfoils.
2nd Symposium on Numerical and Physical Aspects of Aerodynamic Flows,
Long Beach.

Nielsen, P. (ed.) (1981)
Measurements on the Nibe Wind Turbines.
The Wind Power Program of the Ministry of Energy and the Electric Utilities in Denmark, Report no.EEV 81-04.

Piquet, J. & Visonneau, M. (1985)
Inverse mode solution of the three dimensional boundary layer equations about a shiplike hull.
3rd Symposium on Numerical and Physical Aspects of Aerodynamic Flows, pp.11-1 - 11-11.

Pletcher, R.H. (1978)
Prediction of incompressible turbulent separating flow.
J.of Fluid Eng., vol.100, pp.427-433.

Radwan, S.F. & Lekoudis, S.G. (1984)
Boundary-layer calculations in the inverse mode for incompressible flows over infinite swept wings.
AIAA J., vol.22, no.6, pp.737-743.

Rasmussen, F. (1983)
Blade and rotor loads for Vestas 15.
Risø-M-2402, Roskilde, Denmark.

Rott, N. & Smith, W.E. (1956)
Some examples of laminar boundary-layer flow on rotating blades.
J.Aero.Sci., vol.23, no.11, pp.991-996.

Reyhner, T.A. & Flügge-Lotz, I. (1968)
The interaction of a shock wave with a laminar boundary layer.
Int.J.Nonlinear Mech., vol.3, no.2, pp.173-199.

Savino, J.M. & Nyland, T.W. (1985)
Wind turbine flow visualization studies.
NASA Lewis Research Center, Cleveland, Ohio.

Sears, W.R. (1950)
Potential flow around a cylindrical blade.
J.Aero.Sci., vol.17, no.3, pp.183-184.

Simpson, R.L., Strickland, J.H. & Barr, P.W. (1974)
Laser and hot-film measurements in a separating turbulent layer.
Technical Report WT-3, Southern Methodist Univ., Termal and Fluid Sciences Center, Dallas, Texas.

Smith, P.D. (1982)
The numerical computation of three-dimensional boundary layers.
IUTAM Symposium, pp.265-285, Berlin, March 29 - April 1.

Stewartson, K. (1969)
On the flow near the trailing edge of a flat plate II.
Mathematika 16, pp.106-121.

Sørensen, J.N. (1986)
Prediction of separated flow past airfoil using viscous-inviscid interaction technique.
To be published.

Takematsu, M. (1972)
Laminar boundary layer on a rotating round-nosed blade.
AIAA J., vol.10, no.3, pp.333-334.

Tanner, W.H. & Yaggy, P.F. (1966)
Experimental boundary layer study on hovering rotors.
J.of the American Helicopter Society,
vol.11, no.3, pp.22-37.

Vatsa, V.N. (1985)
A three-dimensional boundary-layer analysis including heat-transfer and blade-rotation effects.
3rd Symposium on Numerical and Physical Aspects of Aerodynamic Flows, pp.10-45 - 10-59, Long Beach.

Veldman, A.E,P. (1979)
A numerical method for the calculation of laminar, incompressible boundary layers with strong viscous-inviscid interaction.
National Aerospace Laboratory, NLR TR 79023 U,
Amsterdam, The Netherlands.

Veldman, A.E.P. (1980)
The calculation of incompressible boundary layers with strong viscous-inviscid interaction.
AGARD CP 291, paper 12.

Velkoff, H.R. Blaser, D.A. & Jones, K.M. (1971)
Boundary-layer discontinuity on a helicopter rotor blade in hovering.
J.Aircraft, vol.8, no.2, pp.101-107.

Vries, O. de (1979)
Fluid dynamic aspects of wind energy conversion.
AGARD-AG-243.

Wai, J.C., Baillie, J.C. & Yoshihara, H. (1985)
Computation of turbulent separated flows over wings.
3rd Symposium on Numerical and Physical Aspects of Aerodynamic Flows, pp.11-27 - 11-38, Long Beach.

Williams, P.G. (1975)
A reverse flow computation in the theory of self-induced separation.
Lecture Notes in Physics, vol.35, pp.445-451,
Springer Verlag.

Wilson, R.E. & Lissamann, P.B.S. (1974)
Applied aerodynamics of wind power machines.
Oregon State University, Oregon.

Young, Jr., W.H. & Williams, III, J.C. (1970)
The boundary layer on rotating blades in forward flight.
AIAA paper no.70-49.

Øye, S. (1983)
FIX Dynamic, aeroelastic calculation of wind turbine blade (in Danish).
AFM 83-08, Dept.of Fluid Mech., Technical Univ. of Denmark.

APPENDIX A

Derivation of the Boundary Layer Equations

In order to derive the boundary layer equations in a nonorthogonal, curvilinear and rotating coordinate system it is appropriate to start with a general formulation of the Navier-Stokes equations. The formulation of these equations is most easily carried out by use of tensor notation since this assures the formulation to be independent of the coordinate system chosen. The final formulation of the boundary layer equations is consequently derived by employing tensor algebra and imposing the usual thin-layer approximation on the Navier-Stokes equations. First, some basic concepts of tensor analysis will be presented. These will be used to derive, term by term, the boundary layer equations.

A1 Basic Concepts of Tensor Algebra

In the following pages, some fundamental results of tensor analysis will be given. The presentation is mainly based on Aris (1965), Hawkins (1963), and Grundmann (1984). Here, we consider a Cartesian coordinate system $(\bar{x}^1,\bar{x}^2,\bar{x}^3)$ and a general curvilinear coordinate system (x^1,x^2,x^3). If a variable is to be transformed between the two coordinate systems it is required that the following relations exist and are unique,

$$\begin{aligned} \bar{x}^i &= f^i(x^1,x^2,x^3) \quad , \\ x^i &= h^i(\bar{x}^1,\bar{x}^2,\bar{x}^3) \end{aligned} \tag{A1}$$

A vector is called a contravariant vector if the components of vector $\bar{A}^i$ in coordinate system f^i is transformed to A^i in coordinate system h^i through the expression

$$A^i = \frac{\partial x^i}{\partial \bar{x}^j} \bar{A}^j \quad . \tag{A2}$$

A contravariant vector is always denoted by a superscript.

Similarily, a covariant vector is defined as one whose components transform according to the relation

$$A_i = \frac{\partial \bar{x}^j}{\partial x^i} \bar{A}_j \quad , \tag{A3}$$

where a subscript is used to indicate that it is a covariant vector.

A vector which satisfies eq.(A2) or eq.(A3) is called a tensor of first order. A general definition of tensors of higher order is stated as follows.
A variable $B^{ijk\ldots}_{pqr\ldots}$ with ℓ superscripts and m subscripts is called a tensor of n'th order $(n = \ell+m)$ if and only if it transforms through the expression

$$B^{ijk\ldots}_{pqr\ldots} = \frac{\partial x^i}{\partial \bar{x}^\ell} \frac{\partial x^j}{\partial \bar{x}^m} \frac{\partial x^k}{\partial \bar{x}^n} \cdots \frac{\partial \bar{x}^s}{\partial x^p} \frac{\partial \bar{x}^t}{\partial x^q} \frac{\partial \bar{x}^u}{\partial x^r} \cdots B^{\ell mn\ldots}_{stu\ldots} \tag{A4}$$

The tensor is referred to as a mixed tensor of contravariant dimension ℓ and covariant dimension m .

Consider the distance ds between two points P and Q , having coordinates $\bar{x}^i$ and $\bar{x}^i+d\bar{x}^i$ in the Cartesian coordinate system,

$$ds^2 = \sum_{k=1}^{3} d\bar{x}^k \, d\bar{x}^k \quad . \tag{A5}$$

Using the chain rule of differentiation, we obtain

$$\begin{aligned} ds^2 &= \sum_{k=1}^{3} \left(\frac{\partial \bar{x}^k}{\partial x^i} dx^i\right)\left(\frac{\partial \bar{x}^k}{\partial x^j} dx^j\right) \\ &= g_{ij} \, dx^i \, dx^j \quad , \end{aligned} \tag{A6}$$

where the metric tensor g_{ij} is given by

$$g_{ij} = \sum_{k=1}^{3} \frac{\partial \bar{x}^k}{\partial x^i} \frac{\partial \bar{x}^k}{\partial x^j} \quad . \tag{A7}$$

It can be shown that g_{ij} is a second order covariant and symmetric tensor.

The corresponding contravariant metric tensor reads

$$g^{ij} = \sum_{k=1}^{3} \frac{\partial x^i}{\partial \bar{x}^k} \frac{\partial x^j}{\partial \bar{x}^k} \quad . \tag{A8}$$

Multiplication of the two metric tensors yields the Kronecker delta,

$$g_{ij}\, g^{jk} = \delta_i^k \quad . \tag{A9}$$

Instead of employing eq.(A8), the contravariant metric tensor can be established by inversion of the covariant counterpart

$$g^{ij} = \frac{\text{cofactor}(g_{ij})}{g} \quad , \tag{A10}$$

where g denotes the determinant of g_{ij} .

An important property of the metric tensors is their ability to transform a tensor from one form to another. This transformation is referred to as lowering or raising of indices. Thus to lower the index of the vector B^i , we simply write

$$B_j = g_{ij}\, B^i \quad , \tag{A11}$$

and, in a similar way, the index is raised by writing

$$B^j = g^{ij}\, B_i \quad . \tag{A12}$$

The absolute length A of a contravariant vector A^i is defined as

$$(A)^2 = A^i A_i \quad , \tag{A13}$$

where the covariant vector A_i is formed by lowering the index, according to (A11).
In general we have

$$(A)^2 = A^i A_i = g_{ij} A^i A^j = g^{ij} A_i A_j \quad . \tag{A14}$$

The scalar product of a contravariant vector A^i and a covariant vector B_i is given by

$$A^i B_i = AB \cos\theta \quad , \tag{A15}$$

where θ is the angle between vectors A and B.
Eq.(A15) leads to the general expression for the angle θ_{13} between the tangent vectors along the coordinate axes x^1 and x^3,

$$\cos\theta_{13} = g_{13} / (g_{11}\, g_{33})^{\frac{1}{2}} \quad . \tag{A16}$$

According to the tensor algebra, it can be shown that differentation of a tensor leads to a new tensor. Suppose we wish to find the incremental change of a contravariant vector A^i. This is calculated from

$$\delta A^i = \left[\frac{\partial A^i}{\partial x^j} + \left\{ \begin{matrix} i \\ k\ j \end{matrix} \right\} A^k\right] dx^j \quad , \tag{A17}$$

where the symbol $\left\{ \begin{matrix} i \\ k\ j \end{matrix} \right\}$ is the Christoffel-symbol of second kind, defined as

$$\left\{ \begin{matrix} i \\ j\ k \end{matrix} \right\} = \frac{1}{2}\, g^{i\ell}\left(\frac{\partial g_{k\ell}}{\partial x^j} + \frac{\partial g_{j\ell}}{\partial x^k} - \frac{\partial g_{kj}}{\partial x^\ell}\right) \quad . \tag{A18}$$

The Christoffel-symbol is not a tensor, but the sum within the brackets on the right hand side of eq.(A17) is a mixed tensor of second order. This tensor is referred to as the covariant derivative of the vector A^i and is denoted

$$D_j A^i = \frac{\partial A^i}{\partial x^j} + \left\{ \begin{matrix} i \\ k\ j \end{matrix} \right\} A^k \quad . \tag{A19}$$

The corresponding covariant derivative of a covariant vector is

$$D_j A_i = \frac{\partial A_i}{\partial x^j} - \left\{ \begin{matrix} k \\ i\ j \end{matrix} \right\} A_k \quad . \tag{A20}$$

Note that the plus sign is replaced by a minus sign and that the indices 'i' and 'k' mutually are replaced in the Christoffel-symbol.

If we take the covariant derivative of the metric tensors, we get

$$D_k g_{ij} = 0 \quad , \tag{A21}$$

and

$$D_k g^{ij} = 0 \quad .$$

Contravariant differentation is defined through the usual rules for raising and lowering of indices, thus it is given by

$$D^i = g^{ij} D_j \quad . \tag{A22}$$

The second order derivative of a vector defines a third order tensor. This is most easily shown by taking the covariant derivative of eq.(A19)

$$D_i D_j A_k = D_i \left[\frac{\partial A_k}{\partial x^j} - \left\{ \begin{matrix} m \\ k\ j \end{matrix} \right\} A_m \right]$$

$$= \frac{\partial^2 A_k}{\partial x^j \partial x^i} - \left\{ \begin{matrix} m \\ k\ j \end{matrix} \right\} \frac{\partial A_m}{\partial x^i} - \frac{\partial}{\partial x^i} \left\{ \begin{matrix} m \\ k\ j \end{matrix} \right\} A_m$$

$$- \left\{ \begin{matrix} n \\ k\ i \end{matrix} \right\} \frac{\partial A_n}{\partial x^j} + \left\{ \begin{matrix} n \\ k\ i \end{matrix} \right\} \left\{ \begin{matrix} m \\ n\ j \end{matrix} \right\} A_m$$

$$- \left\{ \begin{matrix} n \\ j\ i \end{matrix} \right\} \frac{\partial A_k}{\partial x^n} + \left\{ \begin{matrix} n \\ j\ i \end{matrix} \right\} \left\{ \begin{matrix} m \\ k\ n \end{matrix} \right\} A_m \quad . \tag{A23}$$

The permutation symbol ε_{ijk} is defined in such a manner that it is 1 if ijk is an even permutation of 123, - 1 if ijk is an odd permutation of 123 and zero if any of i, j and k are equal. It can be shown that ε_{ijk} does not satisfy the transformations required to be a tensor. However, if we multiply ε_{ijk} by the square-root of the determinant of the metric tensor, we get a third order covariant tensor

$$e_{ijk} = g^{\frac{1}{2}} \varepsilon_{ijk} \quad .$$

Similarly, (A24)

$$e^{ijk} = g^{-\frac{1}{2}} \varepsilon^{ijk} \quad .$$

is a third order contravariant tensor.

By using the rules of lowering and raising of indices in combination with eq.(A24), we get the following relation between the permutation symbols

$$\varepsilon^{ijk} g_{jp} g_{kq} = g \varepsilon_{pqr} g^{ir} \quad . \tag{A25}$$

One of the most important rules of the tensor algebra, is that, the indices is always preserved. This rule makes the algebra easy to employ since it gives an easy check on the validity of the manipulations used.

Since tensor operations is valid for all coordinate systems they result in important simplifications, when applied to vector equations. This is illustrated in the following table, where some important vector operations are formulated in a general tensor notation:

Tabel A1 Relations between vector operations and tensor operations.

Vector operation	Tensor operation
$\underline{a} \cdot \underline{b}$	$A^i B_i = A_i B^i = g_{ij} A^i B^j = g^{ij} A_i B_j$
$\underline{a} \times \underline{b}$	$e_{ijk} A^j B^k$ or $e^{ijk} A_j B_k$
$\underline{\nabla} \cdot \underline{a}$	$D_i A^i = D^i A_i = g_{ij} D^i A^j = g^{ij} D_i A_j$
$\underline{\nabla} \times \underline{a}$	$e_{ijk} D^j A^k$ or $e^{ijk} D_j A_k$
$(\underline{a} \cdot \underline{\nabla}) \cdot \underline{b}$	$A_i D^i B_j$ or $A^i D_i B_j$
$\underline{a} \times (\underline{b} \times \underline{c})$	$e_{ijk} e^{k\ell m} A^j B_\ell C_m$
$\underline{\nabla} a$	$D^i a$ or $D_i a$
$\nabla^2 a$	$D_i D^i a$

When using tensor operations to transform a set of equations from Cartesian coordinates into curvilinear coordinates, the tangent base given by eq.A2 or eq.A3 does not in general define a set of unit vectors. Instead, the length of the base vectors depends on the values of the coordinates (x^1,x^2,x^3). Furthermore, the curvilinear coordinates does not necessarily have the same physical dimension. Therefore the covariant and the contravariant vectors differ from the associated physical components.

If we note, however, that the covariant tangent vectors have length's $g_{11}^{\frac{1}{2}}$, $g_{22}^{\frac{1}{2}}$ and $g_{33}^{\frac{1}{2}}$, respectively, the physical components are derived by normalising the contravariant vectors

$$A(j) = g_{jj}^{\frac{1}{2}} A^j \quad . \tag{A26}$$

By lowering the index, we get the corresponding expression for a covariant vector

$$A(j) = g_{jj}^{\frac{1}{2}} g^{ij} A_i \quad . \tag{A27}$$

In a Cartesian coordinate system, the metric tensor is the unit matrix, therefore

$$\bar{A}_i = \bar{A}^i = \bar{A}(i) \quad . \tag{A28}$$

Using the relation eq.(A3) for the transformation of a Cartesian vector into a curvilinear coordinate system, we get

$$A_i = \frac{\partial \bar{x}^j}{\partial x^i} \bar{A}(j) \quad . \tag{A29}$$

Inserting eq.(A29) into eq.(A27), the transformation of a Cartesian vector $\bar{A}(k)$ into its physical components in curvilinear coordinates A(i) is given by

$$A(i) = g_{ii}^{\frac{1}{2}} g^{ij} \frac{\partial \bar{x}^k}{\partial x^j} \bar{A}(k) \quad . \tag{A30}$$

Although only a brief survey of results from the tensor analysis has been presented here, it includes the most fundamental relations necessary to transform the equations of fluid motion into general coordinate frames.

A2 The Navier-Stokes Equations

In a rotating Cartesian frame of reference, the time-averaged, steady and incompressible Navier-Stokes equations are written as

Continuity

$$\frac{\partial \bar{u}_i}{\partial \bar{u}_i} = 0 \quad . \tag{A31}$$

Momentum

$$\bar{u}_j \frac{\partial \bar{u}_i}{\partial \bar{u}^j} + 2\varepsilon_{ijk}\bar{\Omega}_j\bar{u}_k + \varepsilon_{ijk\,k\ell m}\bar{\Omega}_j\bar{\Omega}_\ell\bar{x}^o_m$$
$$= -\frac{1}{\rho}\frac{\partial \bar{p}}{\partial \bar{x}_i} + \frac{\partial}{\partial \bar{x}_j}\left(\nu \frac{\partial \bar{u}_i}{\partial \bar{x}_j} - \overline{\bar{u}_i'\bar{u}_j'}\right) \tag{A32}$$

Here the bars refer to variables defined in the Cartesian frame of reference. The density is denoted by ρ and the kinematic viscosity by ν . $\bar{u}_i$ denotes velocities, $\bar{\Omega}_i$ angular velocities, $\bar{x}^o_i$ is the components of the position vector, and $\bar{p}$ denotes the static pressure.

It shall be noted that the second term on the left hand side of eq.(A32) is the Coriolis acceleration and the third term is the centrifugal acceleration. The term $-\overline{\bar{u}_i'\bar{u}_j'}$ is the contribution to the turbulent diffusion, usually referred to as the Reynolds stress. By use of tensor notation, these equations are readily expressed in a form which is invariant under a general transformation. In general curvilinear coordinates we get

Continuity

$$D_i u^i = 0 \quad . \tag{A33}$$

Momentum

$$u^j D_j u^i + 2e^{ijk}\Omega_j u_k + e^{ijk}e_{k\ell m}\Omega_j\Omega_\ell x^o_m$$

$$= -\frac{1}{\rho} D^i p + D^j\left(\nu D_j u^i - \overline{u'^i u'_j}\right) \tag{A34}$$

Here the terms in the momentum equation represent contravariant vectors.

In the present coordinate system the x^2-coordinate is defined in the normal direction to the surface, hence the covariant metric tensor is formulated as

$$g_{ij} = \begin{bmatrix} g_{11} & 0 & g_{13} \\ 0 & 1 & 0 \\ g_{31} & 0 & g_{33} \end{bmatrix} \quad , \tag{A35}$$

where $g_{13} = g_{31}$.

Using eq.(A10) the corresponding contravariant metric tensor is given by

$$g^{ij} = \frac{1}{g} \begin{bmatrix} g_{33} & 0 & -g_{31} \\ 0 & g & 0 \\ -g_{13} & 0 & g_{11} \end{bmatrix} \quad , \tag{A36}$$

where $g = \det(g_{ij})$ yields

$$g = g_{11} g_{33} - g_{13} g_{31} \quad . \tag{A37}$$

For convenience g_{11} is replaced by h_1^2 and g_{33} by h_3^2 .

We are now in position to derive the boundary layer equations in the coordinate system represented by the above metric, eq.(A35). This is accomplished by deriving the individual terms

in the Navier-Stokes equations and taking advantage of the usual thin-layer approximation.

It should be noted, however, that the expressions can be extremely long and cumbersome. As a consequence, the algebraic manipulations are carried out on a computer by using the symbolic language FORMAC.

The equation of continuity

Combining eq.(A33) and eq.(A19), the equation of continuity reads

$$D_i u^i = \frac{\partial u^i}{\partial x^i} + \left\{ \begin{matrix} i \\ j \; i \end{matrix} \right\} u^j = 0 \quad . \tag{A38}$$

From the definition of the Christoffel-symbol it can be demonstrated that

$$\left\{ \begin{matrix} i \\ j \; i \end{matrix} \right\} = \frac{1}{g^{\frac{1}{2}}} \frac{\partial g^{\frac{1}{2}}}{\partial x^j} \quad . \tag{A39}$$

Inserting this expression in eq.(A38) we get

$$\frac{1}{g^{\frac{1}{2}}} \frac{\partial}{\partial x^i} \left(g^{\frac{1}{2}} u^i \right) = 0 \quad , \tag{A40}$$

which in physical components yields

$$\frac{\partial}{\partial x^1} \left(\frac{g^{\frac{1}{2}}}{h_1} u(1) \right) + \frac{\partial}{\partial x^2} \left(g^{\frac{1}{2}} u(2) \right) + \frac{\partial}{\partial x^3} \left(\frac{g^{\frac{1}{2}}}{h_3} u(3) \right) = 0 \quad . \tag{A41}$$

The convective terms

Representing the convective contribution as a contravariant vector we get

$$a^i = u^j D_j u^i = u^j \frac{\partial u^i}{\partial x^j} + \left\{ \begin{matrix} i \\ j \; k \end{matrix} \right\} u^j u^k \quad . \tag{A42}$$

In physical components this equation is written as

$$a(i) = \left(\frac{g_{ii}}{g_{jj}}\right)^{\frac{1}{2}} u(j) \frac{\partial}{\partial x^j}\left(\frac{u(i)}{g_{ii}^{\frac{1}{2}}}\right) + \left(\frac{g_{ii}}{g_{jj}g_{kk}}\right)u(j)u(k) \quad , \qquad (A43)$$

which yields the resulting equations

$$a(1) = \frac{u(1)}{h_1}\frac{\partial u(1)}{\partial x^1} + u(2)\frac{\partial u(1)}{\partial x^2} + \frac{u(3)}{h_3}\frac{\partial u(3)}{\partial x^3}$$

$$+ \frac{u(1)^2 g_{13}}{g}\left[\frac{g_{13}}{h_1^2}\frac{\partial h_1}{\partial x^1} + \frac{\partial h_1}{\partial x^3} - \frac{1}{h_1}\frac{\partial g_{13}}{\partial x^1}\right]$$

$$+ \frac{u(1)u(3)}{g}\cdot\left[\left(\frac{g_{13}^2}{h_1 h_3} + h_1 h_3\right)\frac{\partial h_1}{\partial x^3} - 2g_{13}\frac{\partial h_3}{\partial x^1}\right]$$

$$+ \frac{u(3)^2 h_1}{g}\cdot\left[\frac{\partial g_{13}}{\partial x^3} - \frac{g_{13}}{h_3}\frac{\partial h_3}{\partial x^3} - h_3\frac{\partial h_3}{\partial x^1}\right] \quad , \qquad (A44)$$

$$a(2) = \frac{u(1)}{h_1}\frac{\partial u(2)}{\partial x^1} + u(2)\frac{\partial u(2)}{\partial x^2} + \frac{u(3)}{h_3}\frac{\partial u(2)}{\partial x^3} \quad , \qquad (A45)$$

$$a(3) = \frac{u(1)}{h_1}\frac{\partial u(3)}{\partial x^1} + u(2)\frac{\partial u(3)}{\partial x^2} + \frac{u(3)}{h_3}\frac{\partial u(3)}{\partial x^3}$$

$$+ \frac{u(1)^2 h_3}{g}\cdot\left[\frac{\partial g_{13}}{\partial x^1} - \frac{g_{13}}{h_1}\frac{\partial h_1}{\partial x^1} - h_3\frac{\partial h_1}{\partial x^3}\right]$$

$$+ \frac{u(1)u(3)}{g}\cdot\left[\left(\frac{g_{13}^2}{h_1 h_3} + h_1 h_3\right)\frac{\partial h_3}{\partial x^1} - 2g_{13}\frac{\partial h_1}{\partial x^3}\right]$$

$$+ \frac{u(3)^2 g_{13}}{g}\cdot\left[\frac{g_{13}}{h_3^2}\frac{\partial h_3}{\partial x^3} + \frac{\partial h_3}{\partial x^1} - \frac{1}{h_3}\frac{\partial g_{13}}{\partial x^3}\right] \quad . \qquad (A46)$$

According to boundary layer theory, the velocity in the normal direction $u(2)$ is small compared to $u(1)$ and $u(3)$, and so is the streamwise and crosswise derivatives of $u(2)$. Therefore we put

$$a(2) \cong 0 \quad . \qquad (A47)$$

The Coriolis acceleration

In tensor notation, the Coriolis acceleration is

$$a_{co}^{i} = 2e^{ijk}\Omega_j u_k \quad . \tag{A48}$$

Introducing the permutation symbol, according to eq.(A24), and raising the indices of Ω_j and u_k, eq.(A48) yields

$$a_{co}^{i} = 2g^{-\frac{1}{2}}\varepsilon^{ijk}g_{jm}g_{kn}\Omega^m u^n \quad . \tag{A49}$$

Combining this expression with eq.(A25) results in

$$a_{co}^{i} = 2g^{\frac{1}{2}}\varepsilon_{\ell mn}\, g^{i\ell}\,\Omega^m u^n \quad ,$$

which in physical components is written as

$$a_{co}(i) = 2\cdot\left(\frac{g\cdot g_{ii}}{g_{mm}g_{nn}}\right)^{\frac{1}{2}}\Omega(m)u(n) \quad . \tag{A50}$$

Here the physical components of the angular velocity are defined in the curvilinear coordinate system. But, since the angular velocity is given in the Cartesian coordinate system, we need to transform $\Omega(m)$ into its Cartesian components $\bar{\Omega}(m)$. By taking advantage of eq.(A30), this is accomplished as follows

$$a_{co}(i) = 2\,\varepsilon_{\ell mn}\, g^{i\ell}\left(\frac{g\cdot g_{ii}}{g_{nn}}\right)^{\frac{1}{2}} g^{mj}\,\frac{\partial \bar{x}^k}{\partial x^j}\,\bar{\Omega}(k)u(n) \quad , \tag{A51}$$

where

$$\begin{aligned} \bar{\Omega}(1) &= 0 \quad , \\ \bar{\Omega}(2) &= -\Omega \quad , \\ \bar{\Omega}(3) &= 0 \quad . \end{aligned} \tag{A52}$$

Note that the minus sign appears because the Cartesian coordinate system is defined as left-handed.

Performing the summation of eq.(A51) gives

$$a_{co}(1) = -\frac{2\Omega}{g^{\frac{1}{2}}}\left[g_{13}\,\frac{\partial\bar{x}^2}{\partial x^2}\,u(1) - h_1\,\frac{\partial\bar{x}^2}{\partial x^3}\,u(2) + h_1h_3\,\frac{\partial\bar{x}^2}{\partial x^2}\,u(3)\right] \quad , \tag{A53}$$

$$a_{co}(2) = -\frac{2\Omega}{g^{\frac{1}{2}}}\left[u(1)\cdot\left(h_1\,\frac{\partial\bar{x}^2}{\partial x^3} - \frac{g_{13}}{h_1}\,\frac{\partial\bar{x}^2}{\partial x^1}\right) + u(3)\cdot\left(\frac{g_{13}}{h_3}\,\frac{\partial\bar{x}^2}{\partial x^3} - h_3\,\frac{\bar{x}^2}{\partial x^1}\right)\right] \quad , \tag{A54}$$

$$a_{co}(3) = -\frac{2\Omega}{g^{\frac{1}{2}}}\left[-h_1h_3\,\frac{\partial\bar{x}^2}{\partial x^2}\,u(1) - h_3\,\frac{\partial\bar{x}^2}{\partial x^1}\,u(2) - g_{13}\,\frac{\partial\bar{x}^2}{\partial x^2}\,u(3)\right] \quad . \tag{A55}$$

To be consistent with boundary layer theory, we neglect the Coriolis force in the normal direction. Assuming $u(2)$ to be small compared with $u(1)$ and $u(3)$, the boundary layer approximation yields

$$a_{co}(1) \cong -\frac{2\Omega}{g^{\frac{1}{2}}}\,\frac{\partial\bar{x}^2}{\partial x^2}\,(g_{13}\,u(1) + h_1h_3\,u(3)) \quad , \tag{A56}$$

$$a_{co}(2) \cong 0 \quad , \tag{A57}$$

$$a_{co}(3) \cong \frac{2\Omega}{g^{\frac{1}{2}}}\,\frac{\partial\bar{x}^2}{\partial x^2}\,(h_1h_3\,u(1) - g_{13}\,u(3)) \quad . \tag{A58}$$

The centrifugal acceleration

According to eq.(A34) the contribution due to the centrifugal acceleration reads

$$a_c^i = e^{ijk}e_{k\ell m}\,\Omega_j\Omega_\ell x_m^o \quad . \tag{A59}$$

Note that both the angular velocity and the position vector belongs to the Cartesian coordinate system. Therefore it is

appropriate to carry out the mathematical manipulations in this coordinate system, before recasting the expressions into the curvilinear one.

Recalling eq.(A32), the centrifugal acceleration in the Cartesian coordinate system reads

$$\bar{a}_c(i) = \varepsilon_{ijk}\varepsilon_{k\ell m}\,\Omega(j)\Omega(\ell)\bar{x}(m) \quad . \tag{A60}$$

Taking advantage of eq.(A52), we get

$$\begin{aligned} \bar{a}_c(1) &= -\,\Omega^2\bar{x}^1 \quad , \\ \bar{a}_c(2) &= 0 \quad , \\ \bar{a}_c(3) &= -\,\bar{\Omega}^2\bar{x}^3 \quad . \end{aligned} \tag{A61}$$

According to eq.(A30), $\bar{a}_c(i)$ is transformed into curvilinear coordinates by

$$a_c(i) = g_{ii}^{\frac{1}{2}}\, g^{ij}\, \frac{\partial\bar{x}^k}{\partial x^j}\, \bar{a}_c(k) \quad , \tag{A62}$$

combining this equation with eq.(A61) yields

$$a_c(1) = \frac{h_1}{g}\,\Omega^2\cdot\left[g_{13}\left(\frac{\partial\bar{x}^1}{\partial x^3}\,\bar{x}^1 + \frac{\partial\bar{x}^3}{\partial x^1}\,\bar{x}^3\right) - h_3^2\cdot\left(\frac{\partial\bar{x}^1}{\partial x^2}\,\bar{x}^1 + \frac{\partial\bar{x}^3}{\partial x^1}\,\bar{x}^3\right)\right] \quad , \tag{A63}$$

$$a_c(2) = -\,\Omega^2\cdot\left(\frac{\partial\bar{x}^1}{\partial x^2}\,\bar{x}^1 + \frac{\partial\bar{x}^3}{\partial x^2}\,\bar{x}^3\right) \quad , \tag{A64}$$

$$a_c(3) = \frac{h_3}{g}\,\Omega^2\cdot\left[g_{13}\cdot\left(\frac{\partial\bar{x}^1}{\partial x^1}\,\bar{x}^1 + \frac{\partial\bar{x}^3}{\partial x^1}\,\bar{x}^3\right) - h_1^2\cdot\left(\frac{\partial\bar{x}^1}{\partial x^3}\,\bar{x}^1 + \frac{\partial\bar{x}^3}{\partial x^3}\,\bar{x}^3\right)\right] \quad . \tag{A65}$$

According to the boundary layer approximation, the contribution of the normal pressure gradient induced by the rotation is neglected. That is, we put

$$a_c(2) \cong 0 \quad . \tag{A66}$$

The pressure gradient

The pressure gradient contributes to the equations as

$$a_p^i = -\frac{1}{\rho} D^i p = -\frac{1}{\rho} g^{ij} \frac{\partial p}{\partial x^j} \quad , \tag{A67}$$

which in physical components is

$$a_p(i) = -\frac{1}{\rho} g_{ii}^{\frac{1}{2}} g^{ij} \frac{\partial p}{\partial x^j} \quad , \tag{A68}$$

thus yielding

$$a_p(1) = -\frac{h_1 h_3^2}{g} \frac{1}{\rho} \frac{\partial p}{\partial x^1} + \frac{g_{13} h_1}{g} \frac{1}{\rho} \frac{\partial p}{\partial x^3} \quad , \tag{A69}$$

$$a_p(2) = -\frac{1}{\rho} \frac{\partial p}{\partial x^2} \quad , \tag{A70}$$

$$a_p(3) = \frac{g_{13} h_3}{g} \frac{1}{\rho} \frac{\partial p}{\partial x^1} - \frac{h_1^2 h_3}{g} \frac{1}{\rho} \frac{\partial p}{\partial x^3} \quad . \tag{A71}$$

Neglecting the normal pressure gradient implies that

$$a_p(2) \cong 0 \quad . \tag{A72}$$

The diffusive terms

Cast into tensor form, the diffusive terms reads

$$a_D^i = D^j\left(\nu D_j u^i - \overline{u'^i u'_j}\right) \tag{A73}$$

The thin-layer approximation assumes that stress gradients in directions parallel to the surface are negligible in comparison with stress gradients normal to the surface. This combined with $g_{12} = g_{21} = g_{32} = g_{23} = 0$ and $g_{22} = 1$ implies that

the contribution of the diffusion in the curvilinear coordinate system is the same as in the Cartesian one. Therefore, the diffusion is readily obtained as

$$a_D(1) \cong \frac{\partial}{\partial x^2}\left(\nu \frac{\partial u(1)}{\partial x^2} - \overline{u'(1)u'(2)}\right) \quad , \tag{A74}$$

$$a_D(2) \cong 0 \quad , \tag{A75}$$

$$a_D(3) \cong \frac{\partial}{\partial x^2}\left(\nu \frac{\partial u(3)}{\partial x^2} - \overline{u'(2)u'(3)}\right) \quad . \tag{A76}$$

A3 The Boundary Layer Equations

Before writing down the full boundary layer equations, the variables are recasted into the notation of the main text. That is $(\bar{x}^1,\bar{x}^2,\bar{x}^3)$ is replaced by $(\bar{x},\bar{y},\bar{z})$, (x^1,x^2,x^3) is replaced by (x,y,z) and $(u(1),u(2),u(3))$ is replaced by (u,v,w).

In order to make a compact formulation of the equations, we denote the angle between the coordinate curves x and z as θ. According to eq.(A16), we get

$$g_{13} = h_1 h_3 \cos\theta \quad , \tag{A77}$$

which, inserted in eq.(A37), yields

$$g = h_1^2 h_3^2 \sin^2\theta \quad . \tag{A78}$$

Recalling the transformation derived in section 3.1 of the main text, we note that

$$\frac{\partial \bar{x}^2}{\partial x^2} = \frac{R}{h_1 h_3 \sin\theta} \frac{\partial \bar{x}^1}{\partial x^1} \quad . \tag{A79}$$

Inserting eqs.(A77)-(A79) into the boundary layer equations, we get

Continuity

$$\frac{\partial}{\partial x}(uh_3\sin\theta) + \frac{\partial}{\partial y}(vh_1h_3\sin\theta) + \frac{\partial}{\partial z}(wh_1\sin\theta) = 0 \quad . \tag{A80}$$

x-momentum

$$\frac{u}{h_1}\frac{\partial u}{\partial x} + v\frac{\partial u}{\partial y} + \frac{w}{h_3}\frac{\partial u}{\partial z} - \frac{2\Omega\ R\cos\theta}{h_1h_3\sin^2\theta}\frac{\partial\bar{x}}{\partial x}u - \frac{2\Omega\ R}{h_1h_3\sin^2\theta}\frac{\partial\bar{x}}{\partial x}w$$

$$+ \frac{\Omega^2\bar{r}}{\sin^2\theta}\left(\frac{\cos\theta}{h_3}\frac{\partial\bar{r}}{\partial z} - \frac{1}{h_1}\frac{\partial\bar{r}}{\partial x}\right) - \cot\theta\ K_1u^2 + K_{13}uw + \frac{K_3}{\sin\theta}w^2$$

$$= -\frac{1}{h_1\sin^2\theta}\frac{1}{\rho}\frac{\partial p}{\partial x} + \frac{\cos\theta}{h_3\sin^2\theta}\frac{1}{\rho}\frac{\partial p}{\partial z} + \frac{\partial}{\partial y}\left(\nu\frac{\partial u}{\partial y} - \overline{u'v'}\right) \quad . \tag{A81}$$

z-momentum

$$\frac{u}{h_1}\frac{\partial w}{\partial x} + v\frac{\partial w}{\partial y} + \frac{w}{h_3}\frac{\partial w}{\partial z} + \frac{2\Omega\ R}{h_1h_3\sin^2\theta}\frac{\partial\bar{x}}{\partial x}u + \frac{2\Omega\ R\cos\theta}{h_1h_3\sin^2\theta}\frac{\partial\bar{x}}{\partial x}w$$

$$+ \frac{\Omega^2\bar{r}}{\sin^2\theta}\left(\frac{\cos\theta}{h_1}\frac{\partial\bar{r}}{\partial x} - \frac{1}{h_3}\frac{\partial\bar{r}}{\partial z}\right) + \frac{K_1}{\sin\theta}u^2 + K_{31}uw - \cot\theta\ K_3w^2$$

$$= \frac{\cos\theta}{h_1\sin^2\theta}\frac{1}{\rho}\frac{\partial p}{\partial x} - \frac{1}{h_3\sin^2\theta}\frac{1}{\rho}\frac{\partial p}{\partial z} + \frac{\partial}{\partial y}\left(\nu\frac{\partial w}{\partial y} - \overline{v'w'}\right) \quad . \tag{A82}$$

Where

$$\bar{r} = \sqrt{\bar{x}^2 + \bar{z}^2} \quad , \tag{A83}$$

$$K_1 = \frac{1}{h_1h_3\sin\theta}\left[\frac{\partial}{\partial x}(h_3\cos\theta) - \frac{\partial h_1}{\partial z}\right] \quad , \tag{A84}$$

$$K_3 = \frac{1}{h_1h_3\sin\theta}\left[\frac{\partial}{\partial z}(h_1\cos\theta) - \frac{\partial h_3}{\partial x}\right] \quad , \tag{A85}$$

$$K_{13} = \frac{1}{\sin\theta}\left[\cos\theta\left(K_3 + \frac{1}{h_3}\frac{\partial\theta}{\partial z}\right) - K_1 - \frac{1}{h_1}\frac{\partial\theta}{\partial x}\right] \quad , \tag{A86}$$

$$K_{31} = \frac{1}{\sin\theta}\left[\cos\theta\left(K_1 + \frac{1}{h_1}\frac{\partial\theta}{\partial x}\right) - K_3 - \frac{1}{h_3}\frac{\partial\theta}{\partial z}\right] \quad . \tag{A87}$$

It can be demonstrated that K_1 and K_3 represent the geodestic curvatures of the z = constant curves and x = constant curves, respectively.

Evaluating the momentum equations on the edge of the boundary layer yields the Euler equations

$$
\begin{aligned}
&- \frac{1}{h_1 \sin^2\theta}\,\frac{1}{\rho}\,\frac{\partial p}{\partial x} + \frac{\cos\theta}{h_3 \sin^2\theta}\,\frac{1}{\rho}\,\frac{\partial p}{\partial z} \\
&= \frac{U_e}{h_1}\,\frac{\partial U_e}{\partial x} + \frac{W_e}{h_3}\,\frac{\partial U_e}{\partial z} - \frac{2\Omega\, R\cos\theta}{h_1 h_3 \sin^2\theta}\,\frac{\partial \bar{x}}{\partial x}\,U_e \\
&- \frac{2\Omega\, R}{h_1 h_3 \sin^2\theta}\,W_e + \frac{\Omega^2\,\bar{r}}{\sin^2\theta}\left(\frac{\cos\theta}{h_3}\,\frac{\partial \bar{r}}{\partial z} - \frac{1}{h_1}\,\frac{\partial \bar{r}}{\partial x}\right) \\
&- \cot\theta\, K_1 U_e^2 + K_{13}\, U_e W_e + \frac{K_3}{\sin\theta}\,W_e \quad . \qquad \text{(A88)}
\end{aligned}
$$

$$
\begin{aligned}
&\frac{\cos\theta}{h_1 \sin^2\theta}\,\frac{1}{\rho}\,\frac{\partial p}{\partial x} - \frac{1}{h_3 \sin^2\theta}\,\frac{1}{\rho}\,\frac{\partial p}{\partial z} \\
&= \frac{U_e}{h_1}\,\frac{\partial W_e}{\partial x} + \frac{W_e}{h_3}\,\frac{\partial W_e}{\partial z} + \frac{2\Omega\, R}{h_1 h_3 \sin^2\theta}\,\frac{\partial \bar{x}}{\partial x}\,U_e \\
&+ \frac{2\Omega\, R\cos\theta}{h_1 h_3 \sin^2\theta}\,\frac{\partial \bar{x}}{\partial x}\,W_e + \frac{\Omega^2\, r}{\sin^2\theta}\left(\frac{\cos\theta}{h_1}\,\frac{\partial \bar{r}}{\partial x} - \frac{1}{h_3}\,\frac{\partial \bar{r}}{\partial z}\right) \\
&+ \frac{K_1}{\sin\theta}\,U_e^2 + K_{31}\, U_e W_e - \cot\theta\, K_3 W_e^2 \quad . \qquad \text{(A89)}
\end{aligned}
$$

Here it has been utilized that $\frac{\partial u}{\partial y} = \frac{\partial w}{\partial y} = 0$ at the edge of the boundary layer.

APPENDIX B

Discretization of the Boundary Layer Equations

In the following, various versions of the Keller-box scheme and the zig-zag scheme will be used to discretize the three-dimensional boundary layer equations and the equations defining the initial conditions (i.e. the initial line equations, the infinite-swept-wing equations and the stagnation line equations).

B1 Discretization of the Initial Line Equations

The initial line equations defines a set of one-dimensional flow equations in the sence that they only have one independent variable η. It is therefore only necessary to discretize the equations about an η-column, as shown in fig. B1.

The discretization is accomplished by using centred differences for the derivatives and averages for the variables at the center between two adjoining net points.

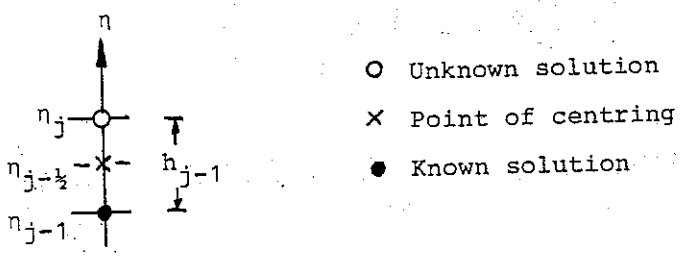

Fig. B1 Difference molecule of the initial line equations.

Denoting the distance between net points η_{j-1} and η_j by h_{j-1}, the derivatives are written as

$$( )'_{j-\frac{1}{2}} = h_{j-1}^{-1}[( )_j - ( )_{j-1}] \quad , \tag{B1}$$

and the averaged variables are given by

$$( )_{j-\frac{1}{2}} = \frac{1}{2}[( )_j + ( )_{j-1}] \quad . \tag{B2}$$

Eqs.(3.137a)-(3.137d) and eqs.(3.147a)-(3.147c) defines together the initial line equations. In discretized form they are written as

$$F_j - F_{j-1} - \frac{1}{2}h_{j-1}(U_j + U_{j-1}) = 0 \tag{B3}$$

$$G_j - G_{j-1} - \frac{1}{2}h_{j-1}(W_j + W_{j-1}) = 0 \tag{B4}$$

$$U_j - U_{j-1} - \frac{1}{2}h_{j-1}(V_j + V_{j-1}) = 0 \tag{B5}$$

$$W_j - W_{j-1} - \frac{1}{2}h_{j-1}(T_j + T_{j-1}) = 0 \tag{B6}$$

$$\begin{aligned} &h_{j-1}^{-1}\left[(b\,V)_j - (b\,V)_{j-1}\right] + \frac{1}{4}(E_j + E_{j-1})(V_j + V_{j-1}) \\ &- \frac{1}{2}\bar{m}_2\bar{U}_{xe}(U_j^2 + U_{j-1}^2) - \frac{1}{2}\bar{K}_{13}\left[(U\,W)_j + (U\,W)_{j-1}\right] \\ &+ \frac{1}{2}\bar{m}_5(U_j + U_{j-1}) + \bar{m}_2\bar{U}_{xe} + \bar{K}_{13}\left(\frac{\bar{W}_e}{W_{ref}}\right) - \bar{m}_5 = 0 \quad . \end{aligned} \tag{B7}$$

$$\begin{aligned} &h_{j-1}^{-1}\left[(b\,T)_j - (b\,T)_{j-1}\right] + \frac{1}{4}(E_j + E_{j-1})(T_j + T_{j-1}) \\ &+ \frac{1}{2}\bar{m}_8(W_j^2 + W_{j-1}^2) - \frac{1}{2}\bar{m}_{11}(W_j + W_{j-1}) \\ &- \bar{m}_8\left(\frac{\bar{W}_e}{W_{ref}}\right)^2 + \bar{m}_{11}\left(\frac{\bar{W}_e}{W_{ref}}\right) = 0 \quad . \end{aligned} \tag{B8}$$

$$h_{j-1}^{-1}(E_j - E_{j-1}) - \frac{1}{2}\bar{m}_2\bar{U}_{xe}(U_j + U_{j-1}) + \frac{1}{2}\bar{m}_{13}(W_j + W_{j-1}) = 0 \quad . \tag{B9}$$

Note that bars denote quantities which are known apriori.

Denoting the variables evaluated at the surface by supscript 'o' and at the edge of the boundary layer by subscript 'J', the boundary conditions become

$$U_o = W_o = E_o = 0 \quad , \tag{B10a}$$

and

$$U_J = 1 \quad , \quad W_J = \frac{W_e}{W_{ref}} \quad , \quad F_J = \eta_J - 1 \quad . \tag{B10b}$$

B2 Discretization of the Infinite-Swept-Wing Equations

In order to discretize the infinite-swept-wing equations, we consider the two-dimensional difference molecule shown in fig. B2.

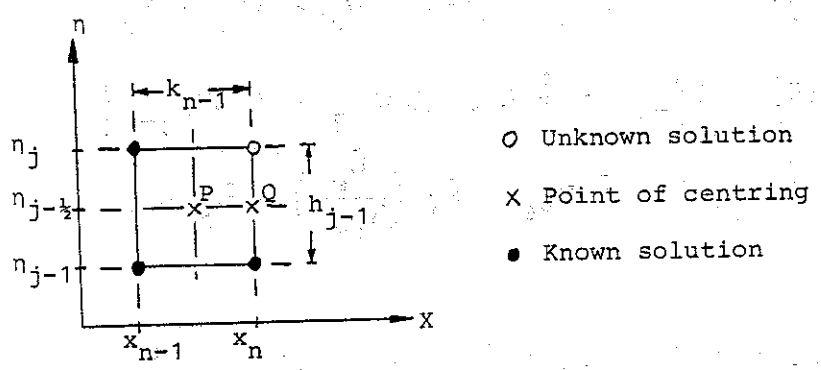

Fig. B2 Difference molecule of the infinite-swept-wing equations

On the net shown in the figure, we denote the node points by

$$x_n = x_{n-1} + k_{n-1} \quad , \quad n = 1,2, \ldots , N \tag{B11a}$$

and

$$\eta_j = \eta_{j-1} + h_{j-1} \quad , \quad j = 1,2, \ldots , J \quad . \tag{B11b}$$

The difference equations approximating eqs.(3.137a)-(3.137d) are obtained by averaging about $Q(x_n, \eta_{j-\frac{1}{2}})$, thus yielding

$$F_j - F_{j-1} - \frac{1}{2}h_{j-1}(U_j + U_{j-1}) = 0 \qquad \text{(B12)}$$

$$G_j - G_{j-1} - \frac{1}{2}h_{j-1}(W_j + W_{j-1}) = 0 \qquad \text{(B13)}$$

$$U_j - U_{j-1} - \frac{1}{2}h_{j-1}(V_j + V_{j-1}) = 0 \qquad \text{(B14)}$$

$$W_j - W_{j-1} - \frac{1}{2}h_{j-1}(T_j + T_{j-1}) = 0 \quad . \qquad \text{(B15)}$$

For simplicity, variables evaluated at (x_n, η_j) and at (x_n, η_{j-1}) are denoted by $(\ )_j$ and $(\ )_{j-1}$, respectively.

In eqs.(3.145a)-(3.145c), all variables except E are approximated by averaging about the midpoint $P(x_{n-\frac{1}{2}}, \eta_{j-\frac{1}{2}})$. Hence derivatives may be written

$$\left[\frac{\partial(\ )}{\partial x}\right]_P = k_{n-1}^{-1}\left[\frac{1}{2}(\ )_j + \frac{1}{2}(\ )_{j-1} - (\ )_{j-\frac{1}{2}}^{n-1}\right] \qquad \text{(B16}$$

and

$$(\ )_P' = \frac{1}{2}h_{j-1}^{-1}\left[(\ )_j - (\ )_{j-1} + (\ )_j^{n-1} - (\ )_{j-1}^{n-1}\right] \quad , \qquad \text{(B17)}$$

where

$$(\ )_{j-\frac{1}{2}}^{n-1} = \frac{1}{2}\left[(\ )_j^{n-1} + (\ )_{j-1}^{n-1}\right] \quad . \qquad \text{(B18)}$$

Averaged values are given by

$$(\ )_P = \frac{1}{2}\left[(\ )_j + \frac{1}{2}(\ )_{j-1} + (\ )_{j-\frac{1}{2}}^{n-1}\right] \qquad \text{(B19)}$$

In order to avoid possibly oscillations due to the discretization of the normal velocities, the variable E is averaged as

$$E_P = \frac{1}{2}(E_j + E_{j-1}) \qquad \text{(B20)}$$

and

$$E_P' = h_{j-1}^{-1}(E_j - E_{j-1}) \quad , \qquad \text{(B21)}$$

where $E_j = \frac{1}{2}(E_j^n + E_j^{n-1})$ is taken as the unknown.

Thus, eqs. (3.145a)-(3.145c) are approximated by

$$\frac{1}{2}\, h_{j-1}^{-1}\left[\left(b\ V\right)_j - \left(b\ V\right)_{j-1} + \left(b\ V\right)_j^{n-1} - \left(b\ V\right)_{j-1}^{n-1}\right]$$

$$+ \frac{1}{4}\left(E_j + E_{j-1}\right)\left(\frac{1}{2}\, V_j + \frac{1}{2}\, V_{j-1} + V_{j-\frac{1}{2}}^{n-1}\right)$$

$$+ \frac{1}{2}\left[\frac{1}{2}\, \bar{m}_1\left(U_e + U_e^{n-1}\right) - \bar{m}_2 \lambda_j\, k_{n-1}^{-1}\left(U_e - U_e^{n-1}\right)\right]$$

$$\cdot\left[\frac{1}{2}\left(U^2\right)_j + \frac{1}{2}\left(U^2\right)_{j-1} + \left(U^2\right)_{j-\frac{1}{2}}^{n-1}\right]$$

$$- \frac{1}{2}\left[\bar{K}_{13} + \bar{m}_3\, \frac{\overline{\partial U}_e}{\partial z}\, \frac{2}{U_e + U_e^{n-1}}\right]\left[\frac{1}{2}\left(UW\right)_j + \frac{1}{2}\left(UW\right)_{j-1} + \left(UW\right)_{j-\frac{1}{2}}^{n-1}\right]$$

$$- \frac{1}{2}\, \bar{m}_4\, \frac{2}{U_e + U_e^{n-1}}\left[\frac{1}{2}\left(W^2\right)_j + \frac{1}{2}\left(W^2\right)_{j-1} + \left(W^2\right)_{j-\frac{1}{2}}^{n-1}\right]$$

$$+ \frac{1}{2}\, \bar{m}_5\left(\frac{1}{2}\, U_j + \frac{1}{2}\, U_{j-1} + U_{j-\frac{1}{2}}^{n-1}\right) + \bar{m}_6\, \frac{\frac{1}{2}\, W_j + \frac{1}{2}\, W_{j-1} + W_{j-\frac{1}{2}}^{n-1}}{U_e + U_e^{n-1}}$$

$$- \frac{1}{4}\, \bar{m}_2 \lambda_j\, k_{n-1}^{-1}\left(U_e + U_e^{n-1}\right)\left[\frac{1}{2}\left(U^2\right)_j + \frac{1}{2}\left(U^2\right)_{j-1} - \left(U^2\right)_{j-\frac{1}{2}}^{n-1}\right]$$

$$- \frac{1}{2}\, \bar{m}_1\left(U_e + U_e^{n-1}\right) + \bar{m}_2 k_{n-1}^{-1}\left(U_e - U_e^{n-1}\right)$$

$$+ \left(\bar{K}_{13} + \bar{m}_3\, \frac{\overline{\partial U}_e}{\partial z}\, \frac{2}{U_e + U_e^{n-1}}\right)\left(\frac{\bar{W}_e}{W_{ref}}\right)$$

$$+ \bar{m}_4\left(\frac{\bar{W}_e}{W_{ref}}\right)^2 \frac{2}{U_e + U_e^{n-1}} - \bar{m}_5 - \bar{m}_6\left(\frac{\bar{W}_e}{W_{ref}}\right) \frac{2}{U_e + U_e^{n-1}} = 0 \quad . \quad \text{(B22)}$$

$$\frac{1}{2}\, h_{j-1}^{-1}\left[\left(b\ T\right)_j - \left(b\ T\right)_{j-1} + \left(b\ T\right)_j^{n-1} - \left(b\ T\right)_{j-1}^{n-1}\right]$$

$$+ \frac{1}{4}\left(E_j + E_{j-1}\right)\left(\frac{1}{2}\ T_j + \frac{1}{2}\ T_{j-1} + T_{j-\frac{1}{2}}^{n-1}\right)$$

$$- \frac{1}{4}\ \bar{m}_7\ \left(U_e + U_e^{n-1}\right)\left[\frac{1}{2}\left(UW\right)_j + \frac{1}{2}\left(UW\right)_{j-1} + \left(UW\right)_{j-\frac{1}{2}}^{n-1}\right]$$

$$+ \frac{1}{2}\ \bar{m}_8\ \left[\frac{1}{2}\left(W^2\right)_j + \frac{1}{2}\left(W^2\right)_{j-1} + \left(W^2\right)_{j-\frac{1}{2}}^{n-1}\right]$$

$$- \frac{1}{4}\ \bar{m}_9\ \left[\left(U_e^2\right) + \left(U_e^2\right)^{n-1}\right]\left[\frac{1}{2}\left(U^2\right)_j + \frac{1}{2}\left(U^2\right)_{j-1} + \left(U^2\right)_{j-\frac{1}{2}}^{n-1}\right]$$

$$- \frac{1}{4}\ \bar{m}_{10}\left(U_e + U_e^{n-1}\right)\left(\frac{1}{2}\ U_j + \frac{1}{2}\ U_{j-1} + U_{j-\frac{1}{2}}^{n-1}\right)$$

$$- \frac{1}{2}\ \bar{m}_{11}\left(\frac{1}{2}\ W_j + \frac{1}{2}\ W_{j-1} + W_{j-\frac{1}{2}}^{n-1}\right)$$

$$- \frac{1}{4}\ \bar{m}_2\ \left(U_e + U_e^{n-1}\right)\left(\frac{1}{2}\ U_j + \frac{1}{2}\ U_j + U_{j-\frac{1}{2}}^{n-1}\right)k_{n-1}^{-1}\left(\frac{1}{2}\ W_j + \frac{1}{2}\ W_{j-1} - W_{j-\frac{1}{2}}^{n-1}\right]$$

$$+ \frac{1}{2}\ \bar{m}_7\left(\frac{\bar{W}_e}{W_{ref}}\right)\left(U_e + U_e^{n-1}\right) - \bar{m}_8\left(\frac{\bar{W}_e}{W_{ref}}\right)^2$$

$$+ \frac{1}{2}\ \bar{m}_9\left[U_e^2 + \left(U_e^2\right)^{n-1}\right] + \frac{1}{2}\ \bar{m}_{10}\left(U_e + U_e^{n-1}\right)$$

$$+ \bar{m}_{11}\left(\frac{\bar{W}_e}{W_{ref}}\right) + \frac{1}{2}\left(\frac{\bar{m}_2}{W_{ref}}\right)\frac{\partial \bar{W}_e}{\partial x}\left(U_e + U_e^{n-1}\right) = 0 \quad . \qquad \text{(B23)}$$

$$h_{j-1}^{-1}\left(E_j - E_{j-1}\right)$$

$$- \frac{1}{2}\left\{\frac{1}{2}\bar{m}_{12}\left(U_e + U_e^{n-1}\right) + \bar{m}_2 \frac{2}{\delta^* + \delta^{*n-1}} k_{n-1}^{-1}\left[\left(U_e\delta^*\right) - \left(U_e\delta^*\right)^{n-1}\right]\right\}$$

$$\cdot\left(\frac{1}{2}U_j + \frac{1}{2}U_{j-1} + U_{j-\frac{1}{2}}^{n-1}\right) - \frac{1}{2}\bar{m}_{13}\left(\frac{1}{2}W_j + \frac{1}{2}W_{j-1} + W_{j-\frac{1}{2}}^{n-1}\right)$$

$$- \frac{1}{2}\bar{m}_2\left(U_e + U_e^{n-1}\right) k_{n-1}^{-1}\left(\frac{1}{2}U_j + \frac{1}{2}U_{j-1} - U_{j-\frac{1}{2}}^{n-1}\right) = 0 \quad . \tag{B24}$$

Here, bars denote averaged quantities which are known apriori.

To employ the present discretization to the case of reverse flow, we have implemented the Flare approximation via the coefficient λ_j . Here we take

$$\lambda_j = \begin{cases} 1 & \text{for } U_{j-\frac{1}{2}}^{n-\frac{1}{2}} \geq 0 \\ 0 & \text{for } U_{j-\frac{1}{2}}^{n-\frac{1}{2}} < 0 \end{cases} \quad . \tag{B25}$$

If the approximated equations are solved in the direct manner, U_e is known and δ^* is treated as the unknown. Correspondingly, if the equations are solved by the inverse method, δ^* is known and U_e is treated as the unknown. In both cases the discretized equations are subject to the boundary conditions

$$U_o = W_o = E_o = 0 \quad , \tag{B26a}$$

and

$$U_J = 1 \quad , \quad W_J = \frac{W_e}{W_{ref}} \quad , \quad F_J = \eta_J - 1 \quad . \tag{B26b}$$

However, if an interactive solution procedure is employed, both U_e and δ^* are treated as unknown and the relation given by eq.(3.175) is taken as a boundary condition in addition to those given by eq.(3.146a) and (3.146b). That is

$$U_e\left(1 - d_{n,n}\delta^*\right) - e_{n,n}\left(\eta_J W_e - G_J W_{ref}\right)\delta^* - K = 0. \tag{B27}$$

B3 Discretization of the Stagnation Line Equations

When discretizing the stagnation line equations, we approximate the difference equations as if the stagnation line locally coincides with a x = constant line. Hence, we obtain a difference molecule as shown in fig. B3.

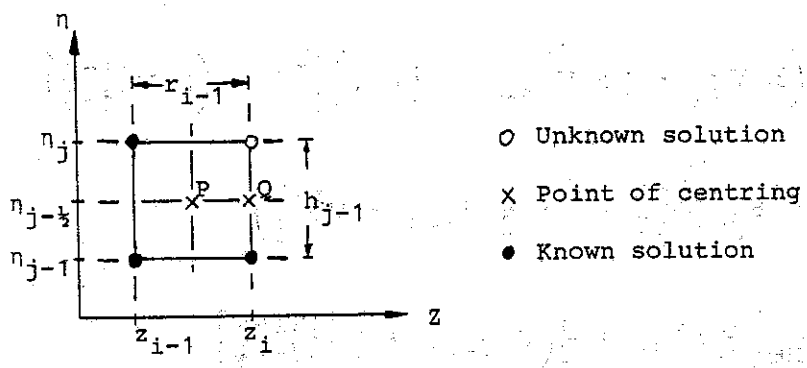

Fig. B3 Difference molecule of the stagnation line equations.

The node points are denoted by

$$z_i = z_{i-1} + r_{i-1} \quad , \quad i = 1,2, \ldots , I \qquad \text{(B28a)}$$

$$\eta_j = \eta_{j-1} + h_{j-1} \quad , \quad j = 1,2, \ldots , J \qquad \text{(B28b)}$$

In order to discretize the equations, we employ the same procedure as in the infinite-swept-wing case. That is eqs. (3.137a) - (3.137d) are averaged about $Q(\eta_{j-\frac{1}{2}}, z_i)$ and eqs.(3.143a)-(3.143c) are averaged about $P(\eta_{j-\frac{1}{2}}, z_{i-\frac{1}{2}})$. Thus we obtain

$$F_j - F_{j-1} - \frac{1}{2} h_{j-1} (U_j + U_{j-1}) = 0 \qquad \text{(B29)}$$

$$G_j - G_{j-1} - \frac{1}{2} h_{j-1} (W_j + W_{j-1}) = 0 \qquad \text{(B30)}$$

$$U_j - U_{j-1} - \frac{1}{2} h_{j-1} (V_j + V_{j-1}) = 0 \qquad \text{(B31)}$$

$$W_j - W_{j-1} - \frac{1}{2} h_{j-1} (T_j + T_{j-1}) = 0 \qquad \text{(B32)}$$

$$\begin{aligned}
&\frac{1}{2} h_{j-1}^{-1} \left[\left(b\ V \right)_j - \left(b\ V \right)_{j-1} + \left(b\ V \right)_j^{i-1} - \left(b\ V \right)_{j-1}^{i-1} \right] \\
&+ \frac{1}{4} \left(E_j + E_{j-1} \right) \left(\frac{1}{2} V_j + \frac{1}{2} V_{j-1} + V_{j-\frac{1}{2}}^{i-1} \right) \\
&- \frac{1}{2} \bar{m}_2 \bar{U}_{xe} \left[\frac{1}{2} \left(U^2 \right)_j + \frac{1}{2} \left(U^2 \right)_{j-1} + \left(U^2 \right)_{j-\frac{1}{2}}^{i-1} \right] \\
&- \frac{1}{2} \left(\bar{K}_{13} + \frac{\bar{m}_3}{\bar{U}_{xe}} \frac{\partial \bar{U}_{xe}}{\partial z} \right) \left[\frac{1}{2} \left(UW \right)_j + \frac{1}{2} \left(UW \right)_{j-1} + \left(UW \right)_{j-\frac{1}{2}}^{i-1} \right] \\
&+ \frac{1}{2} \bar{m}_5 \left(\frac{1}{2} U_j + \frac{1}{2} U_{j-1} + U_{j-\frac{1}{2}}^{i-1} \right) \\
&- \frac{1}{2} \bar{m}_3 r_{i-1}^{-1} \left(\frac{1}{2} W_j + \frac{1}{2} W_{j-1} + W_{j-\frac{1}{2}}^{i-1} \right) \left(\frac{1}{2} U_j + \frac{1}{2} U_{j-1} - U_{j-\frac{1}{2}}^{i-1} \right) \\
&+ \bar{m}_2 \bar{U}_{xe} + \left(\bar{K}_{13} + \frac{\bar{m}_3}{\bar{U}_{xe}} \frac{\partial \bar{U}_{xe}}{\partial z} \right) \left(\frac{\bar{W}_e}{\bar{W}_{ref}} \right) - \bar{m}_5 = 0 \quad . \qquad \text{(B33)}
\end{aligned}$$

$$\frac{1}{2}\, h_{j-1}^{-1}\left[\left(b\,T\right)_j - \left(b\,T\right)_{j-1} + \left(b\,T\right)_j^{i-1} - \left(b\,T\right)_{j-1}^{i-1}\right]$$

$$+ \frac{1}{4}\left(E_j + E_{j-1}\right)\left(\frac{1}{2}\,T_j + \frac{1}{2}\,T_{j-1} + T_{j-\frac{1}{2}}^{i-1}\right)$$

$$+ \frac{1}{2}\,\bar{m}_8\left[\frac{1}{2}\left(W^2\right)_j + \frac{1}{2}\left(W^2\right)_{j-1} + \left(W^2\right)_{j-\frac{1}{2}}^{i-1}\right]$$

$$- \frac{1}{2}\,\bar{m}_{11}\left(\frac{1}{2}\,W_j + \frac{1}{2}\,W_{j-1} + W_{j-\frac{1}{2}}^{i-1}\right)$$

$$- \frac{1}{2}\,\bar{m}_3 r_{i-1}^{-1}\left[\frac{1}{2}\left(W^2\right)_j + \frac{1}{2}\left(W^2\right)_{j-1} - \left(W^2\right)_{j-\frac{1}{2}}^{i-1}\right]$$

$$- \bar{m}_8\left(\frac{\bar{W}_e}{\bar{W}_{ref}}\right)^2 + m_{11}\left(\frac{\bar{W}_e}{\bar{W}_{ref}}\right) + \frac{\bar{m}_3}{\bar{W}_{ref}}\left(\frac{\bar{W}_e}{\bar{W}_{ref}}\right)\frac{\partial \bar{W}_e}{\partial z} = 0 \qquad . \quad \text{(B34)}$$

$$h_{j-1}^{-1}\left(E_j - E_{j-1}\right) - \frac{1}{2}\,\bar{m}\,\bar{U}_{xe}\left(\frac{1}{2}\,U_j + \frac{1}{2}\,U_{j-1} + U_{j-\frac{1}{2}}^{i-1}\right)$$

$$- \frac{1}{2}\left(\bar{m}_{13} + 2\,\bar{m}_3 r_{i-1}^{-1}\,\frac{\delta^* - \delta^{*i-1}}{\delta^* + \delta^{*i-1}}\right)\left(\frac{1}{2}\,W_j + \frac{1}{2}\,W_{j-1} + W_{j-\frac{1}{2}}^{i-1}\right)$$

$$- \bar{m}_3 r_{i-1}^{-1}\left(\frac{1}{2}\,W_j + \frac{1}{2}\,W_{j-1} - W_{j-\frac{1}{2}}^{i-1}\right) = 0 \qquad . \quad \text{(B35)}$$

The boundary conditions are given as

$$U_o = W_o = E_o = 0 \qquad , \quad \text{(B36a)}$$

and

$$U_J = 1 \quad , \quad W_J = \frac{W_e}{W_{ref}} \quad , \quad F_J = \eta_J - 1 \qquad . \quad \text{(B36b)}$$

B4 Discretization of the General Boundary Layer Equations using the Box Scheme

In the case of attached flow, we employ the standard Keller-box scheme to discretize the three-dimensional boundary layer equations. A difference molecule of this scheme is shown in fig. B4, where the node points are introduced by

$$x_n = x_{n-1} + k_{n-1} \quad , \quad n = 1,2, \ldots , N \quad , \tag{B37a}$$

$$z_i = z_{i-1} + r_{i-1} \quad , \quad i = 1,2, \ldots , I \quad , \tag{B37b}$$

and

$$\eta_j = \eta_{j-1} + h_{j-1} \quad , \quad j = 1,2, \ldots , J \quad , \tag{B37c}$$

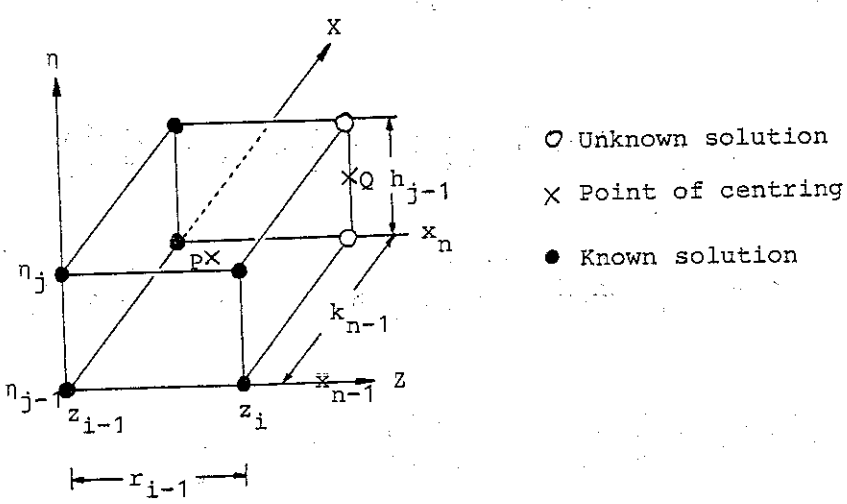

Fig. B4 Difference molecule of the Keller-box scheme.

In this case the definition equations (3.137a)-(3.137d) are discretized by averaging about $Q(x_n, \eta_{j-\frac{1}{2}}, z_i)$ whereas all variables except E appearing in eqs.(3.138a)-(3.138c) are approximated by averaging about the midpoint $P(x_{n-\frac{1}{2}}, \eta_{j-\frac{1}{2}}, z_{i-\frac{1}{2}})$. The unknown E_j, which is related to the normal velocity component, is expressed in terms of its values at the four corner points, i.e. $E_j \equiv \frac{1}{4}\left(E_j^{n,i} + E_j^{n,i-1} + E_j^{n-1,i} + E_j^{n-1,i-1}\right)$.

Thus, we obtain

$$F_j - F_{j-1} - \frac{1}{2} h_{j-1} (U_j + U_{j-1}) = 0 \qquad \text{(B38)}$$

$$G_j - G_{j-1} - \frac{1}{2} h_{j-1} (W_j + W_{j-1}) = 0 \qquad \text{(B39)}$$

$$U_j - U_{j-1} - \frac{1}{2} h_{j-1} (V_j + V_{j-1}) = 0 \qquad \text{(B40)}$$

$$W_j - W_{j-1} - \frac{1}{2} h_{j-1} (T_j + T_{j-1}) = 0 \quad . \qquad \text{(B41)}$$

Letting bars denote quantities which are known apriori and, for convenience, omitting the indices '$n-\frac{1}{2}$', '$i-\frac{1}{2}$', and '$j-\frac{1}{2}$' , eqs.(3.138a)-(3.138c) are approximated as

$$\frac{1}{2}\,h_{j-1}^{-1}\left[\frac{1}{2}\left(bV\right)_j - \frac{1}{2}\left(bV\right)_{j-1} + \frac{1}{2}\left(bV\right)_j^{n-1,i} - \frac{1}{2}\left(bV\right)_{j-1}^{n-1,i} + \left(bV\right)_j^{i-1} - \left(bV\right)_{j-1}^{i-1}\right]$$

$$+ \frac{1}{4}\left(E_j + E_{j-1}\right)\left(\frac{1}{4}\,V_j + \frac{1}{4}\,V_{j-1} + \frac{1}{2}\,V^{i,n-1} + V^{i-1}\right)$$

$$+ \frac{1}{4}\left[\bar{m}_1\left(\frac{1}{2}\,U_e + \frac{1}{4}\,U_e^{i,n-1} + U_e^{i-1}\right) - \bar{m}_2 k_{n-1}^{-1}\left(U_e + U_e^{n,i-1} - 2\,U_e^{n-1}\right)\right]$$

$$\cdot\left[\frac{1}{4}\left(U^2\right)_j + \frac{1}{4}\left(U^2\right)_{j-1} + \frac{1}{2}\left(U^2\right)^{i,n-1} + \left(U^2\right)^{i-1}\right]$$

$$- \frac{1}{2}\left(\bar{K}_{13} + 2\,\bar{m}_3 r_{i-1}^{-1}\,\frac{\frac{1}{2}\,U_e + \frac{1}{2}\,U_e^{n-1,i} - U_e^{i-1}}{\frac{1}{2}\,U_e + \frac{1}{2}\,U_e^{i,n-1} + U_e^{i-1}}\right)\left[\frac{1}{4}\left(UW\right)_j + \frac{1}{4}\left(UW\right)_{j-1} + \frac{1}{2}\left(UW\right)^{i,n-1} + \left(UW\right)^{i-1}\right]$$

$$- \bar{m}_4\,\frac{\left[\frac{1}{4}\left(W^2\right)_j + \frac{1}{4}\left(W^2\right)_{j-1} + \frac{1}{2}\left(W^2\right)^{i,n-1} + \left(W^2\right)^{i-1}\right]}{\left[\frac{1}{2}\,U_e + \frac{1}{2}\,U_e^{i,n-1} + U_e^{i-1}\right]}$$

$$+ \frac{1}{2}\,\bar{m}_5\left(\frac{1}{4}\,U_j + \frac{1}{4}\,U_{j-1} + \frac{1}{2}\,U^{i,n-1} + U^{i-1}\right)$$

$$+ \bar{m}_6\,\frac{\left(\frac{1}{4}\,W_j + \frac{1}{4}\,W_{j-1} + \frac{1}{2}\,W^{i,n-1} + W^{i-1}\right)}{\left(\frac{1}{2}\,U_e + \frac{1}{2}\,U_e^{i,n-1} + U_e^{i-1}\right)}$$

$$- \frac{1}{4}\,\bar{m}_2 k_{n-1}^{-1}\left(\frac{1}{2}\,U_e + \frac{1}{2}\,U_e^{i,n-1} + U_e^{i-1}\right)\left[\frac{1}{4}\left(U^2\right)_j + \frac{1}{4}\left(U^2\right)_{j-1} + \frac{1}{2}\left(U^2\right)^{n,i-1} - \left(U^2\right)^{n-1}\right]$$

$$- \frac{1}{2}\,\bar{m}_3 r_{i-1}^{-1}\left(\frac{1}{4}\,W_j + \frac{1}{4}\,W_{j-1} + \frac{1}{2}\,W^{i,n-1} + W^{i-1}\right)\left(\frac{1}{4}\,U_j + \frac{1}{4}\,U_{j-1} + \frac{1}{2}\,U^{i,n-1} - U^{i-1}\right)$$

$$- \frac{1}{2}\,\bar{m}_1\left(\frac{1}{2}\,U_e + \frac{1}{2}\,U_e^{i,n-1} + U_e^{i-1}\right) + \bar{m}_2 k_{n-1}^{-1}\left(\frac{1}{2}\,U_e + \frac{1}{2}\,U_e^{n,i-1} - U_e^{n-1}\right)$$

$$+ \left[\bar{K}_{13} + 2\,\bar{m}_3 r_{i-1}^{-1}\,\frac{\left(\frac{1}{2}\,U_e + \frac{1}{2}\,U_e^{n-1,i} - U_e^{i-1}\right)}{\left(\frac{1}{2}\,U_e + \frac{1}{2}\,U_e^{i,n-1} + U_e^{i-1}\right)}\right]\left(\frac{\bar{W}_e}{W_{ref}}\right)$$

$$+ 2\left[\bar{m}_4\left(\frac{\bar{W}_e}{W_{ref}}\right) - \bar{m}_6\left(\frac{\bar{W}_e}{W_{ref}}\right)\right]\frac{1}{\left(\frac{1}{2}\,U_e + \frac{1}{2}\,U_e^{i,n-1} + U_e^{i-1}\right)} - \bar{m}_5 = 0 \qquad \text{(B42)}$$

$$\frac{1}{2}\,h_{j-1}^{-1}\left[\frac{1}{2}\left(bT\right)_j - \frac{1}{2}\left(bT\right)_{j-1} + \frac{1}{2}\left(BT\right)_j^{n-1,i} - \frac{1}{2}\left(bT\right)_{j-1}^{n-1,i} + \left(bT\right)_j^{i-1} - \left(bT\right)_{j-1}^{i-1}\right]$$

$$+ \frac{1}{4}\left(E_j + E_{j-1}\right)\left(\frac{1}{4}\,T_j + \frac{1}{4}\,T_{j-1} + \frac{1}{2}\,T^{i,n-1} + T^{i-1}\right)$$

$$- \frac{1}{4}\,\bar{m}_7\left(\frac{1}{2}\,U_e + \frac{1}{2}\,U_e^{i,n-1} + U_e^{i-1}\right)\left[\frac{1}{4}\left(UW\right)_j + \frac{1}{4}\left(UW\right)_{j-1} + \frac{1}{2}\left(UW\right)^{i,n-1} + \left(UW\right)^{i-1}\right]$$

$$+ \frac{1}{2}\,\bar{m}_8\left[\frac{1}{4}\left(W^2\right)_j + \frac{1}{4}\left(W^2\right)_{j-1} + \frac{1}{2}\left(W^2\right)^{i,n-1} + \left(W^2\right)^{i-1}\right]$$

$$- \frac{1}{4}\,\bar{m}_9\left[\frac{1}{2}\left(U_e^2\right) + \frac{1}{2}\left(U_e^2\right)^{i,n-1} + \left(U_e^2\right)^{i-1}\right]\cdot\left[\frac{1}{4}\left(U^2\right)_j + \frac{1}{4}\left(U^2\right)_{j-1} + \frac{1}{2}\left(U^2\right)^{i,n-1} + \left(U^2\right)^{i-1}\right]$$

$$- \frac{1}{4}\,\bar{m}_{10}\left(\frac{1}{2}\,U_e + \frac{1}{2}\,U_e^{i,n-1} + U_e^{i-1}\right)\left(\frac{1}{4}\,U_j + \frac{1}{4}\,U_{j-1} + \frac{1}{2}\,U^{i,n-1} + U^{i-1}\right)$$

$$- \frac{1}{2}\,\bar{m}_{11}\left(\frac{1}{4}\,W_j + \frac{1}{4}\,W_{j-1} + \frac{1}{2}\,W^{i,n-1} + W^{i-1}\right)$$

$$- \frac{1}{4}\,\bar{m}_2 k_{n-1}^{-1}\left(\frac{1}{2}\,U_e + \frac{1}{2}\,U_e^{i,n-1} + U_e^{i-1}\right)\left(\frac{1}{4}\,U_j + \frac{1}{4}\,U_{j-1} + \frac{1}{2}\,U^{i,n-1} + U^{i-1}\right)$$
$$\cdot\left(\frac{1}{4}\,W_j + \frac{1}{4}\,W_{j-1} + \frac{1}{2}\,W^{n,i-1} - W^{n-1}\right)$$

$$- \frac{1}{2}\,\bar{m}_3 r_{i-1}^{-1}\left[\frac{1}{4}\left(W^2\right)_j + \frac{1}{4}\left(W^2\right)_{j-1} + \frac{1}{2}\left(W^2\right)^{i,n-1} - \left(W^2\right)^{i-1}\right]$$

$$+ \frac{1}{2}\left[\bar{m}_7\left(\frac{\bar{W}_e}{\bar{W}_{ref}}\right) + \bar{m}_{10} + \frac{\bar{m}_2}{\bar{W}_{ref}}\,\frac{\partial \bar{W}_e}{\partial x}\right]\left(\frac{1}{2}\,U_e + \frac{1}{2}\,U_e^{i,n-1} + U_e^{i-1}\right)$$

$$+ \frac{1}{2}\,\bar{m}_9\left[\frac{1}{2}\left(U_e^2\right) + \frac{1}{2}\left(U_e^2\right)^{i,n-1} + \left(U_e^2\right)^{i-1}\right]$$

$$- \bar{m}_8\left(\frac{\bar{W}_e}{\bar{W}_{ref}}\right)^2 + \bar{m}_{11}\left(\frac{\bar{W}_e}{\bar{W}_{ref}}\right) + \frac{\bar{m}_3}{\bar{W}_{ref}}\left(\frac{\bar{W}_e}{\bar{W}_{ref}}\right)\frac{\partial \bar{W}_e}{\partial z} = 0 \qquad . \tag{B43}$$

$$\bar{h}_{j-1}\left(E_j - E_{j-1}\right)$$

$$- \frac{1}{2}\left[\frac{1}{2}\bar{m}_{12}\left(\frac{1}{2}U_e + \frac{1}{2}U_e^{i,n-1} + U_e^{i-1}\right) + 2\bar{m}_2 k_{n-1}^{-1}\frac{\frac{1}{2}\left(U_e\delta^*\right) + \frac{1}{2}\left(U_e\delta^*\right)^{n,i-1} - \left(U_e\delta^*\right)^{n-1}}{\frac{1}{2}\delta^* + \frac{1}{2}\delta^{*i,n-1} + \delta^{*i-1}}\right]$$

$$\cdot\left(\frac{1}{4}U_j + \frac{1}{4}U_{j-1} + \frac{1}{2}U^{i,n-1} + U^{i-1}\right)$$

$$- \frac{1}{2}\left[\bar{m}_{13} + 2\bar{m}_3 r_{i-1}^{-1}\frac{\frac{1}{2}\delta^* + \frac{1}{2}\delta^{*i,n-1} - \delta^{*i-1}}{\frac{1}{2}\delta^* + \frac{1}{2}\delta^{*i,n-1} + \delta^{*n-1}}\right]\left(\frac{1}{4}W_j + \frac{1}{4}W_{j-1} + \frac{1}{2}W^{i,n-1} + W^{i-1}\right)$$

$$- \frac{1}{2}\bar{m}_2 k_{n-1}^{-1}\left(\frac{1}{2}U_e + \frac{1}{2}U_e^{i,n-1} + U_e^{i-1}\right)\left(\frac{1}{4}U_j + \frac{1}{4}U_{j-1} + \frac{1}{2}U^{n,i-1} + U^{n-1}\right)$$

$$- \bar{m}_3 r_{i-1}^{-1}\left(\frac{1}{4}W_j + \frac{1}{4}W_{j-1} + \frac{1}{2}W^{i,n-1} + W^{i-1}\right) = 0 \quad . \tag{B44}$$

Solved in the inverse or direct manner, the equations are subject to the boundary conditions

$$U_o = W_o = E_o = 0 \quad , \tag{B45a}$$

and

$$U_j = 1 \quad , \quad W_J = \frac{W_e}{W_{ref}} \quad , \quad F_J = \eta_J - 1 \quad . \tag{B45b}$$

If the equations are solved by the quasi-simultaneous method, an extra boundary condition is introduced as (eq.3.175)

$$U_e(1 - d_{i,i}\delta^*) - e_{i,i}\delta^*(\eta_J W_e - G_J W_{ref}) = K \quad . \tag{B45c}$$

B5 Discretization of the General Boundary Layer Equations using the Zig-Zag Scheme

In the case of separated flow, the zig-zag scheme is employed to discretize the three-dimensional boundary layer equations.

As in the case of the standard Keller-box scheme, the node points are defined by the notation (see fig. B5).

$$x_n = x_{n-1} + k_{n-1} \quad , \quad n = 1,2, \ldots , N \quad , \quad \text{(B46a)}$$

$$z_i = z_{i-1} + r_{i-1} \quad , \quad i = 1,2, \ldots , I \quad , \quad \text{(B46b)}$$

$$\eta_j = \eta_{j-1} + h_{j-1} \quad , \quad j = 1,2, \ldots , J \quad . \quad \text{(B46c)}$$

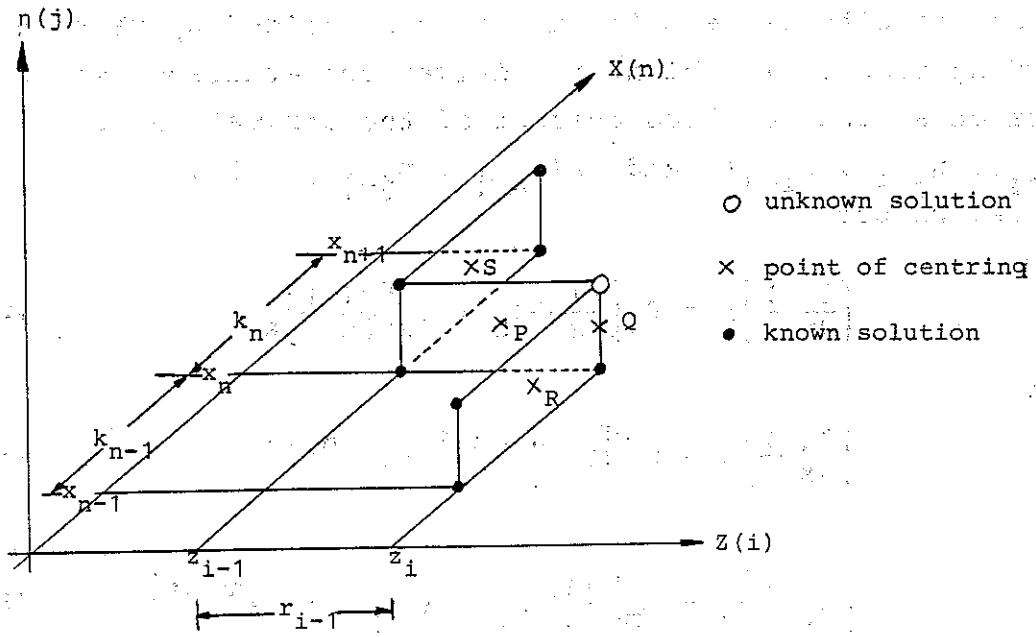

Fig. B5 Difference molecule of the zig-zag scheme

When using the zig-zag scheme the definition equations (3,137a) -(3.137d) are approximated by discretizing about $Q(x_n , \eta_{j-\frac{1}{2}} , z_i)$. To write the difference equations for the remaining equations (3.138a)-(3.138c), we use quantities centered at $P(x_n , \eta_{j-\frac{1}{2}} , z_{i-\frac{1}{2}})$ (see fig. B5). This is done by averaging the the variables about the four corner points of P , that is

$$( )_P = \frac{1}{2}\left[\frac{1}{2}( )_j + \frac{1}{2}( )_{j-1} + ( )^{n,i-1}\right] \quad . \quad \text{(B47)}$$

For convenience, variables evaluated at (x_n , η_{j-1} , z_i) and (x_n , η_j , z_i) are denoted by $( )_{j-1}$ and $( )_j$, respectively, and the index '$j-\frac{1}{2}$' is omitted. That is, for example, we write

$$( )^{n,i-1} = \frac{1}{2}\left[( )_j^{n,i-1} + ( )_{j-1}^{n,i-1} \right] \quad . \tag{B48}$$

The derivatives with respect to η and z are averaged about P by the difference equations

$$( )'_P = \frac{1}{2} h_{j-1}^{-1}\left[( )_j - ( )_j + ( )_j^{n,i-1} - ( )_{j-1}^{n,i-1} \right] , \tag{B49}$$

and

$$\left[\frac{\partial ( )}{\partial z}\right]_P = r_{i-1}^{-1}\left[\frac{1}{2}( )_j + \frac{1}{2}( )_{j-1} - ( )^{n,i-1}\right] \quad . \tag{B50}$$

Derivatives with respect to x are discretized by using an upwinding formula in which the derivatives evaluated at P are taken as the weighted average of the derivatives at $S(x_{n+\frac{1}{2}} , \eta_{j-\frac{1}{2}} , z_{i-1})$ and $R(x_{n-\frac{1}{2}} , \eta_{j-\frac{1}{2}} , z_i)$. That is, we put

$$\left[\frac{\partial ( )}{\partial x}\right]_P = \theta_1\left[\frac{\partial ( )}{\partial x}\right]_S + \theta_2\left[\frac{\partial ( )}{\partial x}\right]_R \quad , \tag{B51}$$

where

$$\left[\frac{\partial ( )}{\partial x}\right]_S = k_n^{-1}\left[( )^{n+1,i-1} - ( )^{n,i-1} \right] \quad , \tag{B52}$$

and

$$\left[\frac{\partial ( )}{\partial x}\right]_R = k_{n-1}^{-1}\left[\frac{1}{2}( )_j + \frac{1}{2}( )_{j-1} - ( )^{n-1,i}\right] \quad . \tag{B53}$$

The weighting coefficients are given as

$$\theta_1 = \frac{x_n - x_{n-1}}{x_{n+1} - x_{n-1}} \quad , \tag{B54}$$

and

$$\theta_2 = \frac{x_{n+1} - x_n}{x_{n+1} - x_{n-1}} \quad . \tag{B55}$$

As in the case of the standard box scheme, special treatment are employed to approximate the variable E . Here we express the unknown E_j as

$$E_j \equiv \frac{1}{2}\left(E_j^{n,i-1} + E_j^{n,i}\right) \quad . \tag{B56}$$

In discretized form the governing equations are written

$$F_j - F_{j-1} - \frac{1}{2}h_{j-1}(U_j + U_{j-1}) = 0 \tag{B57}$$

$$G_j - G_{j-1} - \frac{1}{2}h_{j-1}(W_j + W_{j-1}) = 0 \tag{B58}$$

$$U_j - U_{j-1} - \frac{1}{2}h_{j-1}(V_j + V_{j-1}) = 0 \tag{B59}$$

$$W_j - W_{j-1} - \frac{1}{2}h_{j-1}(T_j + T_{j-1}) = 0 \quad . \tag{B60}$$

$$\frac{1}{2}\,h_{j-1}^{-1}\left[\left(b\,V\right)_j - \left(b\,V\right)_{j-1} + \left(b\,V\right)_j^{n,i-1} - \left(b\,V\right)_{j-1}^{n,i-1}\right]$$

$$+\frac{1}{4}\left(E_j + E_{j-1}\right)\left(\frac{1}{2}\,V_j + \frac{1}{2}\,V_{j-1} + V^{n,i-1}\right)$$

$$+\frac{1}{2}\left[\frac{1}{2}\,\bar{m}_1\left(U_e + U_e^{n,i-1}\right) - \bar{m}_2\left(\theta_1 k_n^{-1}\left(U_e^{n+1,i-1} - U_e^{n,i-1}\right) + \theta_2 k_{n-1}^{-1}\left(U_e - U_e^{n-1,i}\right)\right)\right]$$

$$\cdot\left[\frac{1}{2}\left(U^2\right)_j + \frac{1}{2}\left(U^2\right)_{j-1} + \left(U^2\right)^{n,i-1}\right]$$

$$-\frac{1}{2}\left[\bar{K}_{13} + 2\,\bar{m}\,r_{i-1}^{-1}\,\frac{U_e - U_e^{n,i-1}}{U_e + U_e^{n,i-1}}\right]\left[\frac{1}{2}\left(UW\right)_j + \frac{1}{2}\left(UW\right)_{j-1} + \left(UW\right)^{n,i-1}\right]$$

$$-\frac{\bar{m}_4}{U_e + U_e^{n,i-1}}\left[\frac{1}{2}\left(W^2\right)_j + \frac{1}{2}\left(W^2\right)_{j-1} + \left(W^2\right)^{n,i-1}\right]$$

$$+\frac{1}{2}\,\bar{m}_5\left(\frac{1}{2}\,U_j + \frac{1}{2}\,U_{j-1} + U^{n,i-1}\right)$$

$$+\frac{\bar{m}_6}{U_e + U_e^{n,i-1}}\left(\frac{1}{2}\,W_j + \frac{1}{2}\,W_j + W^{n,i-1}\right)$$

$$-\frac{1}{4}\,\bar{m}_2\left(U_e + U_e^{n,i-1}\right)\left[\theta_1 k_n^{-1}\left(\left(U^2\right)^{n+1,i-1} - \left(U^2\right)^{n,i-1}\right)\right.$$

$$\left. + \theta_2 k_{n-1}^{-1}\left(\frac{1}{2}\left(U^2\right)_j + \frac{1}{2}\left(U^2\right)_{j-1} - \left(U^2\right)^{n-1,i}\right)\right]$$

$$-\frac{1}{2}\,\bar{m}_3 r_{i-1}^{-1}\left(\frac{1}{2}\,W_j + \frac{1}{2}\,W_{j-1} + W^{n,i-1}\right)\left(\frac{1}{2}\,U_j + \frac{1}{2}\,U_{j-1} - U^{n,i-1}\right)$$

$$-\frac{1}{2}\,\bar{m}_1\left(U_e + U_e^{n,i-1}\right)$$

$$+\bar{m}_2\left[\theta_1 k_n^{-1}\left(U_e^{n+1,i-1} - U_e^{n,i-1}\right) + \theta_2 k_{n-1}^{-1}\left(U_e - U_e^{n-1,i}\right)\right]$$

(to be continued)

(continued)

$$+ \left(K_{13} + 2\,\bar{m}_3 r_{i-1}^{-1} \frac{U_e - U^{n,i-1}}{U_e + U_e^{n,i-1}}\right)\left(\frac{\bar{W}_e}{W_{ref}}\right) + 2\left(\frac{\bar{W}_e}{W_{ref}}\right)^2 \frac{\bar{m}_4}{U_e + U_e^{n,i-1}}$$

$$- \bar{m}_5$$

$$- 2\left(\frac{\bar{W}_e}{W_{ref}}\right) \frac{\bar{m}_6}{U_e + U_e^{n,i-1}} = 0 \qquad \text{(B61)}$$

$$\frac{1}{2}\, h_{j-1}^{-1}\Big[\big(b\ T\big)_j - \big(b\ T\big)_{j-1} + \big(b\ T\big)_j^{n,i-1} - \big(b\ T\big)_{j-1}^{n,i-1}\Big]$$

$$+ \frac{1}{4}\Big(E_j + E_{j-1}\Big)\Big(\frac{1}{2}\ T_j + \frac{1}{2} T_{j-1} + T^{n,i-1}\Big)$$

$$- \frac{1}{4}\ \bar{m}_7\Big(U_e + U_e^{n,i-1}\Big)\Big[\frac{1}{2}\big(UW\big)_j + \frac{1}{2}\big(UW\big)_{j-1} + \big(UW\big)^{n,i-1}\Big]$$

$$+ \frac{1}{2}\ \bar{m}_8\Big[\frac{1}{2}\big(W^2\big)_j + \frac{1}{2}\big(W^2\big)_{j-1} + \big(W^2\big)^{n,i-1}\Big]$$

$$- \frac{1}{4}\ \bar{m}_9\Big[U_e^2 + \big(U_e^2\big)^{n,i-1}\Big]\Big[\frac{1}{2}\big(U^2\big)_j + \frac{1}{2}\big(U^2\big)_{j-1} + \big(U^2\big)^{n,i-1}\Big]$$

$$- \frac{1}{4}\ \bar{m}_{10}\Big(U_e + U_e^{n,i-1}\Big)\Big(\frac{1}{2}\ U_j + \frac{1}{2}\ U_{j-1} + U^{n,i-1}\Big)$$

$$- \frac{1}{2}\ \bar{m}_{11}\Big(\frac{1}{2}\ W_j + \frac{1}{2}\ W_{j-1} + W^{n,i-1}\Big)$$

$$- \frac{1}{4}\ \bar{m}_2\Big(U_e + U_e^{n,i-1}\Big)\Big[\theta_1 k_n^{-1}\Big(U^{n+1,i-1} + U^{n,i-1}\Big)\Big(W^{n+1,i-1} - W^{n,i-1}\Big)$$

$$+ \theta_2 k_{n-1}^{-1}\Big(\frac{1}{2}U_j + \frac{1}{2}U_{j-1} + U^{n-i,i}\Big)\Big(\frac{1}{2}W_j + \frac{1}{2}W_{j-1} - W^{n-1,i}\Big)\Big]$$

$$- \frac{1}{2}\ \bar{m}_3 r_{i-1}^{-1}\Big[\frac{1}{2}\big(W^2\big)_j + \frac{1}{2}\big(W^2\big)_{j-1} - \big(W^2\big)^{n,i-1}\Big]$$

$$+ \frac{1}{2}\Big[\bar{m}_7\Big(\frac{W_e}{W_{ref}}\Big) + \bar{m}_{10} + \frac{\bar{m}_2}{W_{ref}}\ \frac{\partial \bar{W}_e}{\partial x}\Big]\Big(U_e + U_e^{n,i-1}\Big)$$

$$+ \frac{1}{2}\ \bar{m}_9\Big[U_e^2 + \big(U_e^2\big)^{n,i-1}\Big]$$

$$- \bar{m}_8\Big(\frac{\bar{W}_e}{W_{ref}}\Big)^2 + \bar{m}_{11}\Big(\frac{\bar{w}_e}{W_{ref}}\Big) + \frac{\bar{m}_3}{W_{ref}}\Big(\frac{\bar{W}}{W_{ref}}\Big)\ \frac{\partial \bar{W}_e}{\partial z} = 0 \qquad . \qquad \text{(B62)}$$

$$h_{j-1}^{-1}\left(E_j - E_{j-1}\right)$$

$$- \frac{1}{2}\Big[\frac{1}{2}\bar{m}_{12}\left(U_e + U_e^{n,i-1}\right) + 2\,\frac{\bar{m}_2}{\delta^* + \delta^{*n,i-1}}\Big(\theta_1 k_n^{-1}\Big[\left(U_e\delta^*\right)^{n+1,i-1} - \left(U_e\delta^*\right)^{n,i-1}\Big]$$

$$+ \theta_2 k_{n-1}^{-1}\Big[U_e\delta^* - \left(U_e\delta^*\right)^{n-1,i}\Big]\Big)\Big]\left(\frac{1}{2}U_j + \frac{1}{2}U_{j-1} + U^{n,i-1}\right)$$

$$- \frac{1}{2}\Big[\bar{m}_{13} + 2\,\bar{m}_3 r_{i-1}^{-1}\,\frac{\delta^* - \delta^{*n,i-1}}{\delta^* + \delta^{*n,i-1}}\Big]\left(\frac{1}{2}W_j + \frac{1}{2}W_{j-1} + W^{n,i-1}\right)$$

$$- \frac{1}{2}\bar{m}_2\left(U_e + U_e^{n,i-1}\right)\Big[\theta_1 k_n^{-1}\left(U^{n+1,i-1} - U^{n,i-1}\right) + \theta_2 k_{n-1}^{-1}\left(\frac{1}{2}U_j + \frac{1}{2}U_{j-1} - U^{n-1,i}\right)\Big]$$

$$- \bar{m}_3 r_{i-1}^{-1}\left(\frac{1}{2}W_j + \frac{1}{2}W_{j-1} - W^{n,i-1}\right) = 0 \quad . \qquad \text{(B63)}$$

As in the case of the standard Keller-box scheme, the equations are subject to the boundary conditions

$$U_o = W_o = E_o = 0 \quad , \qquad \text{(B64a)}$$

and

$$U_J = 1 \quad , \quad W_J = \frac{W_e}{W_{ref}} \quad , \quad F_J = \eta_J - 1 \quad . \qquad \text{(B64b)}$$

If the equations are solved by the quasi-simultaneous method, U_e and δ^* are both treated as unknown, and the additional boundary condition is given as (eq.3.175)

$$U_e\left(1 - d_{n,n}\delta^*\right) - e_{n,n}\delta^*\left(\eta_J W_e - W_{ref}G_J\right) = K_n \quad . \qquad \text{(B64c)}$$

APPENDIX C

Matrix Components for Section 3.4.5

The matrices of eqs.(3.195a) - (3.195c) are given as

$$\underline{\underline{A}}_j = \begin{bmatrix} 1 & 0 & -\frac{h_{j-1}}{2} & 0 & 0 & 0 & 0 \\ 0 & 1 & 0 & -\frac{h_{j-1}}{2} & 0 & 0 & 0 \\ 0 & 0 & (s_1)_j & (s_3)_j & (s_9)_j & (s_5)_j & (s_7)_j \\ 0 & 0 & (s_{11})_j & (s_{13})_j & (s_{19})_j & (s_{15})_j & (s_{17}) \\ 0 & 0 & (s_{21})_j & (s_{23})_j & (s_{25})_j & 0 & 0 \\ 0 & 0 & -1 & 0 & 0 & -\frac{h_j}{2} & 0 \\ 0 & 0 & 0 & -1 & 0 & 0 & -\frac{h_j}{2} \end{bmatrix}, \quad j=1,2,\ldots,J-1 \qquad \text{(C1)}$$

$$\underline{\underline{B}}_j = \begin{bmatrix} -1 & 0 & -\frac{h_{j-1}}{2} & 0 & 0 & 0 & 0 \\ 0 & -1 & 0 & -\frac{h_{j-1}}{2} & 0 & 0 & 0 \\ 0 & 0 & (s_2)_j & (s_4)_j & (s_{10})_j & (s_6)_j & (s_8)_j \\ 0 & 0 & (s_{12})_j & (s_{14})_j & (s_{20})_j & (s_{16})_j & (s_{18})_j \\ 0 & 0 & (s_{22})_j & (s_{24})_j & (s_{26})_j & 0 & 0 \\ 0 & 0 & 0 & 0 & 0 & 0 & 0 \\ 0 & 0 & 0 & 0 & 0 & 0 & 0 \end{bmatrix}, \quad j=1,2,\ldots J \qquad \text{(C2)}$$

$$\underline{\underline{C}}_j = \begin{bmatrix} 0 & 0 & 0 & 0 & 0 & 0 & 0 \\ 0 & 0 & 0 & 0 & 0 & 0 & 0 \\ 0 & 0 & 0 & 0 & 0 & 0 & 0 \\ 0 & 0 & 0 & 0 & 0 & 0 & 0 \\ 0 & 0 & 0 & 0 & 0 & 0 & 0 \\ 0 & 0 & 1 & 0 & 0 & -\frac{h_j}{2} & 0 \\ 0 & 0 & 0 & 1 & 0 & 0 & -\frac{h_j}{2} \end{bmatrix}, \quad j=0,1,\ldots,J-1 \qquad \text{(C3)}$$

$$\underline{\underline{A}}_o = \begin{bmatrix} 1 & 0 & 0 & 0 & 0 & 0 & 0 \\ 0 & 1 & 0 & 0 & 0 & 0 & 0 \\ 0 & 0 & 1 & 0 & 0 & 0 & 0 \\ 0 & 0 & 0 & 1 & 0 & 0 & 0 \\ 0 & 0 & 0 & 0 & 1 & 0 & 0 \\ 0 & 0 & -1 & 0 & 0 & -\frac{h_o}{2} & 0 \\ 0 & 0 & 0 & -1 & 0 & 0 & -\frac{h_o}{2} \end{bmatrix} \qquad \text{(C4)}$$

$$\underline{\underline{A}}_J = \begin{bmatrix} 1 & 0 & -\frac{h_{J-1}}{2} & 0 & 0 & 0 & 0 \\ 0 & 1 & 0 & -\frac{h_{J-1}}{2} & 0 & 0 & 0 \\ 0 & 0 & (s_1)_J & (s_3)_J & (s_9)_J & (s_5)_J & (s_7)_J \\ 0 & 0 & (s_{11})_J & (s_{13})_J & (s_{19})_J & (s_{15})_J & (s_{17})_J \\ 0 & 0 & (s_{21})_J & (s_{23})_J & (s_{25})_J & 0 & 0 \\ 0 & 0 & 1 & 0 & 0 & 0 & 0 \\ 0 & 0 & 0 & 1 & 0 & 0 & 0 \end{bmatrix} \qquad \text{(C5)}$$